Hollow colloidal particles by emulsion templating

from synthesis to self-assembly

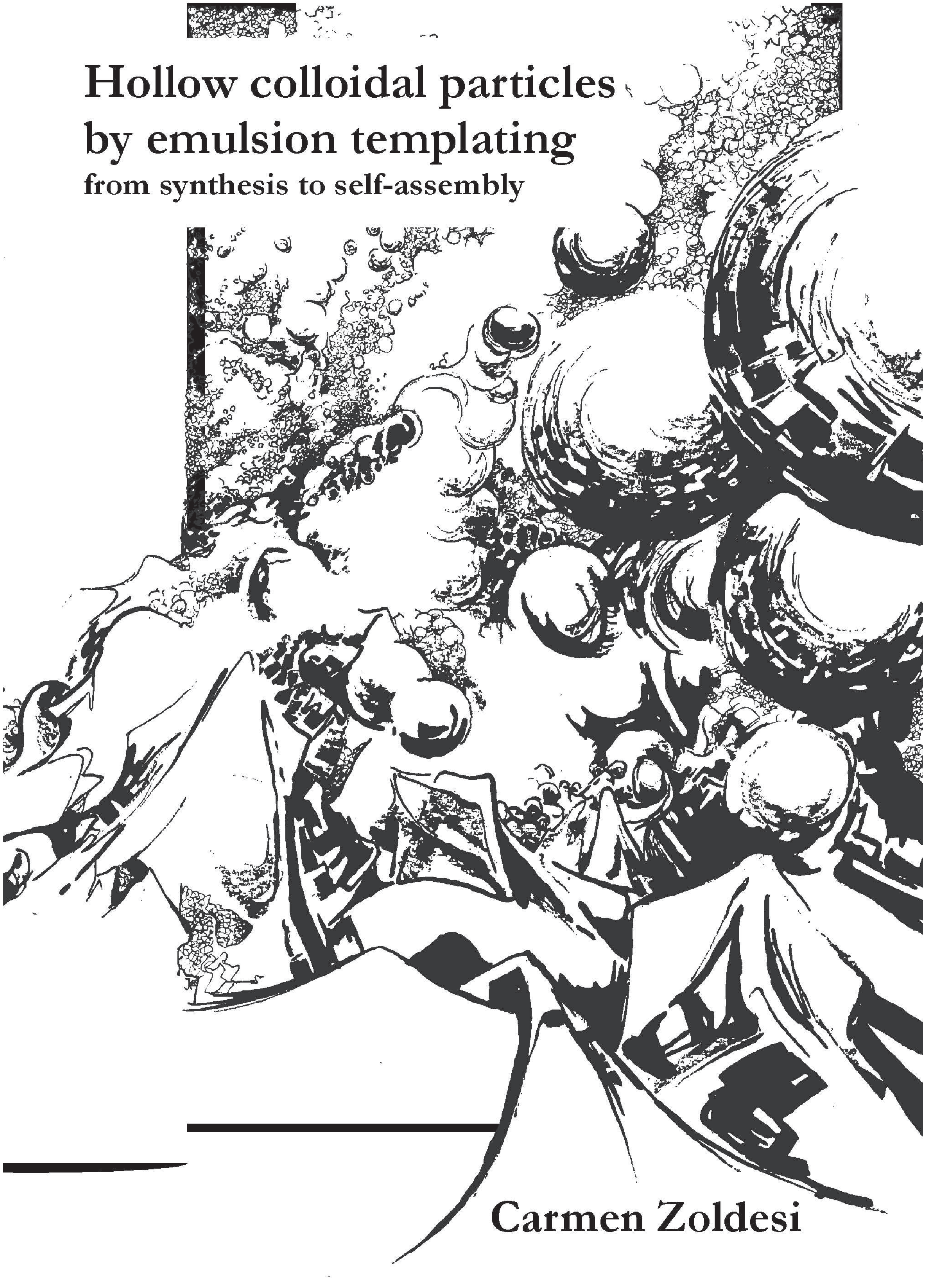

Carmen Zoldesi

Hollow colloidal particles by emulsion templating

from synthesis to self-assembly

Carmen Zoldesi

Universiteit Utrecht

NWO

The work described in this thesis was performed in the Soft Condensed Matter Group, at Utrecht University, The Netherlands. The project was financially supported by the "Nederlandse organisatie voor Wetenschappelijk Onderzoek (NWO)".

ISBN-10: 90-393-4322-5
ISBN-13: 978-90-393-4322-7
Digital version available at: http://www.colloid.nl

HOLLOW COLLOIDAL PARTICLES BY EMULSION TEMPLATING
FROM SYNTHESIS TO SELF-ASSEMBLY

HOLLE COLLOÏDALE DEELTJES DOOR GEBRUIK VAN EEN EMULSIE ALS TEMPLATE
VAN SYNTHESE TOT ZELF-ASSEMBLAGE
(Met een samenvatting in het Nederlands)

Proefschrift

ter verkrijging van de graad van doctor aan de Universiteit Utrecht
op gezag van de
rector magnificus, prof. dr. W.H. Gispen,
ingevolge het besluit van het college voor promoties
in het openbaar te verdedigen
op woensdag 27 september 2006 des middags te 2.30 uur

door

CARMEN IULIA ZOLDESI

geboren op 19 augustus 1974
te Tăsnad, Roemenië

Promotor: prof. dr. A. van Blaaderen

Co-promotor: dr. A. Imhof

CONTENTS

1 INTRODUCTION 5

1.1 Colloidal particles 5

1.2 Core-shell colloidal particles 6

1.3 Colloidal particles from alkoxysilanes 6

1.4 Hollow colloidal particles 7

1.5 This thesis 8

2 PREPARATION OF HOLLOW SPHERES, MICROCAPSULES AND MICROBALLOONS BY SURFACTANT FREE EMULSION TEMPLATING 11

2.1 Introduction 12

2.2 Experimental section 13

2.2.1 Materials 13

2.2.2 Particle synthesis 13

2.2.3 Particle characterization 14

2.3 Results and discussion 14

2.3.1 Microballoons 17

2.3.2 Microcapsules 18

2.3.3 Microspheres 20

2.4 Conclusions 22

3 CHARACTERIZATION AND FORMATION OF MICROSPHERES, MICROCAPSULES AND MICROBALLOONS 25

3.1 Introduction 26

3.2 Experimental section 26

3.2.1 Materials 26

3.2.2 Synthesis 26

3.2.3 Characterization 27

3.3 Results and discussion 29

3.3.1 PDMS oil droplets 29

3.3.2 Droplet growth 29

3.3.3 Solution ^{29}Si NMR of PDMS emulsions 34

3.3.4 Shell thickness vs. core radius 38

3.3.5 EDX analysis of the hollow shells 42

3.3.6 ^{29}Si solid-state NMR of hollow shells 44
3.3.7 Density of the shells 46
3.3.8 Fluorescent shells 48
3.3.9 Shell permeability 49
3.4 Conclusions 51

4 SYNTHESIS OF HOLLOW SPHERES BY SURFACTANT-STABILIZED EMULSION TEMPLATING 53
4.1 Introduction 54
4.2 Experimental section 56
4.2.1 Materials 56
4.2.2 Synthesis 56
4.2.3 Characterization 57
4.3 Results and discussion 58
4.3.1 SDS-stabilized PDMS emulsions 58
4.3.2 Hollow particles from SDS-stabilized oil droplets 62
4.3.3 EDX analysis of the hollow shells 65
4.3.4 Second shell growth 66
4.3.5 Triton X-100-stabilized PDMS emulsions 67
4.3.6 Hollow particles from Triton X-100-stabilized oil droplets 70
4.3.7 Coating different oil droplets with solid shells 73
4.4 Conclusions 74

5 ELASTIC PROPERTIES OF HOLLOW COLLOIDAL PARTICLES: DEFORMATION AND BUCKLING 77
5.1 Introduction 78
5.2 Experimental section 78
5.2.1 Sample preparation 78
5.2.2 Characterization 79
5.3 Results and discussion: indentation 80
5.3.1 Results 80
5.3.2 Discussion 86
5.4 Results and discussion: buckling 90
5.4.1 Study of buckling threshold 90
5.4.2 Simulations of elastic shells 94
5.5 Conclusions 96

6 ASSEMBLY OF MICROCELLULAR STRUCTURES FROM COLLOIDAL PARTICLES PREPARED BY EMULSION TEMPLATING 99
6.1 Introduction 100
6.2 Experimental section 101
6.2.1 Materials 101

6.2.2 Sample preparation 101
6.2.3 Characterization 103
6.3 Results and discussion 103
6.3.1 Small clusters of particles 103
6.3.2 2 -dimensional foams 106
6.3.3 3 -dimensional foams 112
6.3.4 Crystals 114
6.4 Conclusions 116

REFERENCES 117

SUMMARY 127

SAMENVATTING 131

PUBLICATIONS 135

ACKNOWLEDGEMENTS 137

CURRICULUM VITAE 139

1 INTRODUCTION

1.1 COLLOIDAL PARTICLES

The term *colloidal* refers to particles dispersed in a solvent, which have at least in one direction a dimension roughly between 1 nm and 1 μm. The most important considerations behind this definition are that these particles are much larger than the surrounding solvent molecules, but much smaller than macroscopic objects. A characteristic property of particles in this size range is that they undergo Brownian motion due to fluctuations in their random collisions with the solvent molecules. As a result, they exhibit similar phase behavior as atoms and molecules, but their length-scale has several important advantages: colloids are slow, soft and easier to study. They are slow, since the diffusion coefficient is several orders of magnitude smaller than the molecular one, they are soft, because they respond to small external forces, and they can be studied using a variety of experimental techniques such as light scattering and optical microscopy, since their size is comparable to the wavelength of visible light. In addition, the tunability of the interactions between colloids, their size, shape and composition, have made them an important model system for atoms and molecules. The colloidal dispersions also show specific behavior which makes them interesting systems for study. Fundamental differences with molecular systems stem from the presence of fluid between the particles. This gives rise to many new phenomena, for which reason concentrated colloidal dispersions are often referred to as 'complex fluids'. Thanks to their 'complex fluidity', colloidal dispersions also find many applications in practice and in biological systems, for instance in paint, drilling mud, photographic emulsions, magnetic fluids and blood. They are therefore widespread in chemical engineering, pharmaceutical and biological applications. Monodisperse colloidal particles also represent attractive building blocks from which ordered and complex materials can be created.

1.2 CORE-SHELL COLLOIDAL PARTICLES

In recent years, considerable effort has been devoted to the design and controlled fabrication of nano- and micro-structured materials with functional properties. The interest in these materials stems from the fact that their properties (optical, electrical, mechanical, chemical, etc.) are a function of their size, composition and structural order. Therefore, effective strategies to build tailored materials reliably and predictably are required in order to meet the increasing demands placed on materials synthesis and performance. In this respect, over the last years, there has been an immense effort to fabricate core-shell colloidal particles with tailored structural, optical, and surface properties, as precursors for such materials. [1–4] Investigations have been intensified not only by the applicability of such colloids in modern materials science, but also by their technological importance. The synthesis of core-shell particles with defined morphologies and properties typically involves tailoring the surface properties of particles, often accomplished by coating or encapsulating them with a shell of a preferred material. Composite colloids are utilized in the area of coatings, ceramics, electronics, catalysis, separations, and diagnosis. Core-shell particles often exhibit improved physical and chemical properties over their single-component counterparts, and hence are potentially useful in a broad range of applications. They can be used to produce materials with new properties, such as composites, hybrid organic/inorganic materials, porous materials, optical materials to modify scattering/absorptive properties. The fabrication of core-shell particles is also of interest from a fundamental and academic point of view, especially in the fields of colloid and interface science. They can be used as model systems to investigate factors governing colloidal interactions and stabilizations and to gain valuable information on the properties of concentrated dispersions.

1.3 COLLOIDAL PARTICLES FROM ALKOXYSILANES

Over the last decades, there has been an extensive interest in preparation of colloidal particles from alkoxysilanes. The pioneering work in this field was done by Stöber, [5] who introduced a method to prepare highly monodisperse spherical silica particles from tetraalkoxysilane, in a solvent containing water, ammonia and an alcohol.

A major contribution to further development of this method came from Utrecht. The formation and growth mechanism of silica particles has been investigated by Van Helden, [6] Philipse, [7] and van Blaaderen. [8] Philipse and Vrij synthesized silica spheres from tetraalkoxysilane and coated them with trialkoxysilane. [9] Van Blaaderen introduced a method to incorporate large amounts of trialkoxysilane inside the particles, by copolymerization with tetraalkoxysilane, which resulted in organo-silica spheres. [10] Using the same approach, a fluorescent dye was first coupled to the trialkoxysilane prior the copolymerization step. [11]

The further growth of silica particles initially prepared from tetraalkoxysilane following the Stöber reaction mixture has been also extensively investigated. [7, 12–14] A particularly interesting approach makes use of much less alcohol than in a Stöber reaction mixture, and the resulting product consist of large, monodisperse and porous silica particles. [15]

Other types of hybrid particles (so-called microgel), based on alkoxysilanes were obtained using mixtures of trialkoxysilanes and dialkoxysilanes, with a dye coupled to the di-functional alkoxysilane. [16–18]

It was shown that monodisperse spherical organo-silica powders can be obtained also in aqueous solutions containing a catalyst (base or acid), but without alcohol, either from trialkoxysilanes, [19] or from mixtures of tri- and tetraalkoxysilanes. [20] Recently, an interesting method was reported in which monodisperse particles were prepared from trialkoxysilane, using emulsions, in aqueous solutions containing ammonia. [21]

The alkoxysilanes found applications also in preparation of emulsions. Difunctional alkoxysilanes have been used to prepare monodisperse oil droplets, in the presence of ammonia as catalyst, work initiated by Vincent and coworkers. [22] The same procedure was extended to mixtures of difunctional and trifunctional alkoxysilanes, and resulted in microgel particles. [23] Solid shells were grown around these microgel particles using tetraalkoxysilane, in an aqueous solution containing ammonia and alcohol. [24]

1.4 HOLLOW COLLOIDAL PARTICLES

Colloidal particles with a hollow interior represent a special class of core-shell particles. The fabrication of uniformly-sized hollow spheres with controllable size and shape has gained increasing attention in recent years. They often exhibit properties that are substantially different from those of particles in general (e.g., their low density, large specific surface area, stability and surface permeability), thus making them attractive from both a scientific and technological viewpoint. The hollow particles represent a distinct class of materials which are of interest in the fields of medicine, pharmaceutics, materials science and the paint industry. They find diverse applications, including encapsulation of chemicals (for the controlled-release of drugs, cosmetics, inks and dyes), protection of sensitive components (as enzymes and proteins), ultrasound-contrast agents, catalysis, coatings, composite materials, artificial cells and fillers. [3, 25–31] Additionally, they can be used to fabricate highly porous structures with applications in light-weight materials, adsorption, insulation and as filters. When sufficiently ordered, these materials are also predicted to have useful properties as optical devices (e.g. photonic bandgap). [32, 33]

Furthermore, the hollow particles can be used as dielectric defects in photonic crystals, acting as microcavities, which could lead to localized photonic states in the gap, whose shape and properties would be dictated by the nature of the defect. [32, 34]

The physicochemical characteristics of the hollow particles have to fulfil a large variety of requirements, depending on the specific applications, such as shell permeability, stability, bio-compatibility, absorptive/reflective properties, etc. Very often, these properties are directly influenced by the preparation techniques. A variety of chemical and physicochemical methods, including heterophase polymerization combined with a sol-gel process, [35, 36] emulsion/interfacial polymerization strategies, [26] spray-drying methods, [37–39] surface polymerization processes, [40] and colloidal templating [41–43] have been employed to prepare hollow spheres. Among these, a templating approach represents one of the most often used techniques which is based on the synthesis of core-shell particles and subsequently removal of the core by dissolution in a solvent or heating (calcination). Although it can be used to prepare hollow particles from very diverse materials, both organic and inorganic, starting with a variety of templating agents, this technique encounters very often limitations related to the polydispersity of the templates and/or the resulting particles, the coating procedure or the removal of the core without affecting the shell properties.

1.5 THIS THESIS

Due to the increasing interest (both from scientific and technological point of view), in colloidal particles, and in particular particles with a hollow interior, in the present research we focus on several aspects regarding this type of colloids:

- developing a new and flexible method to prepare hollow micrometer-sized colloidal particles;
- characterization of both the templates and the resulting particles from physical and chemical point of view;
- investigating some of the materials which can be obtained by self-assembly of the hollow particles.

For the preparation of hollow particles, we used an emulsion templating technique in which monodisperse emulsion droplets were used as templates for the encapsulation with solid shells. This method opens the possibility of preparing different types of hollow particles with tunable size and interesting properties.

The colloids we prepared can be placed in the larger context of particles obtained from alkoxysilanes. We followed the same route started by Vincent and coworkers, but we made use of the copolymerization between the dialkoxysilane used for the oil droplets, and tetraalkoxysilane in order to obtain solid shells around the liquid cores. Moreover, our synthesis was performed in an alcohol free solution.

Our method brings several advantages over the existing techniques, such as control over core and shell size, monodispersity of the particles, and ease of template removal. Both the emulsion droplets used as templates and the resulting hollow shells were investigated with a wide variety of techniques. The special characteristics that these colloids exhibit make them suitable precursors for interesting materials.

The emulsion templating technique and the types of particles obtained are described in Chapter 2. Several interesting aspects related to the reaction course are discussed in Chapter 3, which also includes extensive investigations of a number of chemical and physical properties of the oil droplets and the hollow shells. Chapter 4 is focused on using surfactant-stabilized emulsion droplets as templates for the encapsulation with solid shells. Special emphasis was put on the determination of the elastic properties of the hollow shells (Chapter 5). As shown in Chapter 6, interesting materials can be obtained by the self-assembly of hollow shells prepared by emulsion templating. The deformability of the shells makes it possible to prepare new types of deformed particles, bubble-like clusters and solid microcellular foams.

2 PREPARATION OF HOLLOW SPHERES, MICROCAPSULES AND MICROBALLOONS BY SURFACTANT FREE EMULSION TEMPLATING

We report on the synthesis of new types of monodisperse, micrometer-sized hollow particles obtained by emulsion templating. Monodisperse silicone oil droplets were prepared by hydrolysis and polymerization of dimethylsiloxane monomer and incorporated in a solid shell using tetraethoxysilane. Hollow shells were obtained by dissolution of the core. We developed a facile fabrication method in which simply by tuning the thickness of the shells we can obtain different types of particles, which we designate as microspheres, microcapsules and microballoons.

2.1 INTRODUCTION

Synthesis of new types of colloidal particles represents an intense and rapidly developing field of research because of their potential use in a variety of applications. They are attractive as building blocks for ordered and complex materials, but also for chemical engineering, pharmaceutical and biological purposes. Among them, hollow colloidal particles represent a distinct class of colloids with additional applications in molecular transport, encapsulation, [27,44] controlled storage and release, [45, 46] catalysis, [47] coatings, and manufacturing of highly porous materials.

The procedure to make hollow systems usually involves preparation of core-shell particles, followed by the removal of the cores. Such hybrid particles can often be prepared by controlled precipitation of inorganic precursors onto the core particles. A different approach is to deposit small particles of the coating material on the cores. This is done, for example, in the layer-by-layer technique, in which case successive layers of anionic particles were deposited, alternated by layers of cationic polymer. [25, 48, 49] A variety of templating agents has been used in synthesis of hollow spheres: latex, [3,25,41] silica, [33, 42,50,51] gold [43] or zinc sulfide colloidal particles. [52] If desired, the template can be removed by dissolution of the core (in the case of silica, gold or zinc sulfide), or heating (for the latex cores). Because of limitations related to their polydispersity or difficulties concerning the coating procedures, a considerably smaller number of methods have used liquid cores as templates for the coating. These were either emulsion droplets, [53–55] or vesicles. [56–59] Depending on the type of desired coating, the resulting hollow shells have been made of very diverse materials, from silica, [25, 53–55, 58, 60] gold, [42, 61] titania, [41] to organic polymers, [33,43,50,51,57,62] polyelectrolytes, [59] and their hybrids. [40] Composite particles of high-molecular weight silicone oil and silica were made, but without a core-shell structure. [63]

In this Chapter we will describe the synthesis of new types of micrometer-sized hollow particles obtained by an emulsion templating technique. These results have been published in Ref. [64]. Our method brings important advantages over other techniques. First of all, the liquid cores can be removed under much more benign conditions than solid cores, namely lower temperatures and ordinary solvents like ethanol. Furthermore, simply by tuning the thickness of the shells we can obtain different types of particles, which makes them suitable for various applications. Moreover, by using emulsion droplets as templates this technique can be useful to incorporate functional oils or oil-soluble compounds inside the particles. An important advantage of our technique is that we use a facile synthesis method which leads to monodisperse particles in the micrometer range.

2.2 EXPERIMENTAL SECTION

2.2.1 MATERIALS

Dimethyldiethoxysilane (DMDES, $\geq$97.0 %) and tetraethoxysilane (TEOS, $\geq$98.0 %) were obtained from Fluka. Ammonia (29.7 wt% NH_3) and ethanol (absolute alcohol, analytical grade) were purchased from Merck. All chemicals were used as received. De-mineralized water was used in all described reactions and also for the cleaning of glassware.

2.2.2 PARTICLE SYNTHESIS

The hollow particles were synthesized using an emulsion-templating technique. The two-step fabrication scheme was as follows: silicone oil droplets were first prepared and used as templates for the encapsulation with solid shells. The liquid cores were finally removed by transferring the particles to ethanol. Reactions were performed at room temperature.

Oil droplets. In the first reaction step, monodisperse, stable oil-in-water emulsion droplets, surfactant free, were prepared by hydrolysis and polymerization of the di-functional silane monomer DMDES ($(CH_3)_2Si(OC_2H_5)_2$), following the method described by Vincent and coworkers. [22] The aqueous solutions were prepared using between 1 and 25 volume percent of ammonia (final concentrations of NH_3 between 0.159 M and 3.967 M). Different amounts of monomer, in the range 1 to 6 volume percent were added, followed by vigorously mixing of the reagents for a few minutes. Different methods of mixing were used: vigorous shaking by hand for 2 minutes, continuous or intermittent, lab-minishaker (MS2 minishaker from IKA) for 4 minutes at 2500 rpm, vigorous shaking by hand for 30 s followed by 5 minutes of sonication (using a Bransonic 8510 Ultrasonic Cleaner, at 44 kHz). The emulsion droplets already formed within a few hours, but they were allowed to grow for at least 24 hours before the coating step. The emulsions were left without stirring during droplet growth.

Hollow particles. The encapsulation of the oil droplets with a solid shell was achieved by using a modified version of the classical Stöber procedure [5]. A total of 0.018 M TEOS ($Si(OC_2H_5)_4$) was added to the as prepared emulsion in five steps (5 min. between steps) using an Eppendorf pipette, under magnetic stirring. The coating was started 24, 48 or 72 hours after the preparation of the oil droplets began, in order to obtain different thicknesses of shells. The particles were allowed to complete the shell growth for three days. Finally, they were centrifuged and re-dispersed in ethanol which was found to penetrate the shells and to dissolve the oil.

2.2.3 PARTICLE CHARACTERIZATION

Static light scattering (SLS). The size and polydispersity of the oil droplets and the thickness of the coating were determined from static light scattering (SLS) measurements, performed with home-built equipment using a He-Ne laser as light source (632.8 nm, 10 mW). The measurements were performed on dilute suspensions in de-mineralized water for the oil droplets and the coated droplets and in ethanol for the hollow shells. The angular distribution of the scattered light was measured at scattering angles in the range $19° \leq \theta \leq 135°$ relative to the transmitted beam, with a photomultiplier tube mounted on a turntable goniometer. The data were plotted against the scattering vector $k = 4\pi n sin(\theta/2)/\lambda$, where n is the solvent refractive index and λ the wavelength in vacuum. By comparing the scattering profiles with theoretical ones calculated with the full Mie solution for the scattering factor, [65] the radius and polydispersity were determined. The polydispersity, defined as the standard deviation of the particle size distribution divided by the mean value, represents actually the upper limit of the particles polydispersity and it is usually slightly higher compared to the value obtained from TEM image analysis. The values for the refractive indices used to fit the experimental data were 1.394 for the oil droplets (corresponding to low molecular weight silicone oil [66]), 1.43 for the solid shells (found by matching their refractive index with dimethylformamide (DMF) which has a refractive index of ≈ 1.43), 1.333 for water and 1.361 for the ethanol.

Transmission electron microscopy (TEM). The morphology of the different types of shells, after drying, was studied with a Philips Tecnai 12 microscope with an accelerating voltage of 120 keV. Samples for TEM were prepared by dipping copper 300 mesh-carrier grids covered with carbon-coated Formvar films into dilute suspensions.

Scanning electron microscopy (SEM). SEM was also used to study the uniformity of the hollow shells. The micrographs were obtained with a Philips XL 30 FEG scanning electron microscope and the samples were prepared by drying a drop of concentrated particle suspension on a glass slide.

Energy dispersive X-ray spectroscopy (EDX). The hollow structure of the shells was evidenced by performing EDX measurements on a Philips Tecnai 20F high resolution microscope operated at 200 keV, in scanning mode (STEM). The same type of samples as for TEM were used.

2.3 RESULTS AND DISCUSSION

The fabrication scheme for the emulsion-templating approach consists, as we described in the synthesis section, of two steps: the preparation of the oil droplets and their encapsulation by a solid shell. Before the coating started, the size and polydispersity of the oil droplets was determined by comparing their scattering profiles with theoretical ones calculated using the full Mie solution for the scattering form factors. [65] Our droplets were highly monodisperse for emulsion standards, as is shown by the many well-defined minima in the SLS profiles for the oil droplets in Fig.2.2, 2.4 and 2.8. The positions of the minima in the scattering curves gives the size of the droplets, whereas the polydispersity affects the depth of the minima: the lower the polydispersity, the deeper the minima. When fitting the experimental points, the most accurate value for the size is obtained by best fitting the first or the second most left minimum in the scattering profile, while the most accurate polydispersity is given by fitting the depth of the most right one.

The coating was achieved by hydrolysis and condensation of tetraethoxysilane, which was added to as prepared emulsions during magnetic stirring, in five steps (5 minutes between steps). The thickness of the coating could be measured from the increase in size after the encapsulation, using SLS. The minima in the scattering curves shift to the left with increasing size of the particles, therefore, by assuming the core size to be the same as before coating, the locations of these minima make possible a detailed comparison with theory, which allows us to obtain the thickness of the shell (Fig.2.2). Moreover, after the exchange of the cores with ethanol, the SLS curves can be fitted well considering the core size to be the same, only this time the core-shell particles are filled with ethanol (Fig.2.4, 2.8). Alternatively, TEM was used for the same investigations and its results were in relatively good agreement with those of the SLS analysis. However, a shrinkage of the particles was determined by TEM, as seen in Table 2.3, which is not unusual, considering that the SLS values were obtained for particles in suspension. Surprisingly, we found that the thickness of the coating did not depend on the amount of TEOS added. Instead, the time elapsed between the beginning of the emulsion preparation and the addition of TEOS was found to be the decisive factor in the final thickness of the shell, with the thickness increasing as TEOS was added sooner. Moreover, the thickness of the coating often exceeded the maximum thickness expected from the amount of TEOS used: when the encapsulation step was started between 24 and 48 hours after the beginning of the emulsion preparation, the expected value for the shell thickness based on the amount of TEOS added, represented only 10 to 20 % of the shell thickness measured with SLS. By monitoring the size and polydispersity of the oil droplets we established that the reaction for the formation of the oil droplets is relatively slow, the droplets taking about three days to reach their final size despite the fact that they are already formed within a few hours. This increase in size of the oil droplets suggests a slow polymerization of the hydrolyzed DMDES monomer and gives us another possibility of choosing the desired size for the templates. Apparently, the un-reacted DMDES monomer still present in the emulsion during the encapsulation process contributes significantly to the shell growth. For a given size of the droplets, the more time elapses between the

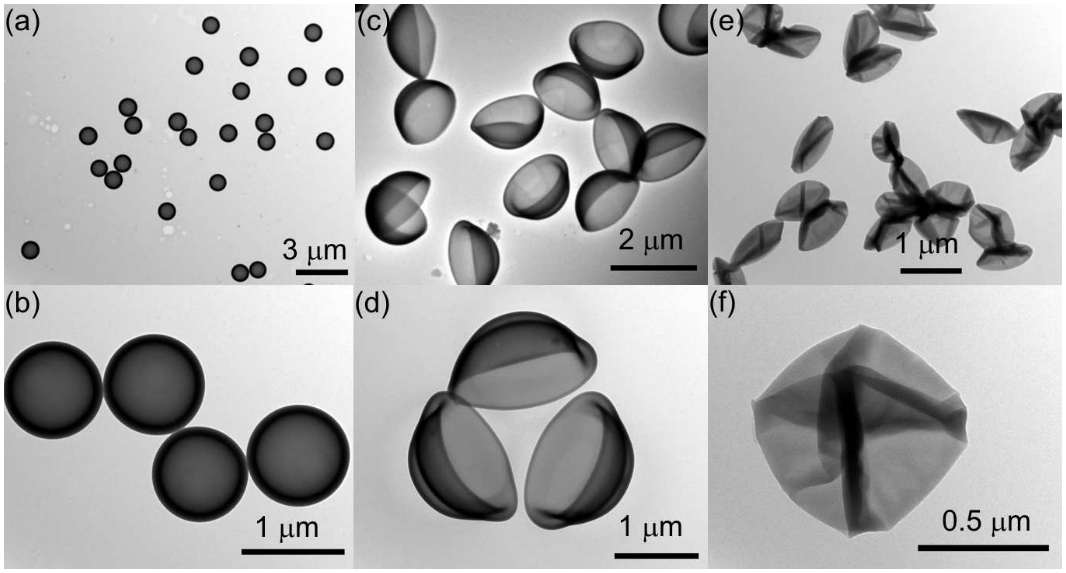

Figure 2.1: *TEM micrographs of hollow particles:(a) microspheres (sample Ss1, core radius 420 nm, shell thickness 150 nm, 7.5 % polydispersity), (b) capsules (sample Sc1, core radius 795 nm, shell thickness 150 nm, 3 % polydispersity), (c) microballoons (sample Sb1, core radius 430 nm, shell thickness 7 nm, 8 % polydispersity). The size and polydispersity obtained from SLS.*

droplet formation and encapsulation, the less monomer there is left and the thinner the resulting shell.

Our approach gives us the opportunity to obtain different hollow spheres. Based on the way in which the particles collapse upon drying, we distinguish three types of hollow spheres: microspheres, microcapsules and microballoons. Typical TEM images of these particles are shown in Fig.2.1. The different spheres were formed when the time between addition of DMDES and TEOS was 24 h, 48 h and 72 h, respectively. The microspheres remain un-deformed as a result of drying; the microcapsules, more flexible and deformable, collapse, forming hemispherical, double-walled caps, while the microballoons have a crumpled appearance. The deformation took place upon drying a sample for TEM. In solution, all coated droplets were found to remain spherical. This was seen by optical microscopy and from the fact that the SLS data could be fitted well with the theory for a (coated) sphere.

The microspheres (Fig.2.1 a,b) were obtained by adding 0.018 M TEOS, under magnetic stirring, to 200 mL of emulsion prepared 24 hours earlier from 1 % v/v DMDES and 10 % v/v ammonia in water at room temperature. For the microcapsules (Fig.2.1 c,d), oil droplets synthesized using the same concentrations of monomer and ammonia (but in 400 mL total volume of emulsion) were coated with a solid shell by adding 0.018 M TEOS after 48 hours since the emulsion preparation. In both cases (microspheres and microcapsules), the shell was allowed to grow for three days after the addition of TEOS. This was necessary because as mentioned earlier, the monomer contributes significantly to the shell thickness and its polymerization was found to be rather slow, as will be discussed in Chapter 3. The third type of particles, microballoons, were obtained by coating oil droplets (prepared in 20 mL emulsion, 3.5 % v/v DMDES and 10 % v/v ammonia) with a solid shell by adding 0.018 M TEOS after 72 hours after their preparation. Alternatively, this type of particles can be obtained also by adding TEOS and ammonia (0.159 M) to the emulsions which were first dialyzed (in order to remove the excess DMDES). The three types of particles are described in more detail in the following sections.

2.3.1 MICROBALLOONS

Table 2.1 gives examples of coated oil droplets with thin solid shells (microballoons), for different size of the templates, as determined by SLS. Typically, the shell thickness for this category of particles never exceeds 30 nm, while we varied the radius of the oil droplets used as templates between 400 nm and 1500 nm. The scattering profile of the oil droplets before and after coating, is illustrated in Fig.2.2. The deep minima in the scattering curves occur only for spherical and monodisperse particles; for non-spherical particles, the average over all orientations, each with a minimum at a different scattering vector, will average the minima away.

TEM micrographs of microballoons (Fig.2.3) show indeed an extremely thin shell, but the thickness cannot be determined from these type of images because of the collapsed shells. From this we conclude that the microballoons are spherical when in suspension and that they deform when dried.

The microballoons are quite interesting because of their potential use in fabrication of microcellular structures, as will be shown in Chapter 6. Due to their very thin shells, when packed and dried, they form highly porous materials with a large volume of voids.

Table 2.1: *Size and polydispersity of microballoons as determined by SLS; R−core radius , d−shell thickness, δ−polydispersity and R_t−total radius of the particle.*

Sample	R(nm)	d (nm)	δ(%)	R_t(nm)	d/R_t
Sb1	430	7	8	437	0.016
Sb2	820	10	3.5	830	0.012
Sb3	1110	30	3	1140	0.026
Sb4	500	15	8	515	0.029
Sb5	710	10	4	720	0.013
Sb6	770	10	5	780	0.012

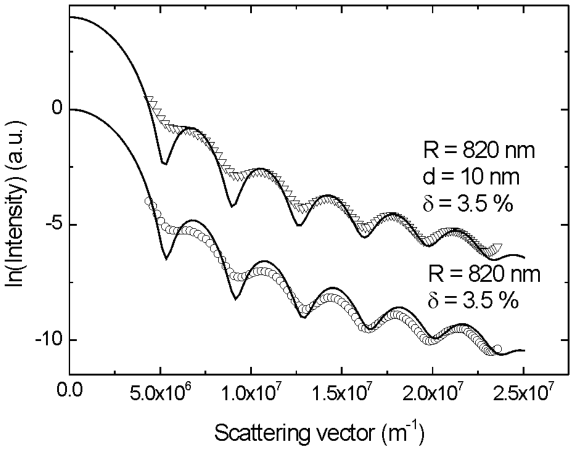

Figure 2.2: *SLS experimental data (scatter points) fitted to theoretical calculations using the full Mie solution of the form factor (lines) for sample Sb2 (microballoons): circles (bottom) represents data from the oil droplets in water, triangles (top) coated oil droplets in water.*

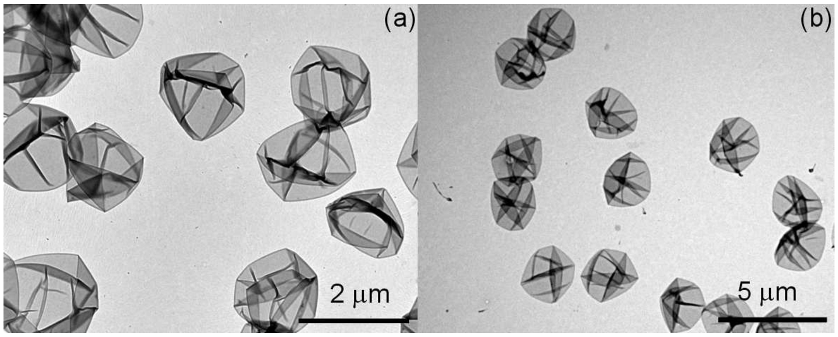

Figure 2.3: *TEM micrographs of microballoons: (a) Sample Sb3, R = 1110 nm, d = 30 nm, δ = 3 %; (b) Sample Sb2, R = 820 nm, d = 10 nm, δ = 3.5 %. Size and polydispersity obtained from SLS.*

2.3.2 MICROCAPSULES

In the case of microcapsules, both the core radius and the thickness of the coating can vary over a relatively large region: the shells obtained have thicknesses between 40 nm and 300 nm, for radii of the droplets used as templates from 300 nm up to 850 nm, as shown in Table 2.2. In Fig.2.4, the minima in the SLS curves obtained for the hollow capsules in ethanol show that these particles maintain their spherical shape in solution, after the oil from the core is removed, being filled in this case with the solvent. Although spherical in solution, after drying, the microcapsules collapse forming hemispherical caps,

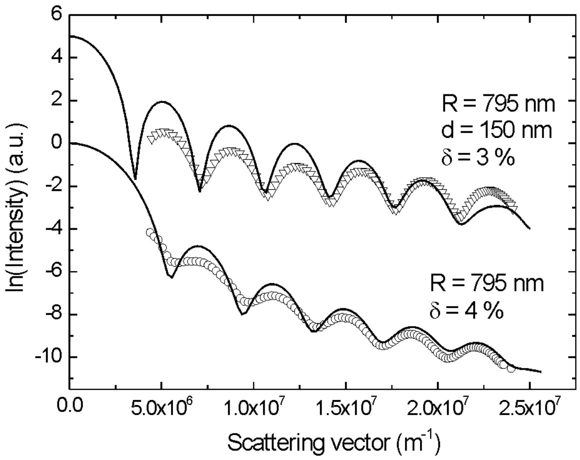

Figure 2.4: *SLS experimental data (scatter points) fitted to theoretical Mie solution (lines) for sample Sc1 (microcapsules): circles (bottom) represents data from the oil droplets in water, triangles (top) capsules in ethanol, filled with the solvent.*

as seen in the TEM (Fig.2.5) or in the SEM (Fig.2.6b) images. This type of deformation is not induced by the vacuum of the TEM but by drying; the same shapes were observed also with a light microscope, in air.

The radii of the templates are not very different in the case of microballoons compared to microcapsules, for the latter shells are much thicker relative to the size of the cores and therefore the difference in shapes after drying. Because of their high uniformity in size, these hollow shells are able to form colloidal crystals when they are in solution, giving rise to colorful Bragg reflections, as shown in Fig.2.6a. However, they collapse when dried, and a typical example of dried "crystal" of microcapsules is presented in Fig.2.6b.

Table 2.2: *Size and polydispersity of microcapsules as determined by SLS; $R-$core radius , $d-$shell thickness, $\delta-$polydispersity and R_t-total radius of the particle.*

Sample	R(nm)	d (nm)	δ(%)	R_t(nm)	d/R_t
Sc1	795	150	3	945	0.158
Sc2	440	130	4.5	570	0.228
Sc3	500	150	6	650	0.230
Sc4	850	230	5	1080	0.213
Sc5	830	300	5	1170	0.256
Sc6	580	210	5	790	0.265
Sc7	390	40	7	430	0.093

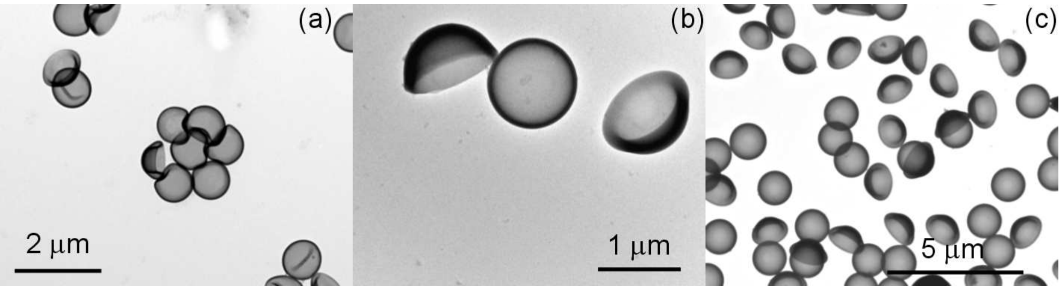

Figure 2.5: *TEM micrographs of microcapsules: (a) Sample Sc2, R = 440 nm, d = 130 nm, $\delta = 4.5$ %; (b) Sample Sc3, R = 500 nm, d = 150 nm, $\delta = 6$ %; (c) Sample Sc6, R = 580 nm, d = 210 nm, $\delta = 5$ %.*

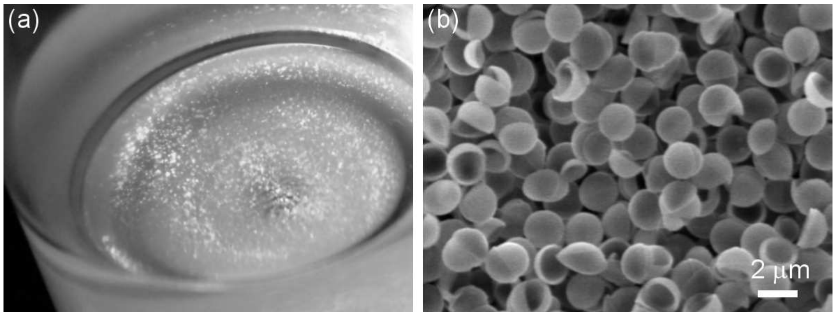

Figure 2.6: *(a) Photograph of a crystal of capsules sedimented in ethanol (sample Sc1, R = 795 nm, d = 150 nm, $\delta = 3$ %). (b) SEM image of a dried crystal of microcapsules obtained from the same sample Sc1.*

As illustrated by their deformation in a dried state, the microcapsules appear to have interesting elastic properties (see Chapter 5), which together with their shell permeability, makes them good candidates for encapsulation. Moreover, when re-suspended in ethanol, after they were dried, the deformed capsules maintain their hemispherical cap-like shape, forming a suspension of non-aggregated, single particles. As a result, they can be used for studying self-assembly of non-spherical colloidal particles.

2.3.3 Microspheres

The hollow microspheres are characterized by shell thicknesses in the same range as for microcapsules, but the ratio between the shell thickness and the total radius of the particle is slightly higher than in the previous case (Table 2.3). Consequently, these shells will maintain their spherical shape even after drying, as shown by the TEM micrographs in Fig.2.7. Fig.2.8 illustrates the scattering curve for the oil droplets used as templates and for the resulting microspheres in ethanol, from which we determined the size and polydispersity of our particles. Additionally, because these shells do not collapse when dried,

Table 2.3: *Size and polydispersity of microspheres as determined by SLS and TEM; R−core radius, d−shell thickness , δ−polydispersity and R_t−total radius of the particle.*

Sample	R(nm)	d (nm)	δ(%)	R_t(nm)	d/R_t	$R_{t,TEM}$(nm)	δ_{TEM}(%)
Ss1	420	150	7.5	570	0.263	535	5.7
Ss2	455	210	5.5	665	0.315	590	6.9
Ss3	500	220	5	720	0.305	603	5
Ss4	327	230	8.5	557	0.412	497	6
Ss5	445	235	6	680	0.345	658	4.7

their size and polydispersity can be determined also by image analysis of the TEM micrographs. The values for the total radii from TEM were found to be in good agreement with those obtained from SLS, with a shrinkage in the TEM of $\approx 6-13\%$ relative to the value obtained using SLS (Table 2.3).

The EDX line scans performed on microspheres revealed the hollow structure of the particles, as well as the shell composition, rich in carbon because of the DMDES contribution. An example of a line scan is presented in Fig.2.9.

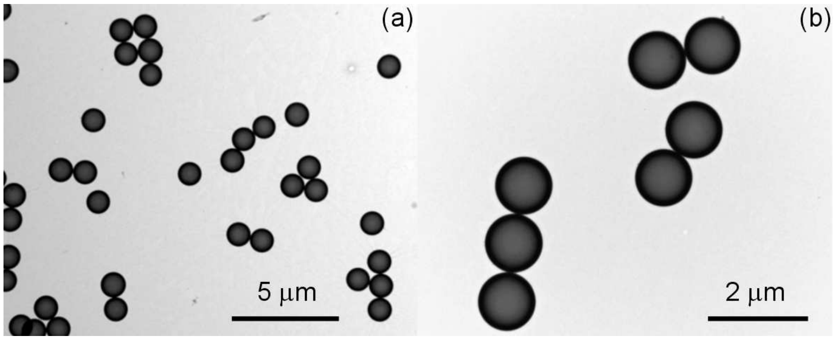

Figure 2.7: *TEM micrographs of hollow microspheres:(a) Sample Ss2, R = 445 nm, d = 210 nm, δ = 5.5 %; (b) Sample Ss3, R = 500 nm, d = 220 nm, δ = 5 %. Size and polydispersity obtained from SLS.*

The microspheres can form dry colloidal crystals similar to those of solid silica spheres. An example of a crystal of hollow microspheres is given in Fig.2.10 and it was obtained by drying a suspension of hollow particles in ethanol, on a microscope cover slip. Because of their ability to form ordered structures which are not destroyed after drying, we are interested in these particles as precursors for crystals of hollow spheres and also as doping agents in crystals of other particles.

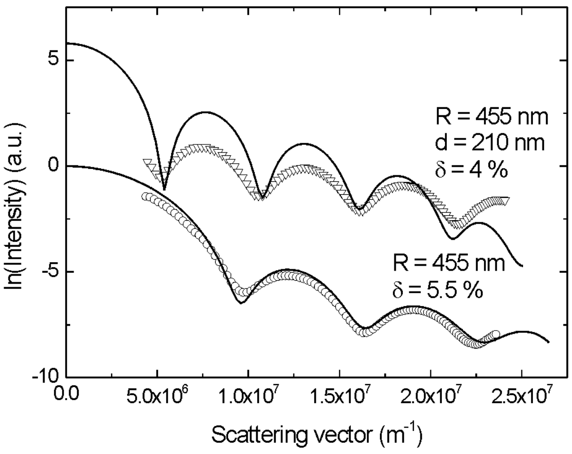

Figure 2.8: *SLS experimental data (scatter points) fitted to theoretical Mie solution (lines) for sample Ss2 (microspheres): circles (bottom) represents data from the oil droplets in water, triangles (top) shells filled with ethanol, in ethanol.*

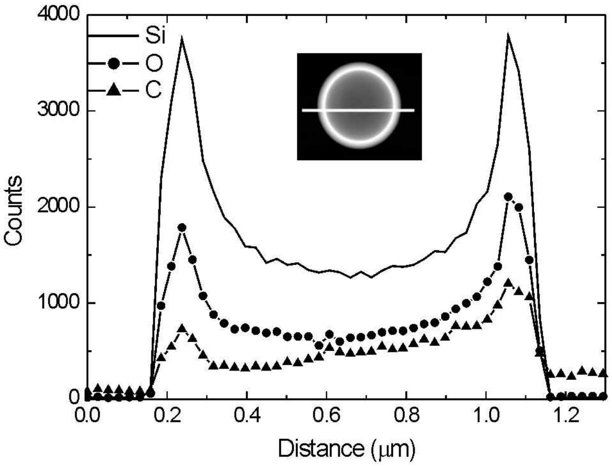

Figure 2.9: *EDX line graph acquired in STEM mode, from a line scan (white line) through the microsphere shown in the inset (TEM dark field image).*

2.4 Conclusions

We demonstrated that emulsion templating can be successfully used to prepare monodisperse, micrometer-sized, hollow particles. Our technique allows us to prepare variable shell thicknesses, from 5 − 300 nm in a simple two-step process. By tuning the ratio between the shell thickness and the particle radius,

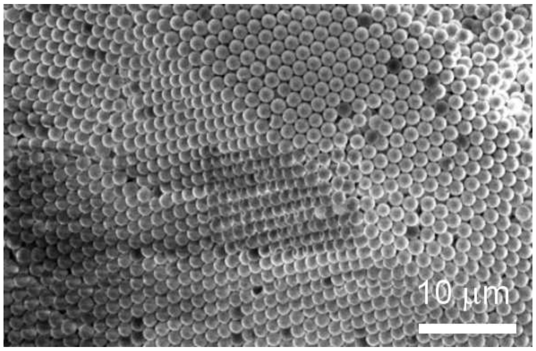

Figure 2.10: *SEM image of a dried crystal of hollow microspheres (sample Ss1, R = 420 nm, d = 150 nm, δ = 8 %;*

three different types of particles can be obtained, with different properties. The monodispersity of our hollow shells may have applications in making ordered materials, either crystalline or porous microcellular structures. Additionally, the permeability and elasticity of the hollow shells might be important for using them in micro-encapsulation or micro-reactors.

3 CHARACTERIZATION AND FORMATION OF MICROSPHERES, MICROCAPSULES AND MICROBALLOONS

We investigated in detail both the silicone oil droplets used as templates and the resulting hollow colloidal particles obtained by the emulsion templating technique we developed. The reaction course of the oil droplets was investigated using light scattering and ^{29}Si solution NMR and the hollow shells were characterized by electron microscopy and light scattering. Depending on the ratio of shell thickness to particle radius, three types of hollow shells can be distinguished depending on the way in which they buckle upon drying. Details on the composition of the shell material were obtained from energy dispersive X-ray analysis and ^{29}Si solid state NMR, showing that the shell consists of a hybrid cross-linked network of silicate and siloxane units. Confocal fluorescence microscopy was used to show that the shells are permeable to small dye molecules.

3.1 Introduction

The fabrication of hollow-shell particles has been the subject of many recent publications in the field of materials science. [3, 25, 27, 33, 40–63] Due to their wide range of applications, the control over synthesis and modification of hollow spheres is of great importance in building new classes of colloids.

We described in Chapter 2 a facile method for preparing monodisperse, hollow colloidal particles based on an emulsion templating technique. As we have shown, the shell thickness of the particle is strongly influenced by the amount of hydrolyzed dimethyldiethoxysilane (DMDES) present in the sample at the beginning of the coating step.

Therefore, in this chapter we first want to understand the formation of the oil droplets in order to explain the formation of the solid shells. This will be done using static light scattering to follow the growth of the oil droplets in time and solution ^{29}Si NMR to determine their chemical composition. Moreover, we discuss how the size of the templates and the thickness of the coating influence the type of particles obtained and their deformability. We present the most relevant characteristics of the hollow shells, such as density and composition of the shell material, which was determined using both solid state ^{29}Si NMR and energy dispersive X-ray investigations. In addition, we show the possibility of incorporating fluorescent dye molecules in the shell material, but also an alternative method to achieve fluorescent particles without having dyes chemically bonded into the shells. The permeability of the shells for small molecules is also illustrated in this chapter, results which have been published in Ref. [67].

3.2 Experimental section

3.2.1 Materials

Dimethyldiethoxysilane (DMDES, $\geq$97.0 %) and tetraethoxysilane (TEOS, $\geq$98.0 %) were obtained from Fluka. 3-aminopropyl-triethoxysilane (APS, $\geq$99.0 %), fluorescein-isothiocyanate (FITC) and rhodamine B-isothiocyanate (RITC) were purchased from Aldrich and ammonia (29.7 % w/w NH_3) and ethanol (absolute alcohol, analytical grade) from Merck. All chemicals were used as received. De-mineralized water was used in all described reactions and also for the cleaning of glassware.

3.2.2 Synthesis

The oil droplets and the non-fluorescent hollow shells were prepared using the procedures described in Chapter 2. The fluorescent shells were obtained by incorporating the RITC dye into the shell during the coating step, using a modified version of the method introduced by van Blaaderen. [11] RITC was first covalently attached to the coupling agent APS by slowly stirring a solution containing 6.5 mg dye and 37.8 mg APS in 1 mL anhydrous ethanol. The reaction was allowed to proceed for at least 12 hours by slowly stirring the dye mixture in the dark. 0.25 mL of the dye solution was added together with 0.018 M TEOS to 400 mL emulsion, during the encapsulation step, after which the procedure described for the hollow particles was followed. Fluorescently labeled shells were obtained also simply by adsorption of RITC molecules at the surface of the particles. This was done by dispersing the particles in water or ethanol containing $\approx 4.4 \times 10^{-3}$ mg/mL RITC.

The growth of the second shell, fluorescently labeled, was obtained by starting with a 5.5 mL dilute suspension of microcapsules in ethanol (core radius 830 nm, shell thickness 300 nm, total shells weight ≈ 0.011 g), to which ammonia and water were added to final concentrations: 1.69 M NH_3 and 3.80 M H_2O. 0.036 M TEOS was added together with 0.007 mL dye mixture containing RITC, APS and ethanol, prepared as described above.

3.2.3 Characterization

The size and polydispersity of the oil droplets and the thickness of the coating were determined with static light scattering (SLS), as described in Chapter 2. In addition, for the experiments in which we determined the growth of the oil droplets in time, we took one or two droplets of emulsion every few hours and dispersed them in de-mineralized water, after which SLS curves were measured. The same procedure was used to determine the increase in shell thickness in time. In this case, every time a sample for SLS was taken, also a TEM grid was prepared in order to determine the type of particles obtained. For all samples, the morphology of the different types of shells after drying was analyzed with transmission electron microscopy (TEM). The elemental microanalysis of the shell material was obtained from energy dispersive X-ray spectroscopy (EDX).
Nuclear magnetic resonance (NMR). Solution ^{29}Si NMR and solid-state ^{29}Si NMR spectroscopy were used to obtain information about the silicon atoms bonded to different groups present in the silicone oil emulsions and in the shell material of hollow spheres, respectively. ^{29}Si NMR spectra in solution were recorded on a Varian Unity Inova spectrometer, at 59.62 MHz with a DEPT (Distortionless Enhancement by Polarization Transfer) technique. A value of 0.7 Hz for the Si-H coupling was used, and a θ pulse of 3 μs. The reference for the chemical shifts was tetramethylsilane (TMS), in $CDCl_3$ as solvent. Both samples from freshly prepared emulsion ($\approx$ 10 hours since preparation) and "old emulsion" ($\approx$ 4 days since preparation) were prepared by dissolving them in deuterated methanol. In the case of the old emulsion, the oil phase was first separated by centrifugation and the remaining water was removed using molecular sieves with a pore diameter of 4 Å. Solid-state ^{29}Si NMR spectra were recorded at 59.62 MHz on a Varian Unity Inova spectrometer

equipped with a 7 mm VT CP/MAS (CP-cross polarization, MAS-magic angle spinning). Samples were spun at 5000 Hz in zirconia rotors. Chemical shifts are given in parts per million (ppm), relative to tetramethylsilane; dodecamethylcyclohexasilane (δ = -42.0 ppm) was used as secondary chemical shift reference. In CP/MAS spectra, a contact time of 5 ms and a relaxation delay of 5 s were used. Spectra were averaged from 1616 FID's. For the solid-state measurements, hollow particles were used, the oil from the core having been removed with ethanol; the samples were dried in air, under a heating lamp, for 12 hours.

Sedimentation experiments The density of the shell material was determined from sedimentation experiments, performed in glass centrifugation tubes (9 cm long, 1 cm diameter), filled with relatively dilute suspension of hollow particles in ethanol. The sedimentation of the particles was followed in time for $\approx$ 3 days. In order to avoid errors due to the meniscus, the particles were let to sediment for $\approx$ 3 hours before we started measuring the sedimentation distances in time. The experiment was stopped before all the particles reached the bottom of the tube. From the sedimentation speed, we determined the density of the particles filled with ethanol and, assuming additivity of volumes, the density of the shell material.

Confocal microscopy. The fluorescently-labelled shells were imaged using an inverted Leica confocal scanning laser microscope (CSLM), type TCS-SP2. The microscope was operated in the fluorescence mode. The 543 nm line of a green He-Ne laser was used for excitation of the rhodamine-labeled particles. Measurements were performed with a 100x oil immersion objective (Leica) with a numerical aperture of 1.4 and a working distance of 100 μm. The samples were prepared by drying a drop of concentrated dispersion of fluorescent shells on a microscope cover slip of 0.15 mm thickness and 22 mm diameter.

The permeability of the shells was investigated using the following experiment: the bottom part of a small glass vial (1.7 mL volume) was replaced by a microscope cover slip (0.15 mm thickness and 22 mm diameter). The vial was filled with a suspension of capsule-like particles, non-fluorescent, which was first centrifuged and the solvent was replaced by ethanol, containing 0.725 mM FITC. The sample was imaged in fluorescence mode, excitation line 488 nm and a 63x oil immersion objective (Leica) with a numerical aperture of 1.4 was used.

3.3 Results and discussion

3.3.1 PDMS oil droplets

Low molecular weight polydimethylsiloxane (PDMS) silicone oil-in-water emulsion droplets were synthesized by the base-catalyzed hydrolysis and polymerization of DMDES. These emulsions do not contain a surfactant, but are charge stabilized. The method we use to prepare the emulsions yields monodisperse droplets, with radii in the range 0.6 to 2 μm and polydispersities between 3 and 8 %. The monomer DMDES is initially insoluble in water, but after a few minutes of mixing (1 - 4 min., depending on the method), a clear solution is obtained as a result of hydrolysis; within $\approx$ 1 hour, the solution starts to become milky, indicating the formation of droplets.

In order to determine which factors influence the oil droplets formation, we prepared emulsions by varying different parameters, such as the monomer and ammonia concentrations, the method of mixing and the temperature. We found that the droplet size hardly depended on the ammonia concentration in the range 1 - 25 % v/v (final concentrations 0.159 - 3.967 M NH_3). However, when we kept the monomer and ammonia concentrations constant, we observed a strong influence of the mixing procedure. For example, in preparations containing 1 % v/v DMDES and 1 % v/v ammonia (0.159 M NH_3) in 15 mL total volume of emulsion, we obtained oil droplets of 300 - 600 nm when we used vigorously shaking by hand (1 min.), about 700 nm for using a lab-minishaker (4 min., 2500 rpm), 300 - 400 nm for shaking by hand (30 s) followed by 5 minutes of sonication. The method of mixing has also a strong influence on the size of the droplets when the total volume of the sample is increased significantly, above 30 mL. When larger amounts of emulsions were needed (typically between 100 - 500 mL), the reagents were mixed by vigorously shaking by hand, for 2 minutes, continuously or intermittent. The size and polydispersity of the droplets obtained were in the same range as for smaller amounts of emulsions, but somewhat less reproducible because of the shaking procedure. In order to obtain reproducible results concerning the formation of the oil droplets, we settled on a 4 minutes shake on a lab-minishaker at 2500 rpm, which gave very good results.

3.3.2 Droplet growth

In one series of experiments, we prepared emulsions varying only the amount of monomer and ammonia used and keeping the rest of the parameters unchanged: 25 mL total volume of the emulsion prepared in a 50 mL glass vial using a lab-minishaker for 4 minutes at 2500 rpm. We used 1, 2, 3, 4 and 6 volume percent of monomer and the ammonia concentrations were taken equal to the concentrations of the monomer. By monitoring the radius of the

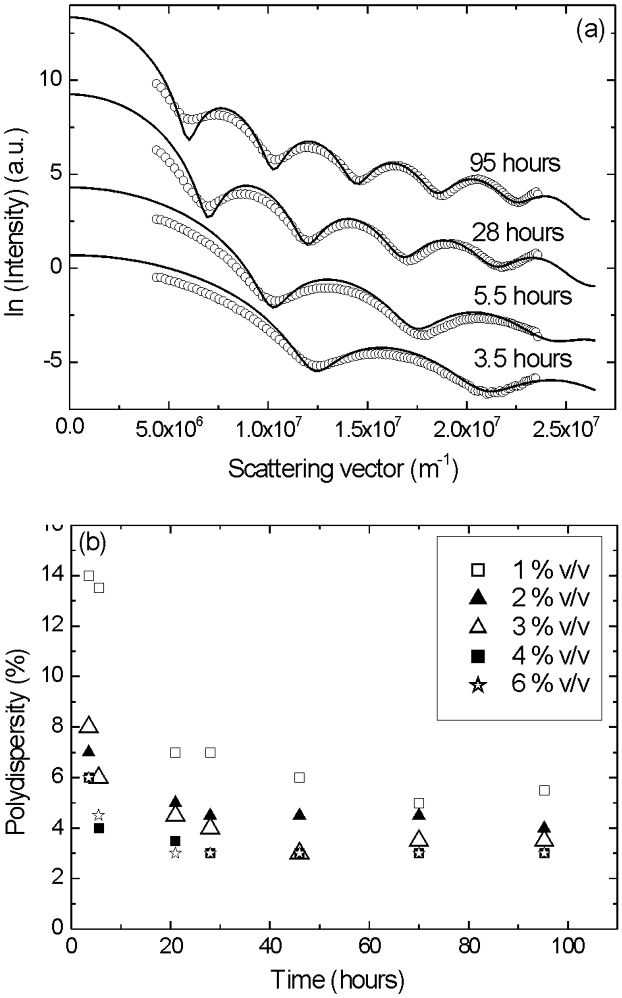

Figure 3.1: *(a) SLS experimental data (scatter) fitted by theoretical calculations with full Mie solution of the form factor (lines) for oil droplets prepared from 2 % v/v DMDES and 2 % v/v ammonia, for different times after preparation. The corresponding radius and polydispersities are as follows: $R = 350$ nm, $\delta = 7$ % after 3.5 hours, $R = 425$ nm, $\delta = 6$ % after 5.5 hours, $R = 625$ nm, $\delta = 4.5$ % after 28 hours and $R = 730$ nm, $\delta = 4$ % after 95 hours; (b) Polydispersity of the oil droplets as a function of time, as determined by SLS, for different DMDES concentrations.*

oil droplets over time with SLS (as exemplified in Fig.3.1a), we observed that even though they are already formed within a few hours, the droplets need about three to four days to reach their final size. After that, their size remains constant, although the larger droplets sometimes begin to coalesce after ≈ 2 weeks, a problem which can be solved by removing the ammonia by dialysis.

Fig.3.1 shows the experimental scattering data and the theoretical fit for the oil droplets prepared with 2 % v/v DMDES and 2 % v/v ammonia, for several time intervals after shaking. In Table 3.1 are shown representative results for

Table 3.1: *Size and polydispersity of oil droplets followed in time, as determined by SLS, for different volume percent of DMDES; R−droplet radius , δ−polydispersity.*

	1 % v/v		2 % v/v		3 % v/v		4 % v/v		6 % v/v	
time (h)	R (nm)	δ (%)	R (nm)	δ (%)	R (nm)	δ (%)	R (nm)	δ (%)	R (nm)	δ (%)
3.5	225	14	350	7	435	8	615	6	670	6
5.5	295	13.5	425	6	530	6	760	4	810	4.5
21	460	7	600	5	725	4.5	1055	3.5	1140	3
28	500	7	625	4.5	770	4	1070	3	1190	3
46	585	6	660	4.5	825	3	1120	3	1250	3
70	650	5	715	4.5	880	3.5	1200	3	1365	3
95	685	5.5	730	4	890	3.5	1250	3	1380	3

the growth of the average droplet size and they are plotted in Fig.3.2. The data can be fitted well by an equation of the form:

$$R(t)^3 = R_f^3[1 - \exp(-\frac{t}{t_1})] \tag{3.1}$$

where R_f is the final droplet radius. The growth rate of the oil droplets was given by $1/t_1$, where t_1 was used as a fitting parameter. The value for t_1 was found to be 27 ± 2 hours for all initial DMDES concentrations, except at 1 % v/v, where it was found to be 45 ± 4.5 hours. The fit parameters are listed in Table 3.2.

We calculated the volume of DMDES present in the sample at each time for which we measured the droplet radius, by making the following assumptions: we considered the number of droplets constant during the entire growth process, we used the value for the radius measured with SLS and we assumed total conversion of DMDES into PDMS. We found that the volume of DMDES changes over the course of the reaction according with:

$$V_{DMDES}(t) = V_{DMDES}(0)\exp(-\frac{t}{t_1}) \tag{3.2}$$

where $V_{DMDES}(0)$ represents the initial amount of monomer used to prepare the emulsions. The decreasing rate for the DMDES volume, $1/t_1$, was found to be the same as the growth rate for the oil droplets. These results suggest that there is a rate limiting step in the condensation reactions, which effectively makes droplet growth a first order process. Although the radius of the droplets is clearly influenced by the DMDES concentration, all the samples show the same behavior in time. The slow increase in droplet size suggests a slow polymerization of the hydrolyzed monomer. Therefore, the desired size of

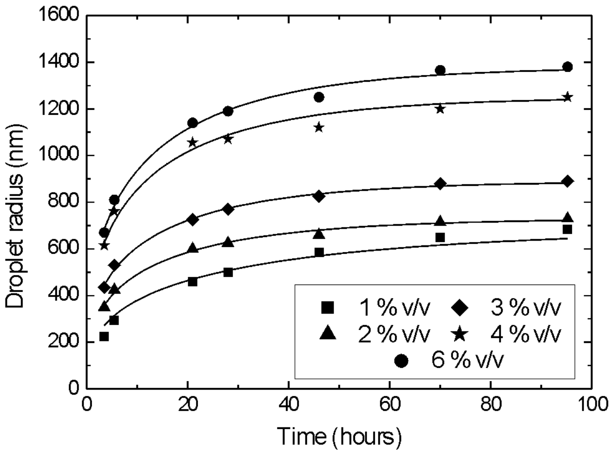

Figure 3.2: *Average droplet radius as a function of time, followed with SLS, for different DMDES concentrations; lines are drawn according to Eqn.3.1 with $1/t_1$ given in Table 3.2.*

the droplets can be obtained by choosing the amount of monomer used, by varying the time elapsed since the beginning of the synthesis, or both. For all samples it was observed that the polydispersity is higher in the first hours after the preparation, gradually decreased within 24 hours and hardly fluctuating afterwards (Fig.3.1b). These observations regarding the polydispersity exclude Oswald ripening as a possible late-stage growth mechanism. Consequently, in order to obtain monodisperse oil droplets (polydispersities better than 5 %), at least 20 hours should elapse after the mixing of the reagents.

Table 3.2: *Final droplet size and growth rate data for different volume percent of DMDES. R_f– final droplet radius as determined from SLS, t_1– fitting parameter obtained by fitting the experimental data (Table 3.1) with the Eqn.3.1 .*

DMDES (%v/v)	R_f (nm)	t_1 (hours)
1	685	45.5 ± 4.6
2	730	27.7 ± 1.2
3	890	26.2 ± 0.9
4	1250	26.0 ± 1.9
6	1380	26.8 ± 1.2

The droplet growth rate could be increased considerably by raising the temperature at which the reaction took place. The same volumes of emulsions were prepared as for the previous experiment, following the same procedure.

Table 3.3: *Size and polydispersity of oil droplets followed in time, as determined by SLS, for different volume percent of DMDES, at two different temperatures; R−droplet radius , δ−polydispersity.*

	2 % v/v (30°C)		4 % v/v (30°C)		2 % v/v (45°C)		4 % v/v (45°C)	
time (h)	R (nm)	δ (%)	R (nm)	δ (%)	R (nm)	δ (%)	R (nm)	δ (%)
1.25	340	8	495	8	380	6	740	5
3	450	8	670	6	450	6	930	4
5	530	6.5	800	6	520	6	1025	4
21.5	750	5	1100	3.5	640	6	1250	4
28.75	780	5	1130	3.5	-		-	
47.75	820	5	1230	3.5	-		-	

The concentrations for the monomer used were 2 % v/v and 4 % v/v, respectively. Again, the ammonia concentrations were chosen to be the same as for the monomer. At each concentration, two samples were prepared and kept at different temperatures during the entire experiment: 30 °C and 45 °C, respectively. The increase in size of the oil droplets was followed in time by taking samples for SLS and the same equation 3.1 was used to fit the data. The results are plotted in Fig.3.3 and compared with those obtained at room

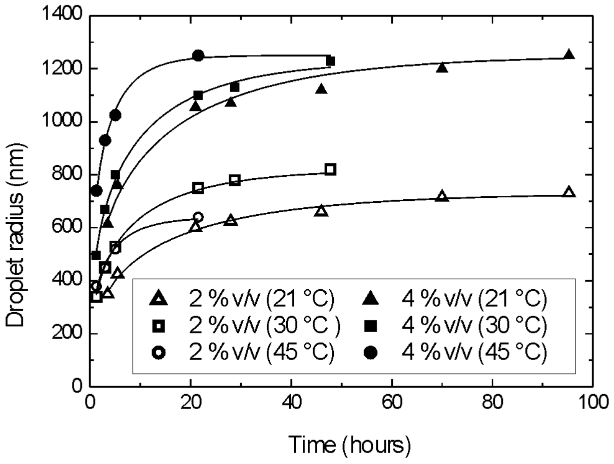

Figure 3.3: *Increase of the droplets radius followed in time, for two monomer concentrations, at three different temperatures (21 °C, 30 °C and 45 °C). Lines are drawn according to eqn.3.1. Data for sample at 21 °C are the same as presented in Fig.3.2a for the corresponding DMDES concentrations.*

Table 3.4: *Final droplet size and growth rate data for different volume percent of DMDES.* R_f- *final droplet radius as determined from SLS,* t_1- *fitting parameter obtained by fitting the experimental data (Table3.3) with the Eqn.3.1.*

DMDES (%v/v)	temperature (°C)	R_f (nm)	t_1 (hours)
2	30	820	15.8 ± 0.5
4	30	1230	16.9 ± 0.7
2	45	640	6.3 ± 0.4
4	45	1250	5.7 ± 0.2

temperature (21 °C). The values for the fitting parameter t_1 were found to be smaller for higher temperatures: $\approx 16 \pm 1$ hours for both samples prepared at 30 °C and $\approx 6 \pm 0.5$ hours for the samples prepared at 45 °C. This shows that the growth rates ($1/t_1$) increase with increasing temperature. However, the final size is not temperature dependent. Clearly, the hydrolyzed monomer polymerizes much faster at higher temperatures, but at the same time, the risk of coalescence increases considerably. This happened for samples prepared at 45 °C, already after $\approx$ 30 hours and for the ones prepared at 30 °C after $\approx$ 50 hours, when no more minima were observed in the static light scattering graphs.

3.3.3 SOLUTION ^{29}SI NMR OF PDMS EMULSIONS

The suitability of ^{29}Si NMR for determining the structure of silicon containing compounds is well established. Therefore, we used solution ^{29}Si NMR to obtain information about the hydrolysis and condensation products present in PDMS emulsions. This is necessary to understand the formation and properties of the shells that are formed in the second reaction step. Because of the slowness of the reaction, we investigated emulsions at two times after preparation: 10 hours old emulsions and emulsions for which the reaction was allowed to complete (4 days).

Figure 3.4a presents the spectrum for the 10 hours old emulsions, prepared with 5 % v/v DMDES and 5 % v/v ammonia. The presence of oil droplets in the sample was checked with SLS shortly before the NMR measurement; their radius was $\approx$ 870 nm. The sample used for the NMR was taken from the bulk of the oil-in-water emulsion in order to get information about all the components present in the solution and not only in the droplets. We were able to identify the resonance lines reported in earlier work [68, 69] on base-catalyzed polymerization of DMDES taking place in ethanolic solutions. Throughout this section, the usual D_{ij} notation [69] will be used, representing

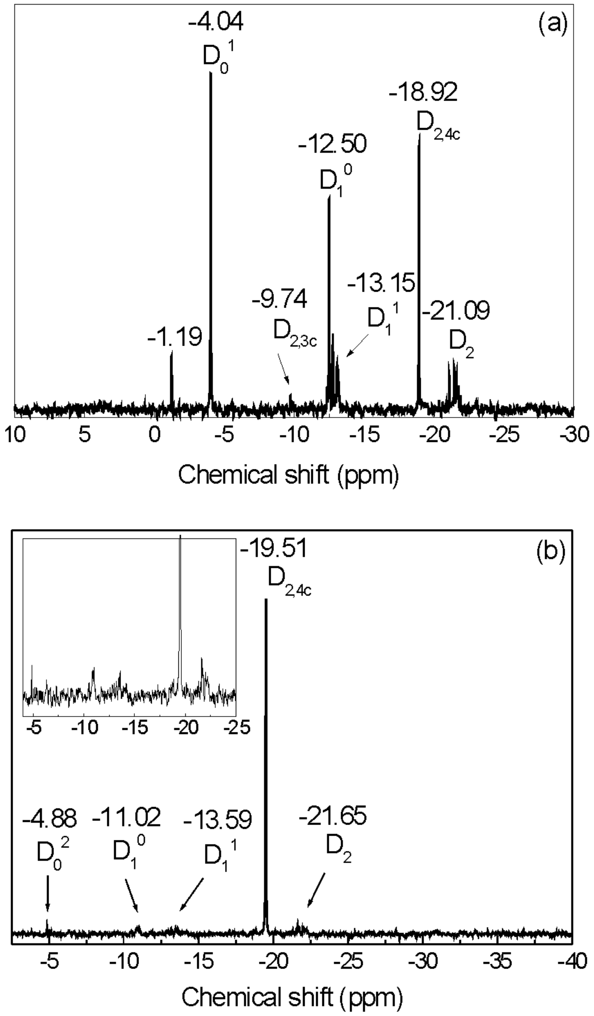

Figure 3.4: *Solution ^{29}Si NMR spectra for PDMS emulsions (a) 10 hours old, prepared from 5 % v/v DMDES and (b) isolated oil phase ≈ 4 days after preparation, prepared from 1 % v/v DMDES. The inset is a magnification. Subscripts in the peak assignments indicate the number of siloxane groups attached to the site, with "3c" and "4c" denoting sites in three- and four-membered silicon ring, respectively. Superscripts indicate the number of hydroxyl groups, the remaining groups being ethoxy groups.*

a site with i siloxane bonds and j hydroxyl groups:

$$D_i^j = (CH_3)_2Si(OC_2H_5)_{2-i-j}(OH)_j(O)_{i/2} \qquad (3.3)$$

The corresponding structures are presented in Fig.3.5. Although the emulsion was prepared 10 hours before the NMR spectrum was recorded, there is still a significant amount of monomer which is only hydrolyzed at one end (D_0^1), indicated by the strongest resonance in the spectrum at -4.04 ppm. Units

Table 3.5: *Assignment of ^{29}Si NMR signals of hydrolysis and condensation of DMDES in PDMS emulsions.*

10 hours old emulsion		4 days old emulsion	
Chemical shift (ppm)	Assignment	Chemical shift (ppm)	Assignment
-1.19	not assigned		
-4.04	D_0^1		
		-4.88	D_0^2
-9.74	$D_{2,3c}$		
-12.50	D_1^0	-11.02	D_1^0
-13.15	D_1^1	-13.59	D_1^1
-18.92	$D_{2,4c}$	-19.51	$D_{2,4c}$
-21.09	D_2	-21.65	D_2

having formed a single siloxane bond show up clearly at -12.50 ppm (D_1^0) and -13.15 ppm (D_1^1). The cyclic tetramer (four-membered silicon ring: $D_{2,4c}$), expected for this type of PDMS droplets, is evidenced by the line at -18.92 ppm. Also a small amount of cyclic trimer (three-membered silicon ring: $D_{2,3c}$) units appears at -9.74 ppm. The lines situated at ≈ -21.09 ppm correspond to the linear chains connected by two siloxane bonds (D_2). The fact that there are more lines in this region is probably due to the different positions that a unit can occupy in the chain. The line at -1.19 ppm could not be assigned.

Two important aspects are clearly evidenced by the components identified in our spectrum. Firstly, there is already PDMS oil formed 10 hours after the emulsion was prepared, indicated by the presence of $D_{2,4c}$, $D_{2,3c}$ and D_2 species; the oil is incorporated in the droplets, their presence being confirmed by SLS performed right before the NMR. Secondly, most of the DMDES is not yet polymerized, evidenced by the strong lines corresponding to D_0^1 and D_1^0. The oil droplets already present in the emulsion after 10 hours will grow further on account of the large amount of hydrolyzed monomer identified in the sample. This is consistent with the growth of the droplets observed with SLS and suports the hypothesis of a slow reaction mechanism indicated by the increase of the droplet size in time.

The ^{29}Si NMR spectrum for PDMS emulsions in their final stage is presented in Fig.3.4b. In this case, the oil droplets have been allowed to grow for four days, after which the oil phase was separated by centrifugation. Excess water was removed by using molecular sieves. The spectrum is clearly dominated by the line at -19.51 ppm corresponding to the cyclic tetramer ($D_{2,4c}$), known to be characteristic for this type of emulsions [22, 70]; also some linear chains (D_2) were identified by the resonance at -21.65 ppm. The initial DMDES was completely consumed by this time. Interestingly, a small amount

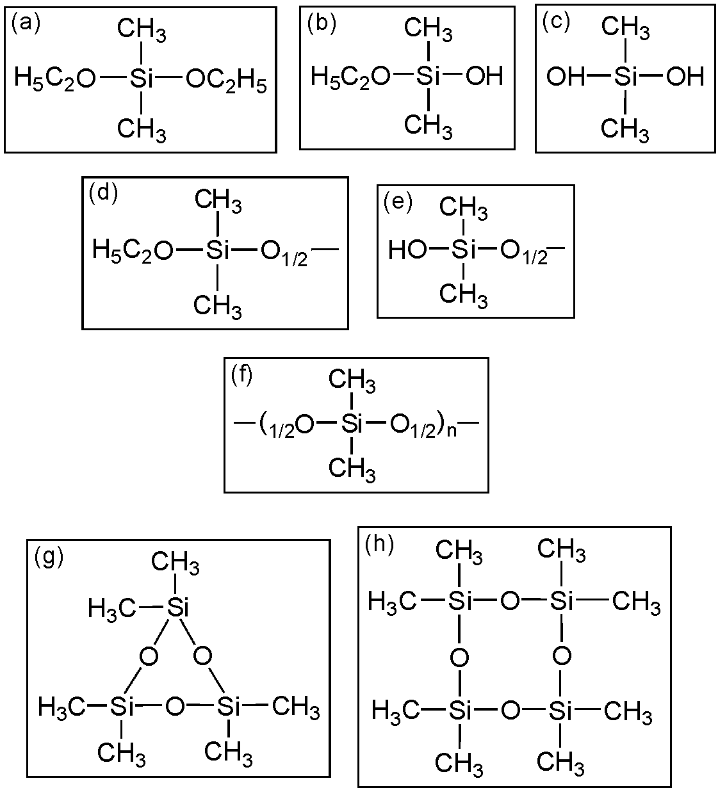

Figure 3.5: *Structural units of products obtained from DMDES hydrolysis and condensation: (a) un-hydrolyzed monomer* D_0^0, *(b) one-end hydrolyzed monomer* D_0^1, *(c) two-ends hydrolyzed monomer* D_0^2, *(d) units with one siloxane bond* D_1^0, *(e) two-ends hydrolyzed monomer with one siloxane bond* D_1^1, *(f) linear chains connected by two siloxane bonds* D_2, *(g) cyclic trimer* $D_{2,3c}$ *and (h) cyclic tetramer* $D_{2,4c}$.

of doubly hydrolyzed monomer is still present at -4.88 ppm (D_0^2). Furthermore, traces of hydrolyzed (-13.59 ppm, D_1^1) and un-hydrolyzed (-11.02 ppm, D_1^0) end groups were detected. These traces of incompletely condensed units will become part of the encapsulation material, as will be demonstrated later.

The studies on the droplet formation show that the silicone oil droplets prepared by hydrolysis and polymerization of DMDES are excellent candidates for templating with solid silica-based shells because of several reasons. First of all their monodispersity and size within the micrometer range makes them suitable templates for colloidal core-shell particles. Secondly, the slow reaction course of their formation allows us to choose the desired size of the cores and the amount of non-polymerized DMDES present in the sample when starting the coating step and which will copolymerize together with TEOS to form the solid shells. Finally, but equally important, the silicone oil obtained is of a low molecular weight, [70] which makes it easy to remove in the final step of the synthesis.

3.3.4 Shell thickness vs. core radius

The procedure described in Chapter 2 was used to obtain hollow colloidal particles with different sizes in the micrometer range. As we specified in section 2.3, we obtained three types of hollow spheres: microspheres, microcapsules and microballoons; they were distinguished based on the way they collapse upon drying (see Fig.2.1). We analyzed the shapes of the hollow shells in the TEM for different values for the core radius and shell thickness and we concluded that the important parameter in distinguishing the three types was the shell thickness (d) relative to the total radius (R_t) of the particle. This is seen from Fig.3.6 which gives an overview of the different types of particles for different values of d/R_t. For high values of this ratio, the hollow shells maintain their spherical shape after drying. This is the case for microspheres, situated in the upper part of the diagram in Fig.3.6, for values of $d/R_t > 0.23$. When the ratio becomes smaller, (0.05 - 0.25), we observed a collapse of the spherical shells, forming hemispherical caps. The lower region of the diagram contains the microballoons, even more deformable shells which collapse showing creases and folds, as a result of their very thin shells ($d/R_t < 0.05$). As can be seen in Fig.3.6, the boundary between two neighboring regions is not perfectly sharp. Close to the transition region, particles of both types can be found in the same sample. Fig.3.6 clearly shows that the main factor determining the shells deformation is the ratio d/R_t. This can be understood from the elasticity

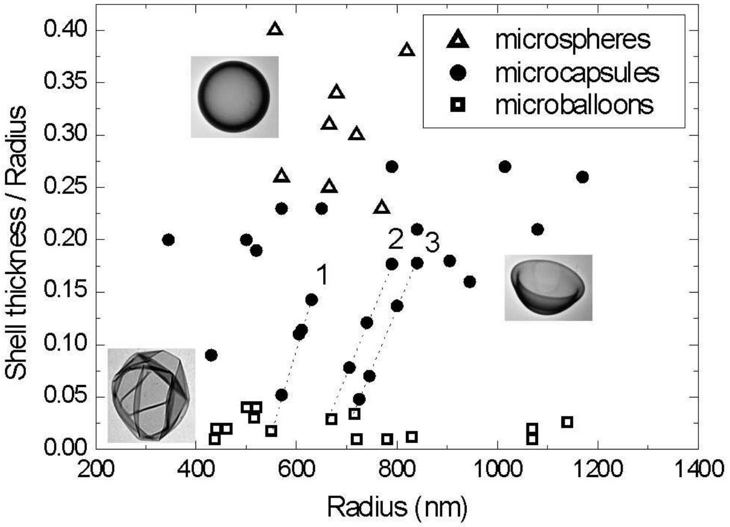

Figure 3.6: *Diagram showing the types of particles corresponding to different ratios between the shell thickness and the total radius of the particle: triangles-microspheres, circles-microcapsules and squares-microballoons. Lines 1, 2 and 3 connect points belonging to three samples for which the growth of the shell was followed in time.*

Table 3.6: *Increase in shell thickness followed in time, with SLS, for three different sizes of the template, corresponding to the samples presented in Fig.3.7: sample S1 540 nm, sample S2 650 nm and sample S3 690 nm; d−shell thickness.*

	Sample S1	Sample S2	Sample S3
time(h)	d(nm)	d(nm)	d(nm)
2.5	10	20	25
7	30	55	35
25	70	90	110
49	90	140	150

theory, which predicts that the pressure difference needed to buckle a hollow ball should be proportional to $(d/R_t)^2$. [71, 72]

A very interesting and potentially useful aspect of the Fig.3.6 is that for the same size of the template, different types of particles can be obtained by tuning the shell thickness. Conversely, for a given shell thickness the behavior of the particle can be varied by suitably choosing its radius. The growth of the shells corresponding to the lines 1, 2 and 3 from Fig.3.6 is presented in Fig.3.7a,b and Table 3.6 and it shows the flexibility of our method in tuning the types of hollow particles. Due to the slow condensation of the monomer, the shell thickness increases gradually and as a result, the particles' behavior will change continuously until the growth is completed. Consequently, microballoon-like particles are obtained after a few hours (≈ 2.5 hours), which evolve to microcapsules with thicker and thicker shell. Although the final shells were quite thick for both samples, the particles still behaved like capsules because the final ratio between the shell thickness and their total radius was just bellow 0.25 (see Fig.3.6). The reaction can be stopped at any time, depending on what type of particles are needed. This can be done either by dialysis against de-mineralized water, for ≈ 3 days or even less if the water is changed more often, or by centrifugation of the samples followed by exchange of the solvent. Consequently, we have two ways of obtaining the desired hollow shells: either by choosing the time when the coating is started and allowing the reaction to proceed to the end, or by monitoring the shell thickness and stopping the reaction when we are satisfied with the shell thickness. The final shell thickness depends on how far the polymerization has proceeded and not on the amount of TEOS added during the encapsulation step. The final shell becomes much thicker than expected based on TEOS alone. For example, the calculated shell thicknesses, only based on the amount of TEOS added, for the samples presented in Table 3.6 are as follows: 10.7 nm for sample S1, 12.9 nm for sample S2 and 13.7 nm for sample S3 (only ≈ 8 - 11 % of the actual shell thickness).

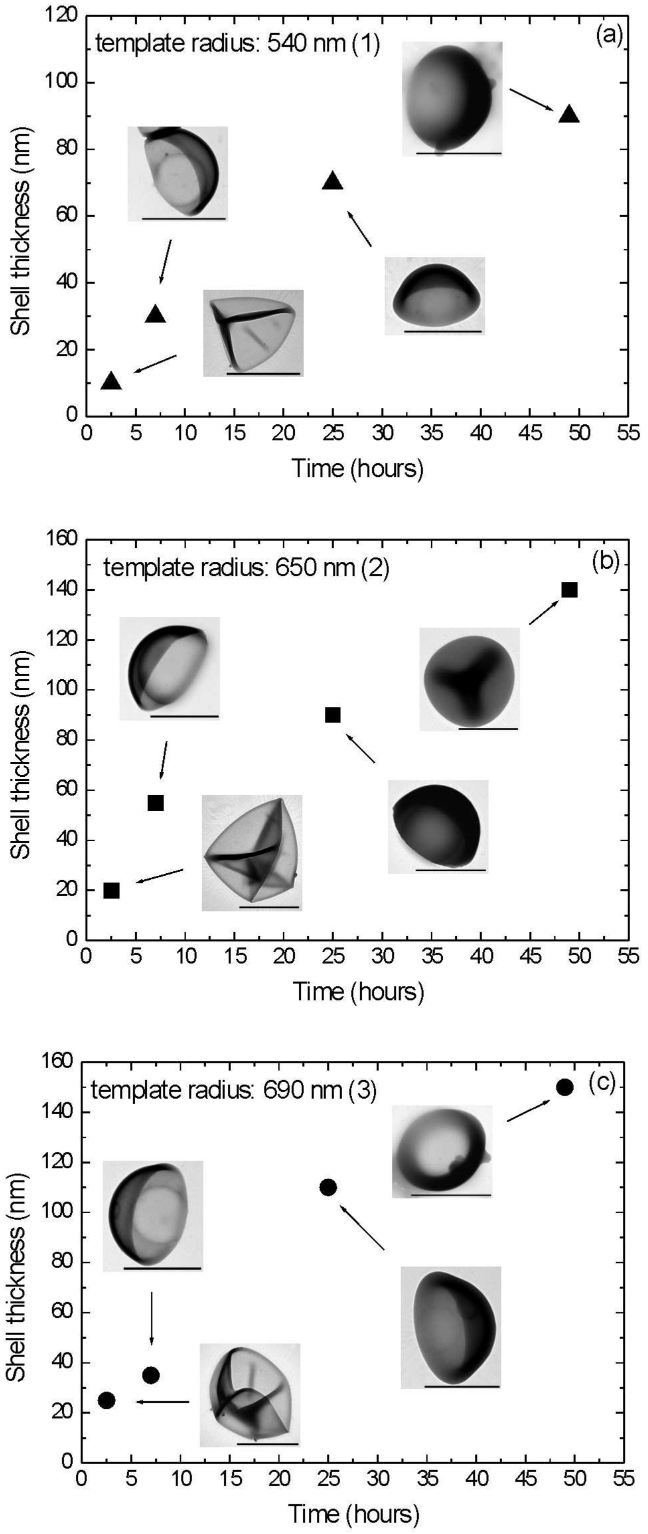

Figure 3.7: *Shell growth followed in time, for the samples indicated in Fig.3.6 by lines 1, 2 and 3: (a) line 1, template radius 540 nm (sample S1), (b) line 2, template radius 650 nm (sample S2) and (c) line 3, template radius 690 nm (sample S3). Scale bars for TEM images: 1 μm.*

As pointed out in Chapter 2, the final shell thickness is directly related to the amount of DMDES left in the sample during the encapsulation step. This means that the shell should grow in time at a similar rate as the oil droplets. Indeed, by following the shell thickness in time (Fig.3.8a), for different size of oil droplets used for encapsulation, we observed a significant growth for a relatively long period of time. All these samples were prepared by adding 0.018 M TEOS to the emulsions prepared with 2 % v/v monomer and 2 % v/v ammonia, except for one (the sample with 740 nm droplet radius was prepared from 3 % v/v DMDES, 3 % v/v ammonia). The coating was started in all cases after 24 hours since the emulsion synthesis began. The evolution of the shells within the first hours (inset in Fig.3.8a) can be characterized as a

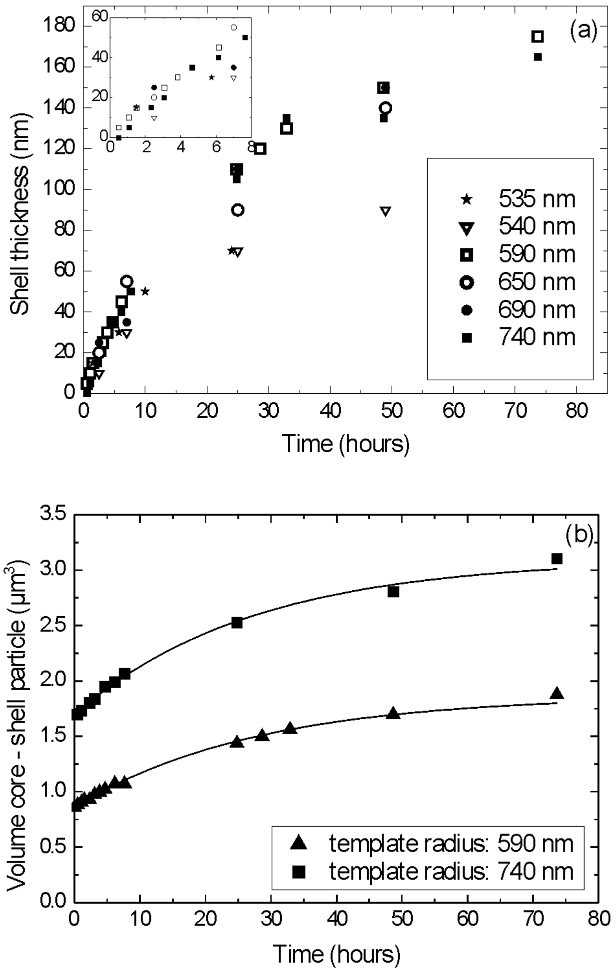

Figure 3.8: *(a) Increase of the shell thickness followed in time, for different radii of the template as indicated in the legend. Inset shows the growth within the first 8 hours after TEOS was added. (b) Average particle volume as a function of time, for two different template size; lines are drawn according to eqn.3.4.*

reaction-limited growth process [8] since the growth rate of the shell thickness is independent of the radius of the template. The overall growth of the coated particles is governed by the same growth rate as found for the oil droplets. This is seen in Fig.3.8b, which shows the increase in volume of the coated droplets, for two different templates. The change in total radius of the coated droplet takes the form:

$$R(t)^3 = R_f^3 - (R_f^3 - R_0^3)exp(-\frac{t}{t_1}) \tag{3.4}$$

where R_f represents the final particle radius and R_0 the radius of the template which remains constant during the encapsulation. The fitted growth rate $1/t_1$ has precisely the same values as found for the emulsion droplets (t_1 = 27 ± 2 hours). This is evidence for our conclusion that the shell growth is less influenced by the TEOS and relies more on the presence of hydrolyzed DMDES and that the latter determines the growth rate through a rate-limiting step which is effectively first order.

3.3.5 EDX analysis of the hollow shells

The large contribution of siloxane units to the shells can be seen in EDX elemental microanalysis on samples in which the liquid cores had been removed by washing in ethanol and drying (Fig.3.9). Differences among the samples are seen by comparing the relative ratios Si/O and Si/C for all types of shells. The Si/O ratio remains almost the same for all three particles, while the Si/C ratio decreases in going from microspheres to microcapsules and microballoons. The increase in carbon content relative to silicon implies a larger proportion of dimethylsiloxane units in the shell material.

As already shown, because of their thick shell relative to their radius, the microspheres maintain their spherical shape after drying. Moreover, their shell can sustain calcination at high temperatures (500 °C) without their structure being affected. The changes in their composition were determined by performing EDX analysis of the shell material before and after calcination.

Table 3.7: *Particle total radius and shell thickness determined with SLS ($R_{t,SLS}$, d_{SLS}) in suspension and with TEM ($R_{t,TEM}$, d_{TEM}) in dried state for microspheres before and after calcination.*

Before calcination				After calcination			
$R_{t,SLS}$ (nm)	d_{SLS} (nm)	$R_{t,TEM}$ (nm)	d_{TEM} (nm)	$R_{t,SLS}$ (nm)	d_{SLS} (nm)	$R_{t,TEM}$ (nm)	d_{TEM} (nm)
570	150	535	120	470	90	470	90

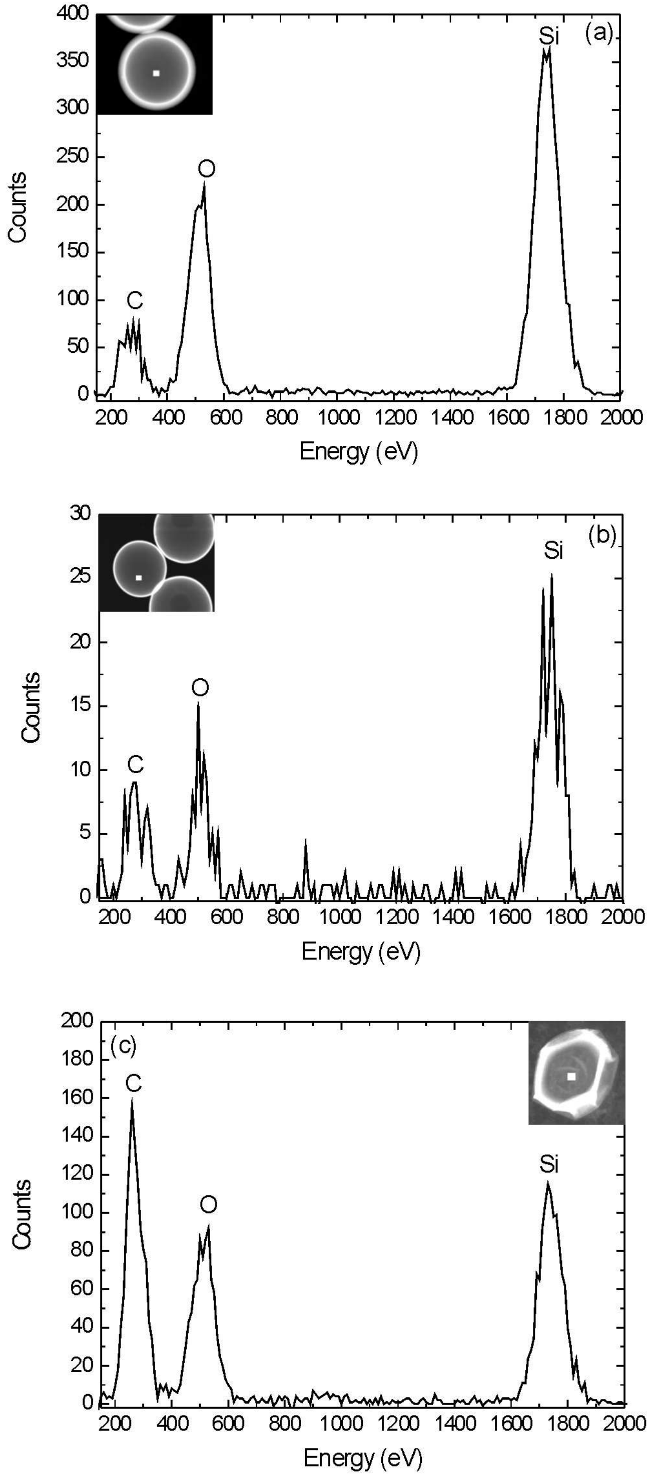

Figure 3.9: *EDX spectra recorded in the middle of the particles, in the points indicated by the white squares from the insets (representing TEM dark field images) for (a) microsphere, (b) microcapsule and (c) microballoon.*

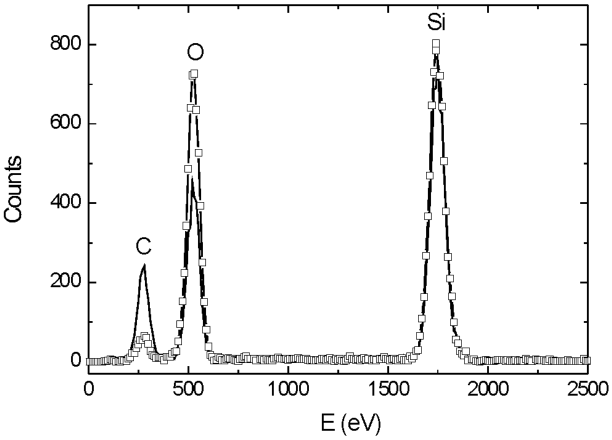

Figure 3.10: *EDX line spectrum recorded in the middle of the shell of a microsphere, before (line) and after (line + scatter) calcination in air at 500 °C for four hours.*

The EDX analysis indicated that the carbon was replaced by oxygen during the calcination in air, as shown in Fig.3.10. The remaining carbon signal, after calcination is due to the carbon-coated sample grids that were used. The calcination has also caused a change in the particle's volume; the shells used for the EDX measurements shown in Fig.3.10, had a total radius of 570 nm before calcination, as determined by SLS, and only 470 nm, afterwards. Interesting to notice is that, for the calcined particles, no difference was found between the radius measured with TEM, in dried state and the value obtained with SLS in suspension. These values are summarized in Table 3.7. From these we conclude that the hybrid silica/siloxane shell can be converted to pure silica by calcination.

3.3.6 ^{29}SI SOLID-STATE NMR OF HOLLOW SHELLS

The chemical structure of the shell material was determined from ^{29}Si solid state CP/MAS NMR spectra. The hollow shells used for these measurements were obtained by adding 0.018 M TEOS to an emulsion prepared from 1 vol.% DMDES and 10 vol.% ammonia and subsequently removing the oil from the core by transferring the coated droplets in ethanol. The resulting hollow shells were dried in air, under a heating lamp, for 12 hours prior to the measurements. This treatment completely removes the liquid cores. The ^{29}Si NMR spectrum is shown in Fig.3.11.

A silicon atom bonded through siloxane bonds (Si - O - Si) with four other silicons is designated as Q_4 (Fig.3.12b). A silicon atom with three O - Si bonds it is named Q_3, the fourth group being ethoxy or hydroxy (Fig.3.12a). They are usually found in silica particles [10, 60], obtained from TEOS following the

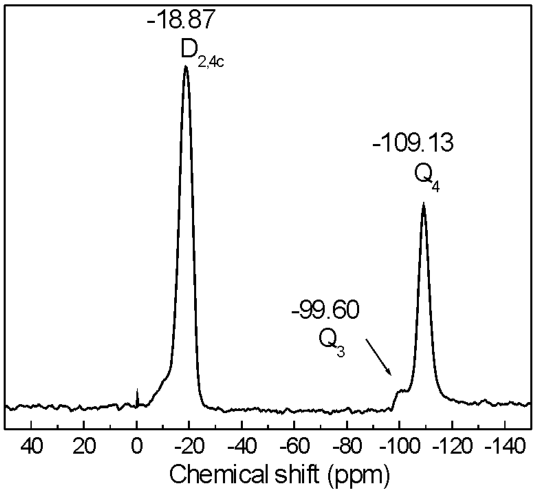

Figure 3.11: ^{29}*Si CP NMR spectrum of hollow shells (core radius: 735 nm, shell thickness: 280 nm). By* Q_3, Q_4 *are designated silicon atoms bonded with three or four other silicon atoms, respectively and* $D_{2,4c}$ *represents a cyclic tetramer*

Stöber procedure. [5] The presence of Q_4 in our spectrum is indicated by the relatively strong resonance situated at - 109.13 ppm; there is also a trace of Q_3 (-99.60 ppm). However, the strongest line in the spectrum belongs to the cyclic tetramer ($D_{2,4c}$, at -18.87 ppm) [73, 74] consisting of di-functional units, built into cyclic tetramers containing also one or more Q_4 units from the TEOS. Such a structural unit is represented in Fig.3.12c, with Si* indicating silicon atoms in di-functional units. Upon copolymerization of mixtures of DMDES and TEOS, the region -11 ppm to -14 ppm has been shown to contain the signals from dimers and end groups of linear oligomers, [73, 74] which can explain the appearance of the shoulder at the left side of $D_{2,4c}$. It has been previously reported [73, 74] that TEOS can indeed act as the linking unit between the cyclic oligomers.

Table 3.8: *Assignment of* ^{29}*Si NMR signals of shell material.*

Chemical shift(ppm)	Assignment
-18.87	$D_{2,4c}$
-99.60	Q_3
-109.13	Q_4

Thus we conclude that our shells consist of a cross-linked silica/siloxane network, in which TEOS plays the role of cross-linker. This explains why a major contribution to the shell comes from the DMDES, and why the shell thickness is mainly determined by the amount of DMDES left in the emulsion.

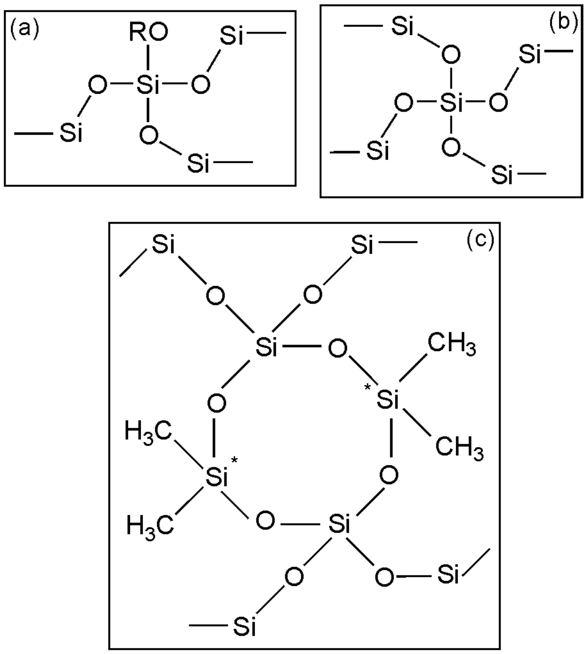

Figure 3.12: *Structure of a tetra-functional silicon atom bonded with (a) three (Q_3) or (b) four (Q_4) other silicon atoms. (c) Cyclic tetramer ($D_{2,4c}$) consisting of di-functional units (silicon atoms in these units indicated by Si*) coming from DMDES, cross-linked with tetra-functional units from TEOS.*

3.3.7 Density of the shells

The density of the shell material was determined from sedimentation experiments. Several diluted suspensions of hollow particles in ethanol, with different core radius and shell thickness were prepared. The sedimentation boundary was followed in time for several days, while they were sedimenting. Representative results are plotted in Fig.3.13. The particles followed a linear sedimentation profile, from which the sedimentation speed was determined as the slope of a linear fit. The total density of the sedimenting particle (ρ_p) in ethanol was determined from:

$$\rho_p = \frac{9\eta v}{2R_t^2 g} + \rho_l \tag{3.5}$$

with η– viscosity of the solvent (1.22×10^{-3} Pa·sec for ethanol at 20 °C), v – sedimentation speed, R_t– total radius of the particle, g– acceleration of gravity and ρ_l– density of the solvent (789 kg/m^3 for ethanol). Considering that the shells are filled with ethanol in solution (R– core radius) and assuming additivity of volumes, the density of the shell material is given by:

$$\rho_{shell} = \frac{\rho_p R_t^3 - \rho_l R^3}{R_t^3 - R^3} \tag{3.6}$$

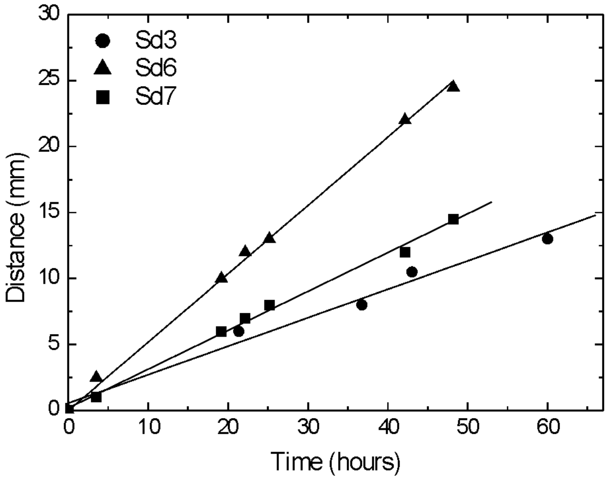

Figure 3.13: *Sedimentation profile of hollow shells in ethanol, for three different samples (Sd3, Sd6 and Sd7), for which the size of the template and shell thickness, are shown in Table 3.9. The lines represent linear fits from which the sedimentation speed was determined.*

The values obtained for the shell density are shown in Table 3.9. The relatively low densities of such particles, combined with the fact that they can sustain calcination and exposure to the vacuum of the TEM, make these materials extremely interesting for applications, when such characteristics are needed.

Table 3.9: *Size of the hollow particles determined with SLS and corresponding densities for the shell material obtained from sedimentation experiments. R − core radius, d − shell thickness, R_t− total radius of the particle and ρ_{shell}− density of the shell material.*

Sample	R(nm)	d(nm)	R_t(nm)	ρ_{shell}(kg/m^3)
Sd1	535	200	735	1040 ± 18
Sd2	500	220	720	1051 ± 24
Sd3	440	130	570	1008 ± 17
Sd4	590	200	790	1005 ± 13
Sd5	850	230	1080	916 ± 2
Sd6	735	280	1015	916 ± 1
Sd7	690	270	960	871 ± 1

3.3.8 Fluorescent shells

In order to fluorescently label our particles, we used a modified version of the procedure to incorporate dyes through covalent bonds into colloidal silica spheres described previously. [11,75] The procedure consists of two steps. First, the dye RITC was chemically bound to the silane coupling agent APS (as described in the synthesis section) and second, the dye mixture was added to the emulsion, together with TEOS, during the encapsulation step; the fluorescent dye ended up chemically incorporated in the particle shell. An example of dye-functionalized hollow shells is presented in Fig.3.14a, showing that the shells were successfully labeled. As an alternative, the dye RITC can be replaced by FITC which can be chemically incorporated into the shell by using the same procedure described above.

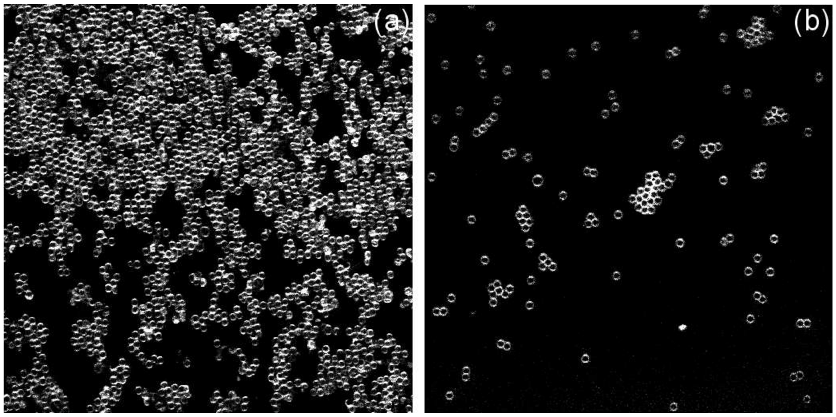

Figure 3.14: *Confocal microscopy images (fluorescence mode, λ = 543 nm) of RITC-labeled particles: (a) the fluorescent dye is chemically incorporated in the shell (image size: 119.05 μm × 119.05 μm) and (b) the fluorescent dye is only adsorbed at the surface of the shell (image size: 106.35 μm × 106.35 μm) .*

Fluorescent particles can be also obtained by simply adding RITC dissolved in ethanol or water (depending on the solvent in which particles are dispersed), to the suspension of particles (final RITC concentration $\approx 4.4 \times 10^{-3}$ mg/mL). In this case, the dye was found to be adsorbed at the surface of the particles (Fig.3.14b), but can be washed away any time by using a mixture of water and ethanol. The FITC dye cannot be used in an adsorption method because instead of being adsorbed at the surface, it stays in solution and can even penetrate the shell (see next section).

Furthermore, the hollow shells dispersed in ethanol can be incorporated in a fluorescent silica shell by using the same procedures as for growing silica shells. [42, 52]. An illustrative example is presented in Fig.3.15, in which the fluorescent shells were obtained as follows: 1.69 M NH_3 and 3.80 M H_2O were added to 5.5 mL dilute suspension of non-fluorescent microcapsules in ethanol (core radius 830 nm, shell thickness 300 nm, total shells weight $\approx$

0.011 g), after which 0.036 M TEOS was added together with 0.007 mL dye mixture containing RITC, APS and ethanol, prepared as described in the synthesis. The suspension was slowly stirred during the addition of TEOS and dye mixture and also after that, for another 3.5 hours. Finally, the resulting particles were cleaned by centrifugation and transfer to ethanol. It is clear from the confocal imaging in fluorescence mode, that the original shells are coated with a fluorescent shell. The total thickness of particles after the extra coating was found (from SLS) to be 400 nm, which means 100 nm thickness of the RITC-labeled shell. Moreover, as can be seen from Fig.3.15, the particles are not collapsed, even when they are dried on the microscope cover slip, whereas initially, before the extra coating, they collapsed when dried, forming hemispherical caps. This is another indication that the shell became indeed thicker.

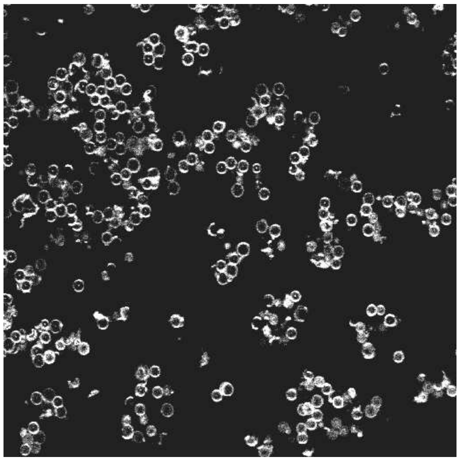

Figure 3.15: *Confocal microscopy image (fluorescence mode, λ = 543 nm) of microcapsules coated with a RITC-labeled silica shell, after they were dried and resuspended in ethanol (image size: 93.78 μm × 93.78 μm).*

The fluorescence achieved for our shells opens up the possibility of using them in confocal microscopy, for studying the properties of concentrated suspensions of hollow particles (Chapter 6).

3.3.9 Shell permeability

As already mentioned, the dissolution of the particle core is possible by using ethanol, which penetrates the shells and dissolves the PDMS oil. This already implies shell porosity sufficiently high for small molecules to pass through. Additionally, we investigated the shell permeability more thoroughly with confocal microscopy. Several qualitative experiments were performed using different capsule-like particles and fluorescently labeled solvents. The experiments proceeded as follows: hollow shells, non-fluorescent, dispersed in ethanol, were allowed to sediment and the solvent was replaced by ethanol containing 0.725 mM FITC; these dispersions were put in the special vials described in the experimental section and imaged in fluorescence mode. The ethanol with FITC, was found to penetrate the shells and as a result, fluorescence is observed also inside of the particles (Fig.3.16a). Taking into account the size of the FITC molecule (the longest distance 1.12 nm), the pores of the shell should be at least ≈ 1.1 nm in diameter to allow the dye to enter the particle. Subsequently, after the particles had sedimented onto the bottom of the vial, the ethanol containing FITC was quickly replaced by fresh ethanol. The fluorescence from the particle cores could still be observed within the first minutes after changing the solvent (Fig.3.16b); subsequently, it slowly diffused out, being replaced by clean ethanol. The particles in Fig.3.16b appear deformed, but this is due to flow resulting from mixing in the fresh ethanol. After ≈ 2 minutes, no more fluorescence could be observed from the particles, indicating that most of the FITC had diffused out. The release of the ethanol with FITC from the microcapsules is captured in close-up in Fig.3.16c. In this experiment, the hollow shells were first dispersed in ethanol containing the same dye concentration as before; subsequently, they were quickly filtered using a filter attached to a syringe and immediately re-suspended in clean ethanol. A glass capillary (0.1 x 2.0 mm) was filled with the new suspension and imaged in fluorescence mode. The particles appear to have ”tails” because the FITC diffusing out of the shells is carried off by the residual flow in the sample.

Although the experiments with fluorescent tracers were just qualitative, they demonstrate the permeability of the shells and the opportunity of refilling

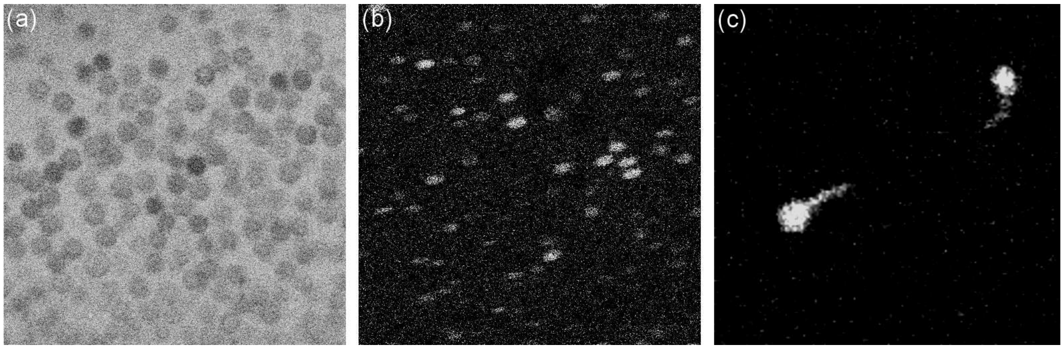

Figure 3.16: *(a) Confocal image (fluorescence mode, λ = 488 nm) of microcapsule-like particles (core radius 795 nm and shell thickness 150 nm), dispersed in ethanol containing 0.725 mM FITC and (b) image taken after the solvent had been quickly replaced with clean ethanol, during scanning, after 40 s. Images size: 29.8 μm × 29.8 μm). (c) Confocal image (fluorescence mode, λ = 488 nm) illustrating the release of the ethanol with FITC from microcapsules (core radius 850 nm and shell thickness 230 nm) dispersed in ethanol, ≈ 4 min. after they were suspended in clean ethanol. Image size: 23.3 μm × 23.3 μm)* .

these microcapsules with different chemicals. This opens the possibility of using them as microreactors or controlled release agents.

3.4 Conclusions

As shown by our investigations, the emulsion templating technique is a suitable approach for preparing hollow colloidal particles with tunable properties. Their size can be controlled not only by the amount of monomer used, but more importantly, also by the time between preparation of the emulsion droplets and addition of the encapsulating material. The monodispersity of the emulsion droplets is an important characteristic for their use as templates. Furthermore, the low molecular weight silicone oil obtained can be easily dissolved in ethanol after the droplets were incorporated in a solid shell. Because of the slow reaction, the PDMS oil droplets obtained from hydrolysis and polymerization of dimethylsiloxane monomer are excellent templates for encapsulation with solid shells using tetraethoxysilane.

We found that shell formation is a copolymerization between TEOS and DMDES. The condensation of the former limits the rate of growth both for the droplets and the shell. The shells consist mainly of dimethylsiloxane units cross-linked with tetra-functional silicate units, as shown by ^{29}Si NMR and EDX analysis. The properties (both chemical and physical) of the shells resemble more closely those of silicone rubber than of silica. The deformability of the particles was found to depend mainly on the ratio between the shell thickness and the particle radius, for our shell material. Of course, in general it depends on many other things as well, such as the elastic modulus of the shell material, which will depend on the cross-link density of TEOS, etc. Therefore, by simply tuning this ratio, three different types of particles can be obtained, with different properties and different perspectives for applications. Due to the specific reaction kinetics, the ratio can be influenced either by varying the time between the preparation of the emulsions and the start of the coating step, or by choosing different times for ending the encapsulation reaction.

The incorporation of fluorescent dyes into the shells opens up the possibility of investigating concentrated suspensions of such particles using confocal microscopy.

4 SYNTHESIS OF HOLLOW SPHERES BY SURFACTANT-STABILIZED EMULSION TEMPLATING

We investigate the possibility of using surfactant-stabilized emulsion droplets as templates for synthesis of hollow colloidal particles. Monodisperse silicone oil droplets were prepared by hydrolysis and polymerization of dimethylsiloxane monomer, using two different surfactants: sodium dodecyl sulphate (anionic) and Triton X-100 (non-ionic). We found a sharp decrease in the average droplet radius with increasing surfactant concentration, with a linear dependence of the droplet radius on the logarithm of the surfactant concentration. The surfactant-stabilized oil droplets were then encapsulated with a solid shell using tetraethoxysilane, and hollow shells were obtained by exchange of the core. In the case of sodium dodecyl sulphate, the resulting shells were relatively thin and rough, while when Triton X-100 was used, smooth shells were obtained which could be varied in thickness from very thick (≈ 150 nm) to very thin shells (≈ 17 nm).

4.1 Introduction

In general, when dealing with emulsions, surfactants are a necessary additive to impart stability. In this respect, the charge-stabilized emulsions used in the previous chapters formed the exception rather than the rule. It is therefore of interest to investigate whether our method to prepare hollow colloids by templating emulsion droplets can be extended to droplets carrying a stabilizing surfactant layer. The emulsions used are again the synthetic PDMS emulsions. These are preferred because they are highly monodisperse. But in order to demonstrate that our method allows coating of emulsions in general, we also tested it on (polydisperse) emulsions of some alkanes.

As their name already implies, surfactants are surface-active agents which adsorb positively at the interface. The common characteristic of these materials is that their molecules consist of a polar 'head' (hydrophilic part) and a hydrocarbon 'tail' (hydrophobic part). This amphiphilic nature of surfactants causes them to have a preference for interfaces. Depending on their chemical structure and properties of the head group, a surfactant is called anionic, cationic, amphoteric or non-ionic. When the head group is negatively charged, we deal with anionic surfactants. Most of the surfactants used industrially can be classified in this category. For cationic surfactants, the head group is positively charged. The surfactants containing head groups that have both positive and negative sites are referred to as amphoteric. In the case of non-ionic surfactants, the head group does not contain charges, but has the propensity to form hydrogen bonds.

Accumulation of surfactant molecules at interfaces causes a reduction in the interfacial tension, even at low concentrations. The impact of a surfactant on the surface tension is described by the Gibbs adsorption equation [76]

$$d\gamma = -\sum \Gamma_i d\mu_i \tag{4.1}$$

with $\Gamma_i = n_i^\sigma / A$ the surface excess per unit interfacial area of species i, defined as the number molecules accumulated at the surface per unit surface area. The solvent is taken to be component 1, and the summation runs over all other components. For ideally diluted solutions, the chemical potential can be written

$$\mu_i = \mu_i^0 + RTlnc_i \tag{4.2}$$

with μ_i^0 the standard chemical potential and c_i the molar concentration of solute i. For a two-component system, Eqn.4.1 becomes:

$$d\gamma = -RT\Gamma_2 dlnc_2 \tag{4.3}$$

Integrating the equation 4.3 at a fixed temperature:

$$\gamma = \gamma_0 - RT\Gamma_2 lnc_2 \tag{4.4}$$

According to the Gibbs adsorption equation, the surface tension should drop as more molecules are adsorbed at the interface. This was seen in the measurements on sodium dodecyl sulphate, [76] where the surface tension of SDS solutions in water was measured as a function of SDS concentration. The surface tension decreases with increasing of surfactant concentration, up to a value at which it becomes almost constant. At this concentration, the surface is already fully saturated with surfactant molecules and adding more surfactant does not lead to more adsorption. Instead, the surfactant molecules form small (a few nm) aggregates in solution called micelles. Each of them consists of about 40 - 100 molecules.The hydrophobic chains cluster together with the polar head groups sticking out into the water. The concentration where micelle formation starts is called the critical micelle concentration (CMC). The value of the CMC depends strongly on the composition of the solution. The addition of salt leads to a reduction of the CMC for both ionic and non-ionic surfactants. [77] However, for the ionic surfactants the effect is more pronounced.

Organic molecules can alter the value of CMC in different ways. Some of them, like the case of small to moderately-sized alcohols, adsorb on the micelles and have a noticeable influence at low concentrations. When they are adsorbed in the surfactant layer, they might be nested between surfactant molecules, thereby lowering the electric repulsion of the polar or ionic head groups; this increases the stability of micelles and therefore lowers the CMC. [78] Organic compounds can also alter the CMC through their influence on the solvation of the surfactant. They can become solubilized in the micelles, forming a small pool of organic molecules surrounded by surfactant. In emulsions, the organic liquid forms a much larger pool. This is not a thermodynamically stable state, but the surfactant layer now stabilizes the droplets kinetically against coalescence.

In this chapter we investigate in detail PDMS emulsions prepared using two surfactants, an anionic one, sodium dodecyl sulphate (SDS) and a non-ionic one, Triton X-100 (TX100). A cationic surfactant, hexadecyltrimethylammonium bromide (CTAB) was also used in several experiments, but it was not possible to determine accurately the influence of surfactant on the droplet size. Although we observed a decrease in the droplets size with increasing the concentration of CTAB, this was accompanied by a large increase in polydispersity. The effect of CTAB on the emulsions could be induced by its cationic head group. The cationic surfactant can cancel the negative surface charge on the droplets (through which the droplets are self stabilized), and destabilize the emulsions.

In the case of surfactant-stabilized emulsions, we are interested in the size and polydispersity of the oil droplets and their growth mechanism. Additionally, we look at the possibility of using the surfactant-stabilized PDMS droplets as templates for encapsulation with solid material, following the procedure described in Chapter 2. Furthermore we make preliminary investigations regarding encapsulation of different types of oil droplets with solid shells, using the same procedure.

4.2 Experimental section

4.2.1 Materials

Dimethyldiethoxysilane (DMDES, $\geq$97.0 %) and tetraethoxysilane (TEOS, $\geq$98.0 %) were obtained from Fluka. The surfactants, sodium dodecyl sulphate (SDS, $\geq$99.0 %), Triton X-100 (TX100) and hexadecyltrimethylammonium bromide (CTAB, $\geq$99.0 %)were purchased from Aldrich and ammonia (29.7 % w/w NH_3) and ethanol (absolute alcohol, analytical grade) from Merck. Cyclohexane ($\geq$99.0 %) was supplied by Acros Organics, hexane ($\geq$98.5 %) by Aldrich, and the oil-soluble fluorescent dye Pyrromethene 580 (PM 580) was obtained from Exciton. All chemicals were used as received. De-mineralized water was used in all described reactions and also for the cleaning of glassware.

4.2.2 Synthesis

Surfactant-stabilized emulsions. The silicone oil-in-water emulsions were prepared by the hydrolysis and polymerization of DMDES in the presence of one of the two surfactants, one anionic (SDS) and one non-ionic (TX100). First, a stock solution of the surfactant was prepared by dissolving a weighted amount of the surfactant in de-mineralized water. The reaction mixtures were prepared in 20 mL glass vials and the total volume of the emulsions was 10 mL. De-mineralized water, surfactant stock solution and ammonia solution were added and mixed together in the reaction vial. DMDES was added to this solution immediately, followed by vigorous mixing for 0.5 or 1 minute with a lab-minishaker (MS2 minishaker from IKA) at 2500 rpm. After shaking, a clear solution was obtained which indicates hydrolysis of the monomer, since the un-hydrolyzed DMDES is insoluble in water. Within $\approx$ 10 minutes, the solution started to become turbid, indicating the formation of the droplets. They were allowed to grow for at least 24 hours before the coating step, except for the cases when the growth of the oil droplets was followed in time. The emulsions were left without stirring during droplet growth. The concentrations of SDS used to prepare the PDMS emulsions varied from 1×10^{-3} to 0.26 % w/w, for 1, 2 and 3 % v/v concentrations of DMDES and 1, 2, 3 and 4 % v/v ammonia solutions. In the case of TX100, the concentration range was from 2×10^{-4} to 0.03 % w/w, for the same concentrations of DMDES and ammonia solution as before. For CTAB, initially the concentrations were in the range 0.005 to 0.02 % w/w and afterwards 2×10^{-4} - 6×10^{-4} % w/w.

Hollow particles. The encapsulation of the surfactant-stabilized PDMS oil droplets with a solid shell was achieved using the same procedure as described in Chapter 2 for the case of surfactant-free emulsions, by adding a small amount of TEOS to the as prepared PDMS emulsions. TEOS was added in concentrations from 0.018 to 0.08 M, under magnetic stirring. This was done either in one single step, four or five steps (5 min. between steps) or by dissolving it first in an aqueous solution containing the same concentration of ammonia as the emulsion used in the coating step. The shells were allowed to grow from 3 to 10 days, after which they were centrifuged and re-suspended in ethanol. The centrifugation/redispersion procedure was repeated several times in order to clean the samples.

Second shell growth. The second shell synthesis was performed in ethanol, using the shells prepared previously as seeds for further growth. [12] The synthesis was carried out using small volumes of hollow shells dispersed in ethanol ($\approx$ 1-3 mL dispersion), to which ammonia solution and TEOS were added; the final concentrations were: 1.5 M NH_3, 0.030 M TEOS and 3.4 M H_2O. The dispersions were stirred for 1 to 2 hours and left for 2 to 3 days before isolation of the shells.

Encapsulation of other oil droplets with solid shells. The emulsions used in these experiments were prepared in 10 mL total volume of a solution of demineralized water containing Triton X-100 (2×10^{-3} % w/w) and 5 % v/v cyclohexane or hexane. The cyclohexane was first fluorescently labelled by dissolving 0.08 mg/mL PM 580 in the oil, followed by magnetic stirring over night. The samples were mixed with the minishaker (2500 rpm) for 1 min., followed by 1 min. of sonication. No fluorescent dye was used for hexane. For the encapsulation step, 3 mL solution of de-mineralized water containing 5 % v/v DMDES and 5 % v/v ammonia was first prepared and vigorously shaken for 30 s. This solution, together with 0.053 mL TEOS (final concentration 0.018 M), was added to the freshly prepared emulsions (right after preparation), during stirring, which was continued for $\approx$ 20 hours.

4.2.3 Characterization

The size and polydispersity of the oil droplets and the thickness of the coating were determined with static light scattering (SLS). The SLS profiles were compared with the theoretical ones calculated with the full Mie solution for the scattering form factor, [65] from which the radius and polydispersity were determined. Usually in a SLS curve, the first minimum (at low value of the scattering vector k) fills up faster than the next ones, due to multiple scattering, which is more severe at low angles. Therefore, the polydispersity is approximated by fitting the depth of the last minima in the scattering profile. In the case of surfactant-stabilized emulsions, due to the small size of the oil droplets, most of the SLS curves contain only one minimum, which makes it difficult to determine accurate values for the polydispersity. The values given must be considered upper bounds.

The hollow shells obtained after encapsulation of the droplets and removal of the cores were analyzed with transmission electron microscopy (TEM). Samples were prepared by dipping a carbon-coated copper grid (covered with Formvar film) in the as prepared suspension. The elemental microanalysis of the shell material was obtained from energy dispersive X-ray spectroscopy (EDX). Confocal microscopy was used to observe the oil droplets encapsulated in solid shells. We used the 543 nm line to excite the PM 580-labeled cyclohexane. The solid shells were observed in transmission mode.

4.3 Results and discussion

4.3.1 SDS-stabilized PDMS emulsions

Fig.4.1a presents the average droplet size for two series of emulsions as a function of surfactant concentration. The emulsions were prepared from 1 and 2 % v/v DMDES, 4 % v/v ammonia solution and concentrations of SDS in the range 1×10^{-3} to 0.25 % w/w. The reagents were mixed for 30 s, using a lab-minishaker at 2500 rpm. The values for the radius and polydispersity of the droplets were measured with SLS, 24 hours after the emulsions preparation and are summarized in Table 4.1. For the emulsions prepared from 1 % v/v DMDES, we observed a significant reduction in the average droplet size as the concentration of surfactant is increased, up to 0.1 % w/w SDS (Fig.4.1a). After that, it slowly increases. The same behavior was observed for the emulsions prepared from 2 % v/v DMDES. However, in the latter case, the concentration of SDS up to which the droplet radius decreases, shifted to a slightly lower value (0.08 % w/w SDS). In the region for which the droplet radius decreases, there is a linear relation between the droplet size and the logarithm of the SDS concentration, as represented in Fig.4.1b. This is in agreement with earlier investigations of surfactant stabilized PDMS droplets, [79] being also consistent with the assumption that SDS mainly influences the droplets through a reduction in interfacial tension of the oil/water interface. According to the Gibbs equation, the interfacial tension also decreases with the logarithm of the surfactant concentration (Eqn.4.4). A lower interfacial tension gives a lower activation energy for homogenous nucleation, which leads to more nuclei; the same volume of oil is formed, but is divided over more droplets.

Usually, in the case of surfactant-stabilized emulsions, the radius of the droplets decreases with the increasing of surfactant concentration until the critical micelle concentration (CMC) is reached. [80] For SDS, the CMC corresponds to a concentration of 0.23 % w/w. [81] Therefore we would expect a minimum in the average droplet size around this value. However, this happens at lower concentrations, as is seen in Fig.4.1a: at 0.1 %w/w for emulsions with 1 % v/v DMDES and at 0.08 %w/w for emulsions with 2 % v/v DMDES. Above these values, the size of the droplets fluctuates, increasing and decreas-

Table 4.1: *Size and polydispersity of oil droplets, as determined by SLS, 24 hours after preparation for different concentrations of SDS and two concentrations of DMDES; R−droplet radius , δ−polydispersity.*

	1 % v/v DMDES		2 % v/v DMDES	
SDS (%w/w)	R (nm)	δ (%)	R (nm)	δ (%)
0.001	650	5		
0.005	467	6		
0.01	383	8		
0.02			390	6
0.04			351	6
0.05	280	12		
0.06			295	8
0.08			272	8
0.1	217	11	325	11
0.12			295	11
0.14			275	16
0.15	250	11		
0.16			295	11
0.18			298	11
0.2	365	11	325	9
0.22			325	9
0.25	325	11		

ing alternately, which makes it difficult to interpret, as a sign that the CMC has been reached. However, the fact that deviations occur at lower concentrations than the CMC might indicate a reduction of the CMC due to the presence of ions (ammonia) and ethanol (hydrolysis of DMDES). It is known that the addition of small amounts of ethanol [78] or ions [77] can decrease the CMC considerably. In our emulsions, the 4 % v/v of ammonia solution corresponds to an ionic strength of ≈ 3.3 mM. Moreover, a small amount of ethanol is formed in the condensation reaction of DMDES, from one mole of DMDES, two moles of ethanol being formed. This leads in our case (1 and 2 % v/v DMDES) to 0.116 and 0.232 M ethanol respectively, considering full conversion of DMDES into PDMS. Consequently, the shift of the minimum in droplet size to a lower concentration for higher DMDES concentration is consistent with this interpretation, although the magnitude of the shift is not fully explained by it.

We investigated the growth of the oil droplets in time by preparing several emulsions with 1, 2 and 3 %v/v DMDES and ammonia respectively, and SDS concentrations in the range 0.02 to 0.1 % w/w. The emulsions were pre-

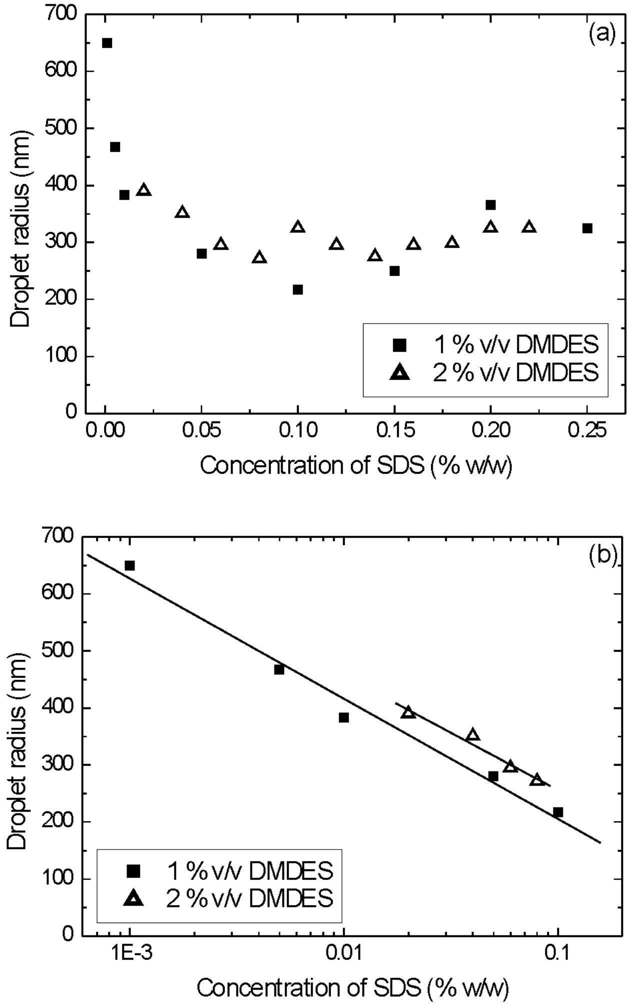

Figure 4.1: *(a) Radius of PDMS droplets as a function of SDS concentration, for emulsions prepared from 1 and 2 % v/v DMDES and 4 % v/v ammonia. (b) The same as (a), but using a logarithmic scale for the SDS concentration. The values for the radius were determined by SLS and are summarized in Table 4.1.*

pared as described in the synthesis section. The radius of the droplets and polydispersity were followed in time with SLS, and the results are plotted in Fig.4.2. Although the droplets are stabilized by SDS and their average size is smaller than in the case of surfactant-free emulsions, their growth shows the same behavior in time. The data can be fitted well by the same relation used in Chapter 3 (Eqn. 3.1).

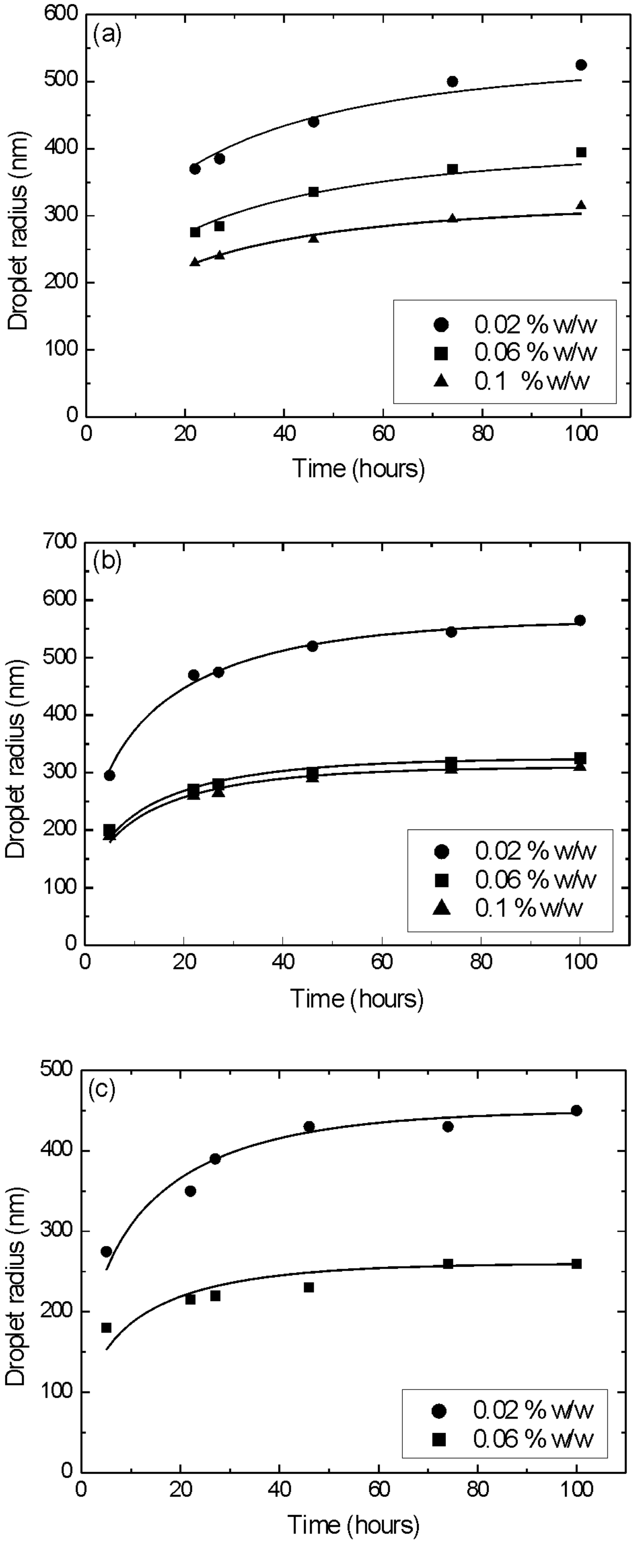

Figure 4.2: *Average droplet radius as a function of time, followed with SLS, for different SDS concentrations, shown in the legend, for emulsions prepared from: (a) 1 % v/v DMDES, 1 % v/v ammonia solution, (b) 2 % v/v DMDES, 2 % v/v ammonia solution and (c) 3 % v/v DMDES, 3 % v/v ammonia solution; lines are drawn according to Eqn.3.1 with* t_1 *given in Table 4.2.*

Moreover the values for the growth rate *1/*t_1, with t_1 a fitting parameter (Table 4.2), are similar as obtained in the case of emulsions without surfactant. Even the peculiar result that the growth rate in emulsions containing 1 % v/v. DMDES is twice as low, is reproduced.

Table 4.2: *Final droplet size and growth rate data for different volume percent of DMDES and different SDS concentrations.* R_f*−final droplet radius as determined from SLS,* t_1*−fitting parameter obtained by fitting the experimental data with the Eqn.3.1.*

SDS (%w/w)	DMDES (%v/v)	R_f (nm)	t_1 (hours)
0.02	1	525	48.2 ± 4.0
0.06	1	395	49.7 ± 4.1
0.1	1	315	45.0 ± 2.8
0.02	2	565	29.3 ± 1.3
0.06	2	325	24.1 ± 1.9
0.1	2	310	23.7 ± 1.6
0.02	3	450	25.8 ± 2.8
0.06	3	260	22.0 ± 4.5

From these results we conclude that even in the presence of SDS, at concentrations below the CMC, the oil droplets are formed by the same reaction mechanism, with a rate limiting step in the condensation reaction as observed in the absence of surfactant. By using SDS in the preparation of PDMS emulsions, we obtained a decrease in the average size of the oil droplets. Although droplets with similar sizes were obtained also in the surfactant-free emulsions in the first hours of the reaction, their polydispersity was quite high; by using surfactant, the polydispersity corresponding to the smaller droplets is improved, and consequently, their potential use for encapsulation.

4.3.2 HOLLOW PARTICLES FROM SDS-STABILIZED OIL DROPLETS

The silicone oil droplets described in the previous section were use as templates for encapsulation with solid shells, using the same two-step procedure described in the case of surfactant-free emulsions. In the first step, we prepared oil droplets from 1 or 2 % v/v DMDES, 1 or 4 % v/v ammonia and several concentrations of SDS. In the second step, the oil droplets were coated with solid shells by adding TEOS to the emulsions. We varied the amount of TEOS used and the addition method. Table 4.3 represents an overview of particles obtained by coating SDS-stabilized oil droplets with solid shells.

Table 4.3: *Size and polydispersity of particles obtained from encapsulation of SDS-stabilized droplets as determined by SLS;* R_d*−radius of the droplets used as templates,* δ*−polydispersity and* d*−shell thickness, obtained by using various amounts of TEOS, which was added 24 hours after the emulsion preparation for all samples, except sample* $S_{4,SDS}$ *when the time interval was 48 hours. The oil droplets were prepared from 1 % v/v DMDES (samples* $S_{1,SDS}$ *-* $S_{4,SDS}$*) and 2 % v/v (samples* $S_{5,SDS}$ *-* $S_{8,SDS}$*) respectively.*

Sample	SDS (% w/w	R_d (nm)	δ(%)	TEOS (M)	d (nm)
$S_{1,SDS}$	0.02	310	7	0.018	40
$S_{2,SDS}$	0.06	290	7	0.018	15
$S_{3,SDS}$	0.04	272	10	0.02	25
$S_{4,SDS}$	0.06	262	12	0.04	15
$S_{5,SDS}$	0.06	237	9	0.04	12
$S_{6,SDS}$	0.06	242	9	0.05	12
$S_{7,SDS}$	0.06	229	9	0.06	17
$S_{8,SDS}$	0.06	229	9	0.08	-

In one series of experiments, we used exactly the same amount of TEOS as previously (0.018 M TEOS), which was added in 5 steps (5 min. between steps), during stirring, to 10 mL emulsion prepared 24 hours before. The samples were stirred for three days, after which the coated droplets were transferred to ethanol in order to remove the cores. The droplets used as templates for these experiments were prepared from 1 % v/v DMDES and 1 % v/v ammonia and 0.02 and 0.06 % w/w SDS, respectively. The hollow shells obtained after dissolution of the core can be seen in Fig.4.3a,b and details about the samples in Table 4.3, samples $S_{1,SDS}$ and $S_{2,SDS}$. Although the shells were allowed to grow for three days, the final thickness was relatively thin compared with the values obtained after three days in the case of surfactant-free emulsions.

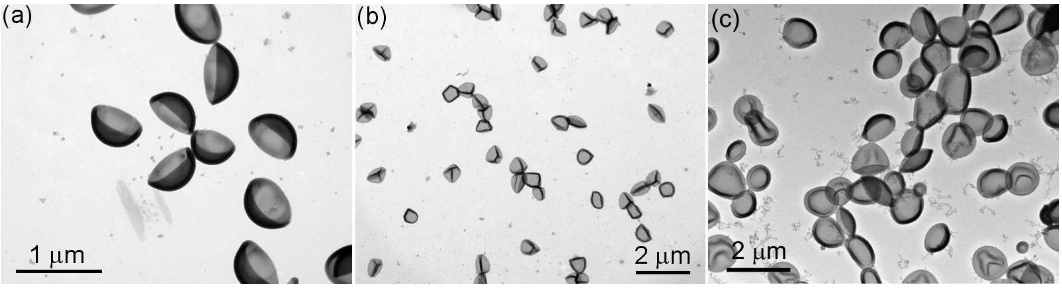

Figure 4.3: *TEM micrographs of hollow shells:(a) Sample* $S_{1,SDS}$*, R = 310 nm, d = 40 nm,* δ *= 7 %; (b) Sample* $S_{2,SDS}$*, R = 290 nm, d = 15 nm,* δ *= 7 %; (c) Sample* $S_{3,SDS}$*, R = 272 nm, d = 25 nm,* δ *= 10 %. Size and polydispersity obtained from SLS.*

Due to the thin shell compared with the total radius, the particles deformed when dried. Also we found evidence of small secondary particles which have not been completely removed by centrifugation. (see Fig.4.4). Moreover, the higher the SDS concentration, the thinner the shell. This indicates that the presence of SDS limits the shell growth.

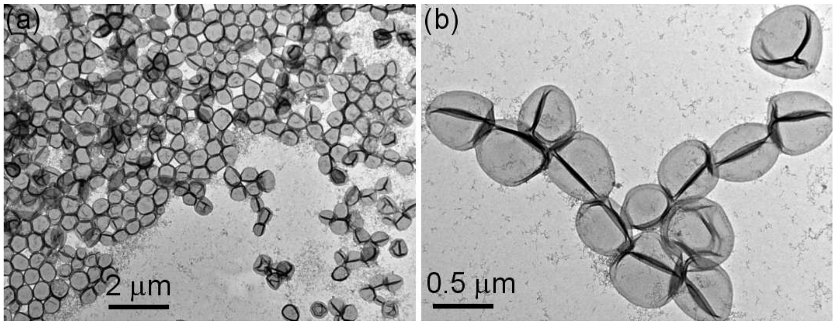

Figure 4.4: *TEM micrographs of hollow shells: Sample* $S_{4,SDS}$*,* $R = 262$ *nm,* $d = 15$ *nm,* $\delta = 12$ *%. Size and polydispersity obtained from SLS.*

The same thin shells were obtained when slightly more TEOS was used (sample $S_{3,SDS}$ from Table 4.3). In this case 10 mL emulsion was prepared from 1 % v/v DMDES, 4 % v/v ammonia and 0.04 % w/w SDS and after 24 hours was diluted once with a solution with the same composition as the initial reaction mixture, except for DMDES. 0.02 M TEOS was added to this mixture during stirring. The resulting shells, after they were transferred to ethanol are shown in Fig.4.3c.

Similar shell thicknesses were obtained when two days old emulsions were used for encapsulation, as is the case of sample $S_{4,SDS}$ from Table 4.3. The emulsion was prepared using 1 % v/v DMDES, 4 % v/v ammonia and 0.06 % w/w SDS, and for the coating step, 0.11 M TEOS was first dissolved into an aqueous solution containing 4 % v/v ammonia, after which 5 mL of this solution was added to the emulsion during stirring. The final TEOS concentration

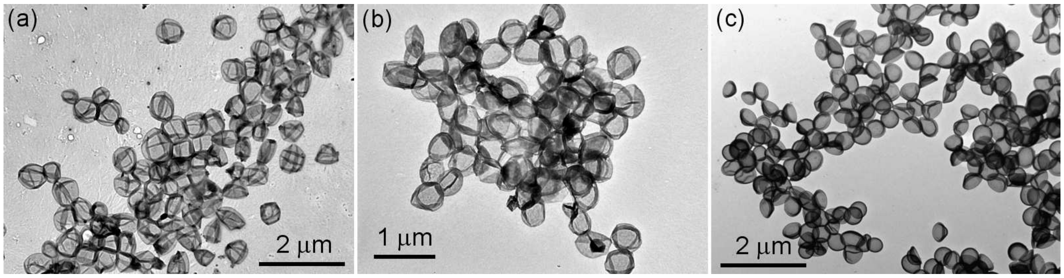

Figure 4.5: *TEM micrographs of hollow shells: (a) Sample* $S_{5,SDS}$*,* $R = 237$ *nm,* $d = 12$ *nm,* $\delta = 9$ *%; (b) Sample* $S_{6,SDS}$*,* $R = 242$ *nm,* $d = 12$ *nm,* $\delta = 9$ *%; (c) Sample* $S_{7,SDS}$*,* $R = 229$ *nm,* $d = 17$ *nm,* $\delta = 9$ *% Size and polydispersity obtained from SLS.*

in the sample was 0.04 M. After 4 days, the coated droplets were transferred to ethanol and the hollow shells are illustrated in Fig.4.4.

In order to investigate the influence of TEOS concentration on the shell thickness, several emulsions were prepared from 2 % v/v DMDES, 4 % v/v ammonia and 0.06 % w/w SDS (samples $S_{5,SDS}$, $S_{6,SDS}$, $S_{7,SDS}$, $S_{8,SDS}$ from Table 4.3). The oil droplets were allowed to grow for 24 hours before the coating step. Aqueous mixtures (5 mL) containing 4 % v/v ammonia and different amounts of TEOS were prepared and added to the emulsions during stirring, which was continued for one hour. The final concentrations of the TEOS in the samples were 0.04 M, 0.05 M, 0.06 M and 0.08 M, respectively. After three days, the particles were transferred to ethanol and cleaned by centrifugation and changing the solvent. For the first three TEOS concentrations we obtained very thin shells: 12 nm, 12 nm and 17 nm, respectively. The hollow shells are shown in Fig.4.5. For 0.08 M TEOS, no particles were obtained, only big aggregates, which indicates that there is a concentration limit for the added TEOS for which stable particles can be obtained. Apparently, the amount of TEOS does not influence the shell thickness significantly. This was also found for the surfactant-free emulsions. Moreover, even when the shells are allowed to grow for several days and TEOS is added already after 24 hours, their thickness doesn't exceed $\approx$ 40 nm, which is completely different from the surfactant-free case.

We conclude that from the encapsulation of SDS-stabilized oil droplets we can obtain hollow shells but we can only obtain microballoon-like particles and microcapsules in this case. The values of d/R_t for these shapes are in agreement with the result of Chapter 3. When SDS-stabilized oil droplets are used for encapsulation with solid shells, apparently a part of the TEOS/DMDES goes into the formation of secondary particles. This is a likely mechanism through which SDS interferes with the shell growth.

4.3.3 EDX analysis of the hollow shells

In order to obtain information about the chemical composition of the shell material, we performed EDX elemental microanalysis on hollow shells obtained by coating SDS-stabilized emulsion droplets. The oil from the core was removed prior to the measurements by washing with ethanol and drying. The EDX spectrum obtained for sample $S_{7,SDS}$ is presented in Fig.4.6a. We found the same composition as for the shells investigated in Chapter 3, namely silicon, oxygen and carbon. We could not detect the presence of surfactant in the shell material, but this does not exclude the possibility that the shell contains some small amount of SDS. If this would be the case, the S and Na signals would be very low considering the small weight percentage of surfactant used in the first place, and as a consequence, very difficult to detect. However, the presence of carbon is an indication that also in this case, the hydrolyzed DMDES contributes to the shell formation.

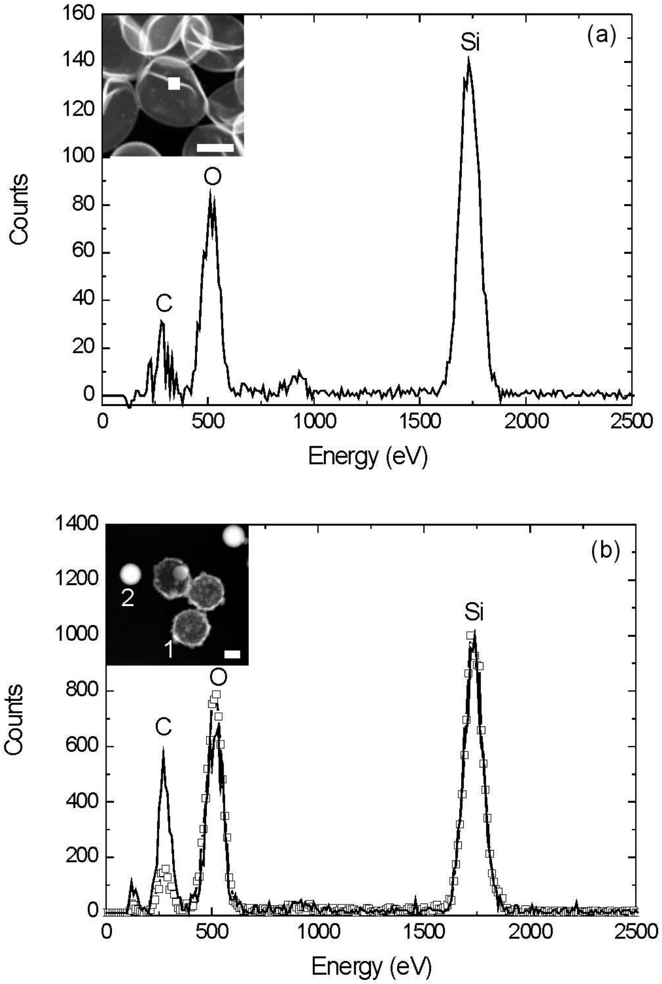

Figure 4.6: *(a) EDX spectrum recorded in the middle of the particle, after the shell growth, in the point indicated by the white square from the inset. (b) EDX spectra recorded after second shell growth: line-EDX in the middle of particle 1, and line + squares-EDX on the particle 2 (secondary nucleation). Insets: TEM dark field images, scale bars 200 nm.*

4.3.4 SECOND SHELL GROWTH

The encapsulation of SDS-stabilized oil droplets leads to a relatively reduced shell thickness. Therefore, in order to obtain thicker shells, we tried to grow an extra silica shell by a regular seeded Stöber growth [5,12] The second shell growth was carried out using the hollow shells dispersed in ethanol from the sample $S_{5,SDS}$ as seeds. 0.011 mL TEOS and 0.16 mL ammonia were added directly to 1.5 mL dispersion of hollow shells in ethanol, during stirring, which

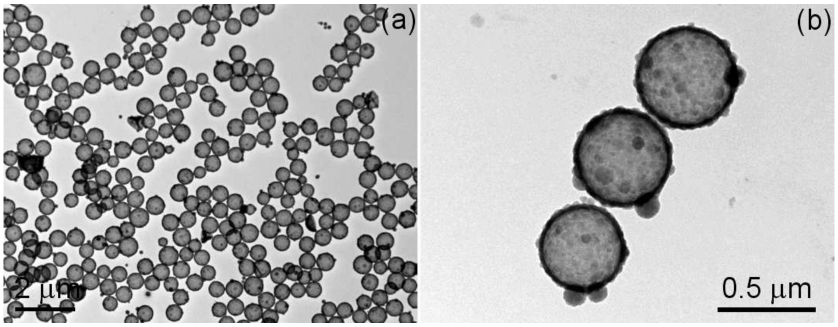

Figure 4.7: *TEM images of particles from sample* $S_{5,SDS}$ *after the second shell growth, at different magnifications.*

continued for two hours. After two days, the samples were cleaned by repeated centrifugation and changing of the solvent. TEM images of the particles obtained from the second growth step are shown in Fig.4.7. Although the particles appear to have a thicker shell and did not collapse as they did before the second coating (Fig.4.5a), they have a very rough surface. The sample contained also somewhat smaller particles which seemed to be secondary nucleation. This same type of shell was obtained in all samples used for second coating.

The EDX analysis (Fig.4.6b) performed on these samples shows the same shell composition as for particles after the first shell growth. By comparing the shell composition with the one of a particle which is part of the secondary nucleation (see Fig.4.6b), it is obvious that the amount of carbon present in the latter one is significantly lower (the small amount comes from the carbon-coated grid, since no background correction was applied).

We concluded that a shell (with the same composition) thick enough to resist deformation can be formed in this way, but unfortunately, these shells are very rough. This might be a consequence of SDS which might have been attached at the surface of the shells during the encapsulation step.

4.3.5 TRITON X-100-STABILIZED PDMS EMULSIONS

We also prepared PDMS emulsions using the non-ionic surfactant Triton X-100, using 2 % v/v DMDES and 2 % v/v ammonia in 10 mL total volume of emulsion, with concentrations of surfactant from 2×10^{-4} to 0.01 % w/w. The samples were prepared by mixing the reagents for 1 min. with a lab-minishaker at 2500 rpm, and after 20 hours, the size of the oil droplets was measured with SLS. The results are presented in Table 4.4 and plotted in Fig.4.8a. The average droplet radius decreases with increasing surfactant concentration up to 0.01 % w/w (Fig.4.8). The concentrations for which Triton X-100 effectively influences the size of the oil droplets are considerably smaller than in the case of SDS due to the fact that it has a much lower cmc of 0.019 % w/w. [82] Also for

Table 4.4: *Size and polydispersity of oil droplets, as determined by SLS, 20 hours after they were prepared from 2 % v/v DMDES, 2 % v/v ammonia solution and different concentrations of Triton X-100; R−droplet radius, δ−polydispersity.*

Triton X-100 (%w/w)	R (nm)	δ (%)
0.0002	690	4
0.0005	580	4
0.001	490	4
0.002	335	6
0.005	285	8
0.01	210	13

Triton X-100, the effective concentration range stops below the cmc, an effect which might be explained by a reduction of the cmc due to the same factors as discussed in section 4.3.1. Similar to the SDS-stabilized emulsions, we found a linear dependence of the radius on the logarithm of the concentration (Fig.4.8b), indicating that the presence of Triton X-100 determines the droplet size through a decrease in the interfacial tension of the oil/water interface.

The growth of the oil droplets stabilized by Triton X-100 in time was investigated for a series of emulsions prepared from 2 % v/v DMDES, 2 % v/v ammonia and TX100 concentrations in the range 2×10^{-4} to 0.01 % w/w. The emulsions were prepared using the same procedure as described earlier in this section and the size and polydispersity of the oil droplets were followed in time with SLS. Table 4.5 contains the average droplet radius and polydispersity and they are plotted vs. time in Fig.4.9. By fitting the data with the same Eqn.

Table 4.5: *Size and polydispersity of oil droplets followed in time, as determined by SLS, for emulsions prepared from 2 % v/v DMDES and ammonia solution and different concentrations of Triton X-100; R−droplet radius , δ−polydispersity.*

	0.0002 %w/w		0.0005 %w/w		0.001 %w/w		0.002 %w/w		0.005 %w/w		0.01 %w/w	
time (h)	R (nm)	δ (%)	R (nm)	δ (%)	R (nm)	δ (%)	R (nm)	δ (%)	R (nm)	δ (%)	R (nm)	δ (%)
3.5	465	5	380	6	330	5	220	8	202	9	-	
20.5	690	4	580	4	490	4	335	6	285	8	210	13
27.5	720	3	610	3	520	3	350	5	295	8	215	13
47	820	3	680	3	570	3	380	5	320	5	230	7
71	840	3	685	3	590	3	400	5	340	6	240	17
95	860	3	685	3	610	3	400	5	350	6	240	17

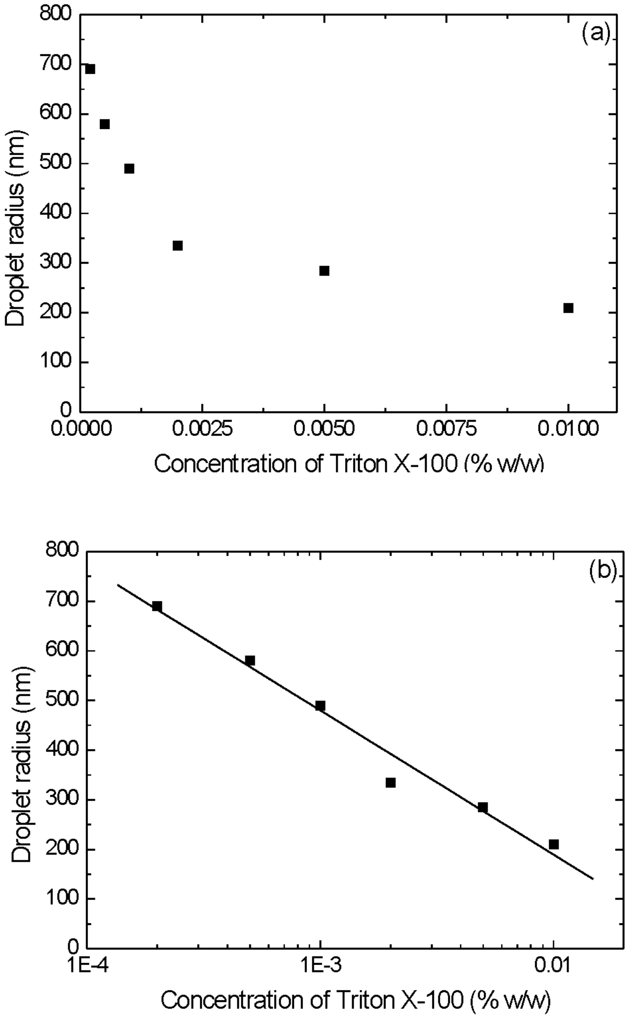

Figure 4.8: *(a) Radius of PDMS droplets as a function of Triton X-100 concentration, for emulsions prepared from 2 % v/v DMDES and 2 % v/v ammonia. (b) The same as (a), but using a logarithmic scale for the TX100 concentration. The values for the radius were determined by SLS and are summarized in Table 4.4.*

3.1 used for all the growth experiments, we obtained values for the growth rate $1/t_1$ quite similar with those found for both surfactant-free and SDS-stabilized emulsions. In Table 4.6 are summarized the values for the fitting parameter t_1. Independent of the presence or the type of surfactant used to stabilize the PDMS droplets prepared through hydrolysis and condensation of DMDES, the reaction mechanism remains the same and can be described by a first order process with a rate limiting step in the condensation reaction.

The influence of Triton X-100 does not differ substantially from the case of SDS, as we observed also in this case a decrease in the average size of the droplets as we increased the surfactant concentration. However, the polydispersities obtained for the Triton-stabilized emulsions are somewhat lower than for SDS-stabilized emulsions (see Fig.4.9b). Additionally, much lower concentrations of Triton X-100 are needed to stabilize the PDMS droplets, which might have important consequences for the encapsulation step.

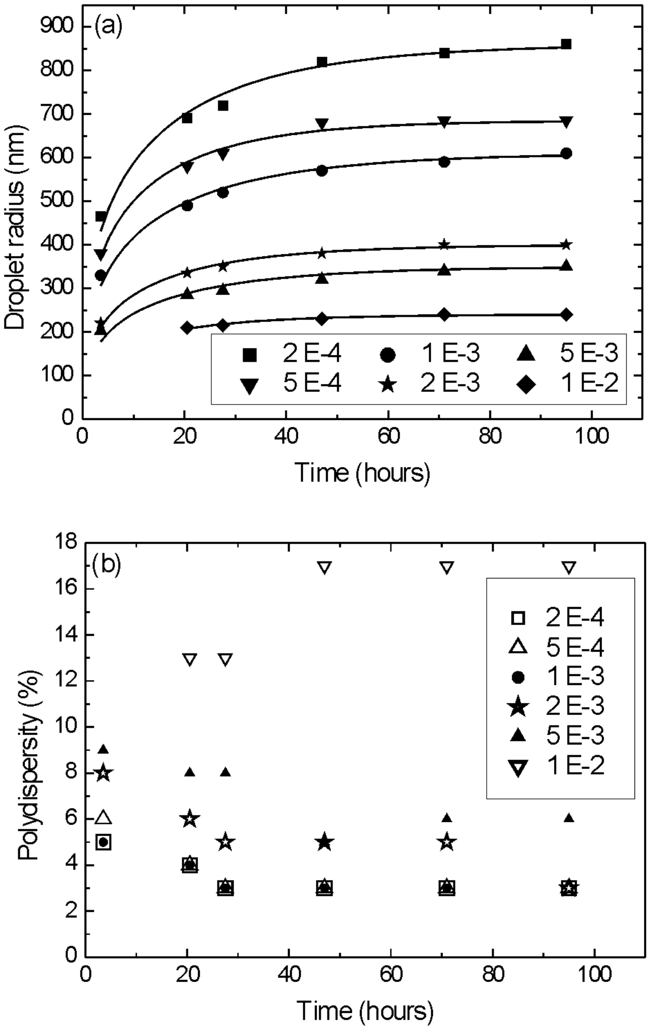

Figure 4.9: *(a) Average droplet radius as a function of time, followed with SLS, for different Triton X-100 concentrations, shown in the legend, for emulsions prepared from 2% v/v DMDES and 2% v/v ammonia solution; lines are fits to Eqn.3.1 with* t_1 *given in Table 4.6.*

4.3.6 Hollow particles from Triton X-100-stabilized oil droplets

PDMS oil droplets prepared from 1 % v/v DMDES and 4 % v/v ammonia or 2 % v/v DMDES and 2 % v/v ammonia and stabilized with different Triton

Table 4.6: *Final droplet size and growth rate data for emulsion droplets prepared from 2 % v/v DMDES, 2 % v/v ammonia solution and different Triton X-100 concentrations.* R_f- *final droplet radius as determined from SLS,* t_1- *fitting parameter obtained by fitting the experimental data with the Eqn.3.1.*

Triton X-100 (% w/w)	R_f (nm)	t_1 (hours)
0.0002	860	26.0 ± 2.0
0.0005	685	20.2 ± 1.2
0.001	610	26.0 ± 1.8
0.002	400	22.2 ± 1.1
0.005	350	24.8 ± 3.0
0.01	240	20.0 ± 0.9

X-100 concentrations, were used as templates for encapsulation experiments. Table 4.7 represents an overview of the emulsions used for coating and contains the concentration of Triton X-100 used to prepare the emulsions, the size and polydispersity of the oil droplets before the coating step, the amount of TEOS added in the second reaction step and the final shell thickness. The samples $S_{1,TX100}$, $S_{2,TX100}$ and $S_{3,TX100}$ were obtained starting with emulsions prepared from 1 % v/v DMDES and 4 % v/v ammonia and three different TX100 concentrations (see Table 4.7). 24 hours after their preparation, 0.02 M TEOS was added in 4 steps (3 min. between steps), during stirring, which continued for one hour. After three days, the cores were removed by washing several times with ethanol. The TEM images of the resulting hollow shells are presented in Fig.4.10. It is very interesting to notice that in contrast to the case of SDS, the Triton X-100 allows the growth of thick shells in one single growth step and microspheres can be formed. Also the amount of secondary nucleation is much reduced.

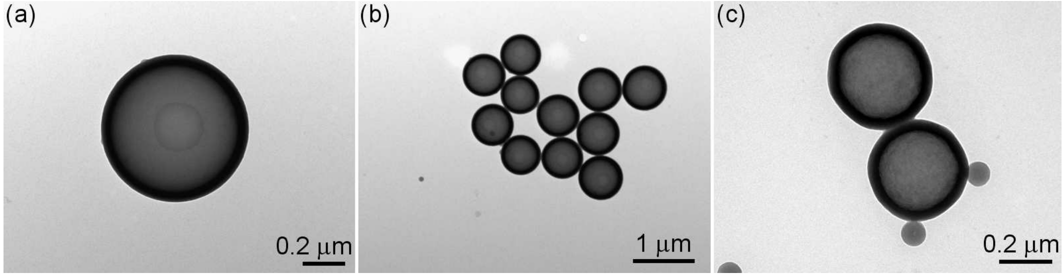

Figure 4.10: *TEM micrographs of hollow shells: (a) Sample* $S_{1,TX100}$, *R = 390 nm, d = 70 nm,* $\delta = 6$ *%; (b) Sample* $S_{2,TX100}$, *R = 320 nm, d = 95 nm,* $\delta = 7$ *%; (c) Sample* $S_{3,TX100}$, *R = 260 nm, d = 85 nm,* $\delta = 16$ *% Size and polydispersity obtained from SLS.*

Table 4.7: *Size and polydispersity of particles obtained from encapsulation of Triton X-100-stabilized droplets as determined by SLS;* R_d*−radius of the droplets used as templates,* δ*−polydispersity and d−shell thickness. The oil droplets were prepared from 1 % v/v DMDES for samples* $S_{1,TX100}$ - $S_{3,TX100}$ *and from 2 % v/v DMDES for the rest of the samples. TEOS was added 24 hours after the emulsion preparation in samples* $S_{1,TX100}$ - $S_{5,TX100}$ *and in samples* $S_{6,TX100}$ - $S_{8,TX100}$ *after 20 hours. For samples* $S_{6,TX100}$ - $S_{8,TX100}$*, the growth of the shell was stopped by dialysis against de-mineralized water.*

Sample	TX100 (% w/w)	R_d (nm)	δ(%)	TEOS (M)	d (nm)
$S_{1,TX100}$	0.001	390	6	0.02	70
$S_{2,TX100}$	0.002	320	7	0.02	95
$S_{3,TX100}$	0.01	260	16	0.02	85
$S_{4,TX100}$	0.001	500	4	0.02	170
$S_{5,TX100}$	0.002	290	9	0.02	100
$S_{6,TX100}$	0.002	265	9	0.02	17.5
$S_{7,TX100}$	0.002	265	9	0.02	27.5
$S_{8,TX100}$	0.002	265	9	0.02	37.5

Fig.4.11 shows TEM images of hollow shells contained in samples $S_{4,TX100}$ and $S_{5,TX100}$, in which the starting emulsion was prepared with 2 % v/v DMDES and 2 % v/v ammonia and two different Triton X-100 concentrations (see Table 4.7). The TEOS was added after 24 hours, following the same procedure described for the previous samples. Except for thick shells, and subsequently microcapsules and microspheres, also microballoon-like particles can be obtained if the shell growth is stopped earlier. This is the case of samples $S_{6,TX100}$, $S_{7,TX100}$ and $S_{8,TX100}$, which were obtained from the same initial emulsion prepared with 2 % v/v DMDES and 2 % v/v ammonia and 0.002 % w/w Triton X-100, to which 0.02 M TEOS was added 20 hours after preparation. The three different samples were obtained by stopping the shell growth after

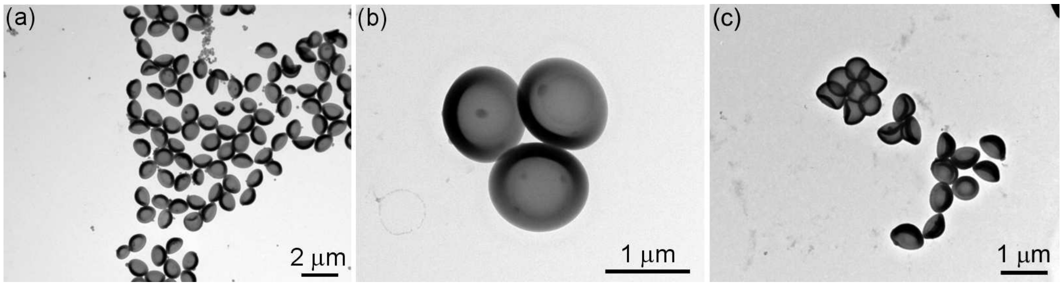

Figure 4.11: *TEM micrographs of hollow shells: (a), (b) Sample* $S_{4,TX100}$*,* $R = 500$ *nm,* $d = 170$ *nm,* $\delta = 4$ *%; (c) Sample* $S_{5,TX100}$*,* $R = 290$ *nm,* $d = 100$ *nm,* $\delta = 9$ *%. Size and polydispersity obtained from SLS.*

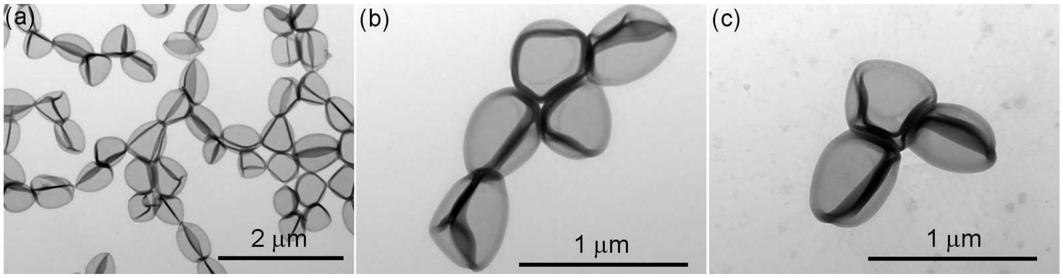

Figure 4.12: *TEM micrographs of hollow shells: (a) Sample* $S_{6,TX100}$*,* $R = 265$ *nm,* $d = 17.5$ *nm,* $\delta = 9$ *%; (b) Sample* $S_{7,TX100}$*,* $R = 265$ *nm,* $d = 27.5$ *nm,* $\delta = 9$ *%; (c) Sample* $S_{8,TX100}$*,* $R = 265$ *nm,* $d = 37.5$ *nm,* $\delta = 9$ *% Size and polydispersity obtained from SLS.*

3 hours, 5 hours and 7 hours respectively, which was done by dialysis against de-mineralized water for two days, after which the samples were washed several times with ethanol. TEM images of the three samples are shown in Fig.4.12.

The encapsulation experiments in which we used Triton X-100-stabilized oil droplets as templates show that this surfactant is more suitable for coating purposes and we can obtain different types of hollow shells, just as without surfactant. The advantage of using Triton X-100 is that it allows us to reduce considerably the size of the particles, which might be important for some experiments, as we will illustrate in Chapter 5.

4.3.7 Coating different oil droplets with solid shells

We preliminarily investigated the possibility of coating also other surfactant-stabilized oil droplets with solid shells, following the same procedure of co-

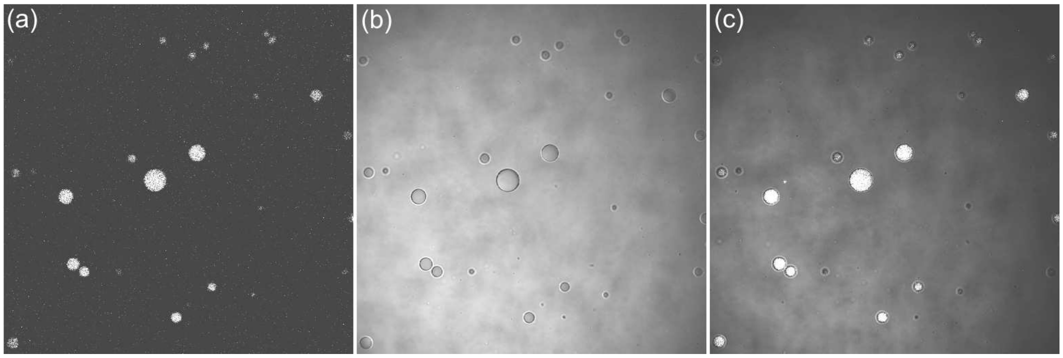

Figure 4.13: *PM 580-labeled cyclohexane droplets coated with a silica/siloxane solid shell in water. (a) The fluorescent droplets imaged in fluorescence mode. (b) Solid shells imaged in transmission mode. (c) Superimposed image of coated cyclohexane droplets in water: light gray - oil droplets in fluorescence mode and dark circles around them - solid shells in transmission mode. Images size: 238* μ*m × 238* μ*m.*

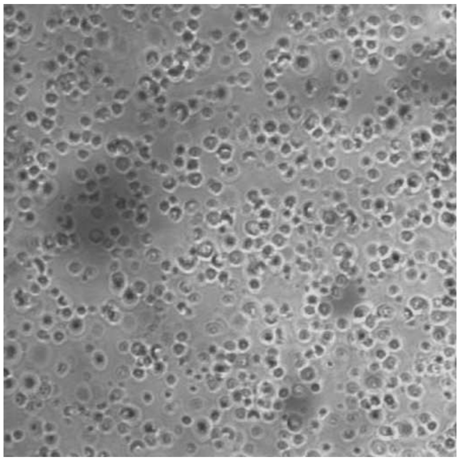

Figure 4.14: *Coated hexane droplets in water showing buckling (transmission mode). Image size: 73 μm × 73 μm.*

polymerization of TEOS with hydrolyzed DMDES. We first prepared Triton X-100-stabilized cyclohexane droplets in water, as described in the synthesis section. The oil was labelled with PM 580. The presence of the droplets was checked, right after their preparation, using confocal microscopy in fluorescence mode. The encapsulation was achieved by adding TEOS together with a solution of hydrolyzed DMDES (see synthesis section), followed by magnetic stirring over night. The coated cyclohexane droplets were observed with confocal microcopy, ≈ 20 hours after the encapsulation: the PM 580-labelled oil droplets were observed in fluorescence mode and the solid shells in transmission (Fig.4.13), which clearly indicated that the oil droplets were surrounded by solid shells.

Hexane droplets in water were prepared following the same procedure but without fluorescent dye. They were also encapsulated in a solid shell using TEOS (see synthesis section) and after ≈ 20 hours after the coating, the core-shell particles were investigated with confocal microscopy in transmission mode. They showed a pronounced buckling (Fig.4.14), probably due to the fast evaporation of hexane. However, the presence of buckled shells it is an indication that the oil droplets are incorporated by solid shells.

We conclude that our method to encapsulate PDMS oil droplets with a silica/siloxane shell can be extended to different oils, but more experiments need to done in order to optimize the procedure.

4.4 Conclusions

In this chapter, we have shown that monodisperse PDMS oil droplets can be prepared also by using surfactants to stabilize them. In our experiments we used two surfactants, one anionic, SDS and one non-ionic, Triton X-100 and we investigated their influence on the size and polydispersity of the oil droplets and on the particles obtained after their encapsulation with solid material. Both surfactants cause a decrease in the average radius of the oil droplets, but they are effective in different concentrations ranges, due to their different CMC. However, the concentrations for which we still observed an influence of the surfactants were somewhat lower than their corresponding CMC's, an effect which we interpreted as a reduction in the CMC value due to the presence of ions and ethanol resulting from the condensation reaction of DMDES. Moreover, in both cases, we found a linear dependence of the droplet radius on the logarithm of the surfactant concentration, indicating that the surfactant mainly influences the oil droplets through a reduction in interfacial tension of the oil/water interface. The formation reaction of the oil droplets in the presence of surfactants was found to take place at the same rate as for the surfactant-free emulsions, with the same growth rates in the average droplet size.

During the encapsulation step, the growth of the shell is limited by the presence of SDS; as a result, by using SDS-stabilized emulsions, we obtained only relatively thin shells which fall into the category of microballoons, towards microcapsules. Although we were not able to detect the presence of SDS in the EDX spectrum, it is very likely that SDS is still present on the surface of the shells and its higher surface charge, possibly in addition to surface wetting properties, prevents the growth of silica monomers and small oligomers to take place. However, the EDX elemental composition indicates that the shells consist of a siloxane/silica copolymer. Attempts to increase the shell thickness in a second growth step resulted in a thicker shell, but extremely rough and inhomogeneous. On the other hand, the presence of Triton X-100 does not seem to disturb the shell growth. By adding TEOS to Triton X-100-stabilized droplets, we can obtain hollow particles of different shell thicknesses, ranging from a few nanometers to ≈ 150 nm in one growth step. It is possible that this difference originates in the much lower amount of Triton X-100 needed to reduce the droplet size.

The fact that we can obtain hollow particles also when surfactant-stabilized PDMS oil droplets are used as templates is important, because it allows us to decrease the final size of the particles, maintaining at the same time reasonably good polydispersities. Moreover, preliminary experiments show that the procedure of coating PDMS droplets with solid shells based on copolymerization of hydrolyzed DMDES and TEOS can be extended also to other types of oil droplets stabilized by surfactants, but more systematic investigations need to be made.

5 Elastic properties of hollow colloidal particles: deformation and buckling

In the first part of this chapter, we probe the elastic properties of micron-sized hollow colloidal particles obtained by emulsion templating by nanoindentation measurements in which point forces were applied to particles supported on a flat substrate. We show that the shells have a linear response up to forces of 7 - 23 nN, depending on the shell thickness. In the linear region, the particle deformation is reversible. The measured Young's modulus ($\approx$ 109 MPa) is comparable with the values for stiff rubbers or soft polymers. We also observed softening and permanent deformation of the shells after probing them repetitively, or beyond the linear regime. In the second part, we present results concerning buckling of oil-filled thin shells in mixtures of water and ethanol. This leads to conformations of nontrivial symmetry, that could be numerically reproduced in a model of homogeneous elastic spherical shells submitted to an isotropic external pressure.

5.1 Introduction

The hollow colloidal particles we prepared by emulsion templating, described in Chapter 2, have shown interesting deformation behavior after drying, as shown in Chapter 3. Therefore, it might be interesting to investigate their elastic properties. Mechanical properties of such particles are potentially important for a variety of applications, such as drug delivery, catalysis and biotechnology. It will also be relevant for the cellular, porous materials that can be assembled from them, as will be shown in the next chapter.

There have been several recent attempts to study the mechanical behavior of various types of shells, and several techniques have been proposed. The developed methods involve observing osmotically induced buckling of polyelectrolyte multilayer capsules immersed in a polyelectrolyte solution, [83, 84] studying of swelling of capsules filled with polyelectrolyte, [84, 85] and measuring the deformation of microcapsules under an applied load using atomic force microscopy. [86–90]

In the first part of this chapter, we investigate the elastic properties of our shells using scanning force microscopy (SFM), following the procedure used in studies on viral capsids. [91, 92] This method allows us to determine in which way the hollow shells respond to an applied point force, what type of deformations appear and most importantly, to extract the material properties. In the second part, we first introduce a simple method to induce buckling of thin shells originally filled with oil, by suspending them in a mixture of ethanol and water. [93] Similar buckling has been reported using osmotic pressure created by polyelectrolyte solutions. [83] However, we additionally find a shape change in which the bowl-shaped shell takes on a polygonal symmetry. We analyzed the buckled conformations using transmission optical microscopy and compared them with configurations obtained from Surface Evolver simulations, using a model of homogeneous elastic spherical shells submitted to an isotropic external pressure. [71]

5.2 Experimental section

5.2.1 Sample preparation

Indentation experiments. The hollow shells used in the scanning-force microscopy (SFM) experiments were prepared by the procedure described in Chapter 4. The polydimethylsiloxane (PDMS) oil droplets used as templates were stabilized with surfactant in order to obtain smaller sizes for the final particles. The emulsions were prepared from 2 % v/v dimethyldiethoxysilane (DMDES), 2 % v/v ammonia and 0.002 % w/w Triton X-100, to which 0.02 M tetraethoxysilane (TEOS) was added 20 hours after preparation. By interrupting the shell growth after 3 hours, 5 hours and 7 hours respectively, we obtained three different samples having the same size of the cores and different shell thicknesses. The particles were washed several times with ethanol in order to remove the oil from the core, after which they were transferred to de-mineralized water. The size of the core and thickness of the shell were measured with static light scattering (as described in Chapter 2). A few experiments were performed on bigger hollow particles (core radius 390 nm and shell thickness 40 nm), prepared by templating surfactant-free emulsions, using the procedure described in Chapter 2 for the capsule-like particles.

The samples used for SFM were prepared as follows: a droplet of 40 μL of the dispersion of shells in water was deposited on a glass slide (0.15 mm thickness and 22 mm diameter) mounted on the piezo holder. After deposition, the excess dispersion was gently removed with a Pasteur pipette, keeping the surface wet and replaced by de-mineralized water. In order to attach the shells to the surface, the glass slides were first coated with 3-aminoprolyl-triethoxysilane (APS) by keeping them for 1.5 hours in a solution containing 170 mL ethanol, 4.5 mL ammonia solution and 23.5 mL APS, after which they were dried under nitrogen.

Buckling experiments. To determine the buckling threshold in solution, we prepared PDMS oil droplets from 2 % v/v DMDES and 2 % v/v ammonia (in 25 mL total volume), with radii of 540 nm, 650 nm and 690 nm respectively. We added TEOS (0.018 M) 24 hours after the emulsion preparation. We took samples at different times during the shell growth (after 2.5 h, 7 h, 25 h and 49 h, respectively) and we measured the shell thickness with SLS. The suspensions were then mixed with equal volumes of ethanol in order to induce buckling. The particles we used for investigating the fine structure of thin shells consisted of much larger PDMS oil droplets coated with very thin solid shells (thickness between 5-20 nm). They were prepared using the same procedure as described in Chapter 2 for microballoon-like particles. In order to obtain bigger particles, we increased the concentration of DMDES and ammonia to 5 % v/v and the droplets were allowed to grow for three days before the encapsulation step. This resulted in somewhat more polydisperse particles with sizes between 3 and 6 μm. The buckling was induced by adding ethanol to the suspensions of particles., which makes the PDMS soluble in the medium. The volume of ethanol added was varied between 10 and 90 %, but we did not observe differences in the phenomena in this range. All the observations discussed in the results section refer to samples for which we used 50 % ethanol by volume.

5.2.2 CHARACTERIZATION

Scanning-force microscopy (SFM). The SFM measurements were performed at the Vrije Universiteit in Amsterdam, with a scanning force microscope (Nanotec, Madrid) operated in "jumping mode" in liquid. [91, 94] In this mode, imaging is achieved by a succession of force-distance (FZ) curves, executed in several milliseconds in a raster scanning fashion. Lateral displacements occur only when the tip is not in contact with the sample, thereby minimizing shear forces. A complete description of the apparatus and the measurement procedure can be found in ref. [94]. The maximal applied force is well defined because each individual approach is stopped at the cantilever deflection corresponding to the set force. FZ curves were recorded by measuring cantilever deflection (force) as a function of the vertical position of the Z-piezo to which the sample was mounted. The relation between the voltage output and the force was first determined by making force-distance (FZ) measurements on the substrate surface next to the shells (FZ on glass). We recorded sample FZ curves after positioning the SFM tip above the center of individual shell, which was located by stopping the cantilever in the middle of a topographical scan of a shell. The tip position was then fine-tuned by making a profile scan and by redirecting the tip to the middle of the shell cross section. The FZ curves were recorded in slow mode ($\approx$ 1 sec), in sequences of three successive curves. The experiments were performed in liquid (water) to investigate the shells in un-deformed state. The cantilevers used (OMCL-RC800PSA, Olympus, Tokyo) had nominal spring constants of 0.05 N/m, 0.07 N/m, 0.1 N/m, 0.39 N/m and 0.76 N/m, respectively. The tip radii of the cantilevers were $\approx$ 20 nm.

Transmission optical microscopy. The buckled shells in solution were observed using a Leica confocal scanning microscope, type TCS-SP2 operated in transmission mode, using glass capillaries (0.1 × 2.0 mm) filled with the suspension.

5.3 RESULTS AND DISCUSSION: INDENTATION

5.3.1 RESULTS

The SFM measurements were performed on different samples consisting of suspensions of hollow shells (filled with water) in water. An overview of the samples used in these experiments is given in Table 5.1. The first three samples used were obtained using the same oil droplets as templates and were encapsulated in solid shells with different thicknesses. The last sample consisted in somewhat bigger particles and was used only in some preliminary experiments. Imaging of the shells was first performed at low resolution and low maximal force (<2 nN) to determine their position (Fig.5.1). High resolution scans of individual shells showed that most of them were intact (except for a small number of shells already deformed due to partially drying during sample preparation) and they were attached firmly to the glass surface. After individual objects were imaged, indentation measurements were performed, following the procedure described in the experimental section.

Table 5.1: *Size and polydispersity of particles used in SFM experiments, as determined by SLS; R_c−core radius , d−shell thickness, δ−polydispersity in the total size and R−average radius of the particle ($R = R_c + d/2$).*

Sample	R_c(nm)	d (nm)	δ(%)	d/R
Sa	265	17.5	9	0.06
Sb	265	27.5	9	0.09
Sc	265	37.5	9	0.12
Sd	390	40	8	0.09

In Fig.5.2 three successive FZ curves for a single shell from sample Sa are shown. For the measurements on this sample we used a cantilever with a spring constant of 0.05 N/m. The dashed line represents the FZ curve performed on the substrate surface next to the shell and it has been translated to match the contact points. The horizontal differences between this line and successive FZ curves correspond to the extent of indentation of the shell. All the shells from this sample exhibited the same behavior. We found that our shells respond linearly to a force of up to 8 ± 0.8 nN (n = 12 shells measured). Above this value, slight deviations from linearity were observed, possibly due to softening of the shells. The maximum force applied for this sample was ≈ 11 nN. At this force, the shells were indented by 31 ± 3.9 nm (n = 12), which represents ≈ 5.5 % of their total height. The shells would still recover to their initial shape after such deformation; images taken immediately after indentation show no evidence of damage. However, we observed a softening of the objects after

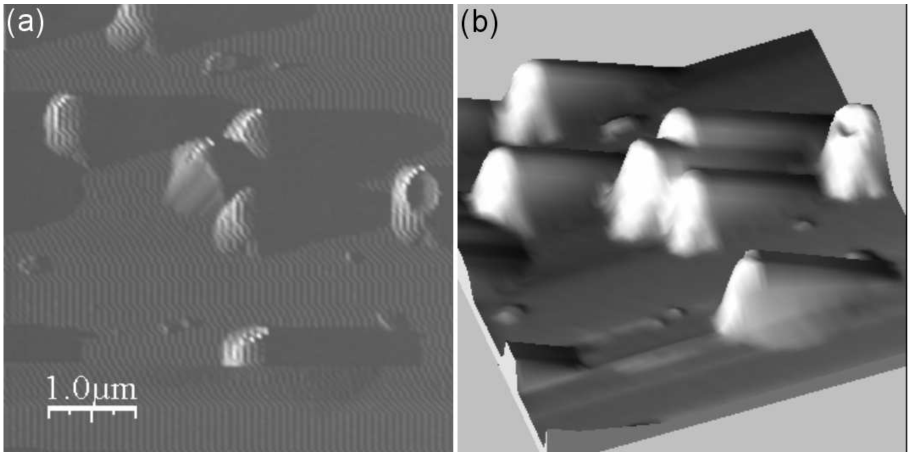

Figure 5.1: *Low resolution SFM images of shells from sample Sc in water (scan area, 5 µm×5 µm, 128×128 pixels): (a) direct topographic image; (b) the same image in 3D representation. A collapsed particle can be seen on the right of the images.*

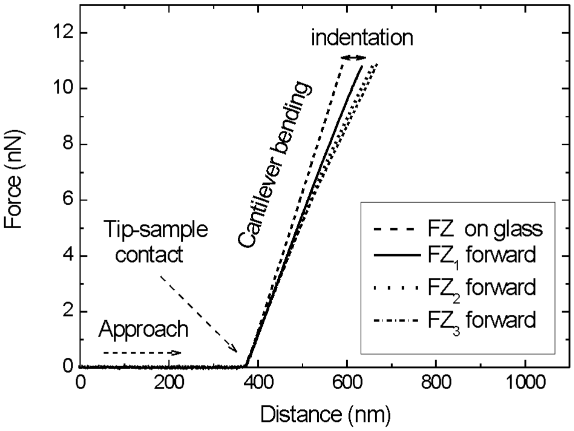

Figure 5.2: *Typical FZ indentation curves on a single shell from sample Sa. Distance represents the vertical z-piezo displacement. The most left dashed curve shows the cantilever on the glass surface. The glass curve was shifted along the z axis to match the tip-sample contact point of the shell and to allow direct readout of the indentation of the shell resulting from the applied force.*

the first FZ curve from the series, indicated by the decrease in the slope of the FZ curves (see Fig.5.2); therefore to determine the elastic response of the shells, we always used the linear part of the first forward FZ curve (FZ_1).

The second sample (Sb, Table 5.1), was measured using a slightly stiffer cantilever, with a spring constant of 0.1 N/m; the maximum force applied in this case was $\approx$ 23 nN. An example of an object from this sample is shown in Fig.5.4a,b, for which we first measured a series of slow FZ curves (see Fig.5.3). At forces beyond $\approx$ 15 nN, deviations from linearity were observed, with the slope of the FZ curves decreasing (Fig.5.3). The maximum deformation of the shell after the FZ series was $\approx$ 67 nm (about 11.5 % of the total diameter). The shell suffered a permanent deformation, as can be seen in the images taken right after the first FZ series. (Fig.5.4c,d).

In order to test the limits of the shell material, we applied on the same object already indented, two more series of FZ curves, up to the same maximum force, recorded this time in fast mode (8ms per curve). The images taken after each series show an increase of the permanent deformation (Fig.5.4e-h). Indentation experiments performed on several more shells from sample Sb showed that these shells respond linearly up to forces of 15 $\pm$ 1.9 nN (n = 8), while the maximum force applied was $\approx$ 23 nN. The deformations induced were permanent in this case, and were in the range 33 - 70 nm.

The third sample, Sc (Table 5.1), was measured using two different cantilevers, with spring constants of 0.39 N/m and 0.76 N/m, which allowed us

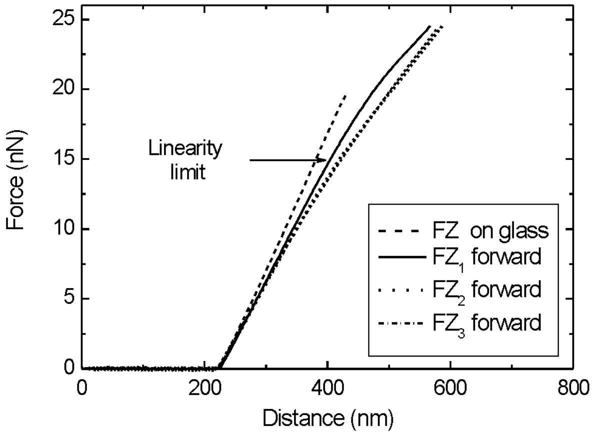

Figure 5.3: *FZ indentation curves on a single shell from sample Sb; the most left dashed curve shows the FZ on the glass. The object before the indentation is shown in Fig.5.4a,b and after the FZ series presented here, in Fig.5.4c,d.*

to apply maximum forces of ≈ 46 nN and ≈ 58 nN, respectively. The shells showed the same behavior in both cases: they responded linearly up to forces

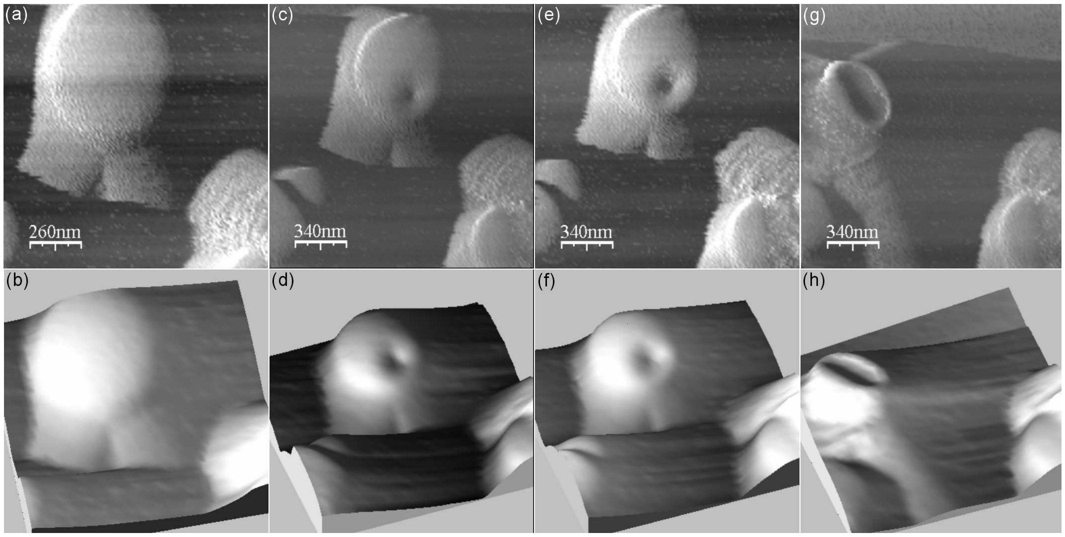

Figure 5.4: *SFM images of a shell from sample Sb in water:(a) direct topographic image of the shell before indentation; (b) the same image in 3D representation; (c) direct image of the same shell after the first FZ series shown in Fig.5.3; (d) the same image in 3D. (e) SFM image of the shell after the second FZ series, with 3D representation in (f). (g) SFM image of the shell after the third FZ series, and (h) the 3D representation of it.*

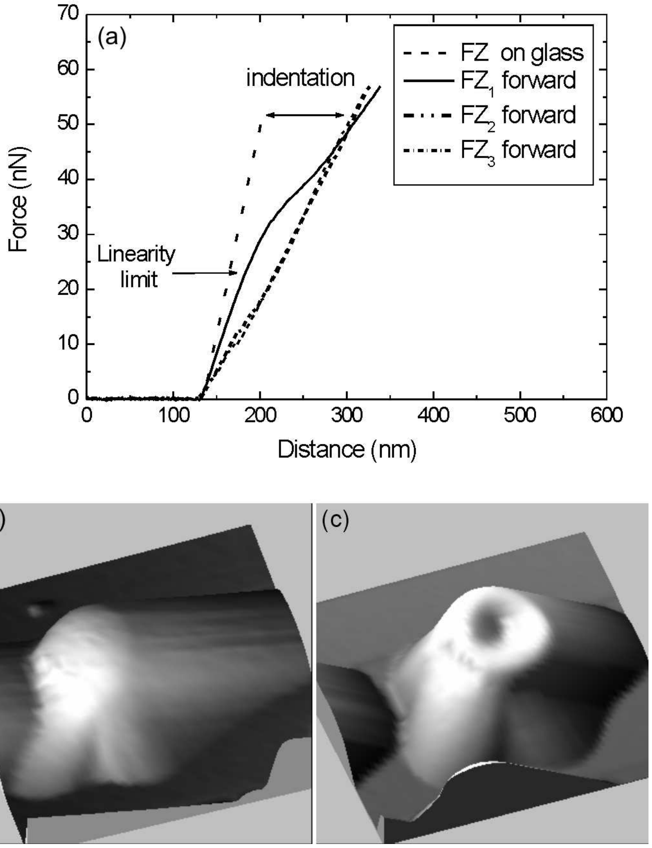

Figure 5.5: *(a) FZ forward indentation curves performed on a shell from sample Sc; (b) 3D SFM image of the shell in water before indentation; (c) 3D SFM image of the shell after the FZ series. For both SFM images, scan area 1.7 μm × 1.7 μm.*

of 23 ± 3.5 nN (n = 16), after which significant deviations from linearity were observed. A typical example of indentation of a shell from sample Sc is presented in Fig.5.5. In this particular case, as a result of the applied force (using the 0.76 N/m cantilever), the maximum indentation achieved was ≈ 110 nm (≈ 18 % of the total diameter). As can be seen from Fig.5.5c, the image taken after the indentation shows a permanent deformation.

The experiments performed on shells from sample Sc, with both cantilevers, revealed a peculiar two-population distribution of particles. The objects appeared to respond slightly differently when the same forces were applied. This is illustrated in Fig.5.6, in which we show two different objects from sample Sc, before and after we applied the same maximum force (≈ 58 nN). The maximum indentation achieved was ≈ 85 nm for object 1, and ≈ 131 nm for object 2. Moreover, the linearity regime was slightly longer extended for object 1 (up to ≈ 31 nN), compared with object 2 (up to ≈ 26 nN). It is clear, both from the FZ curves and SFM images, that the second shell is somewhat softer than the first one.

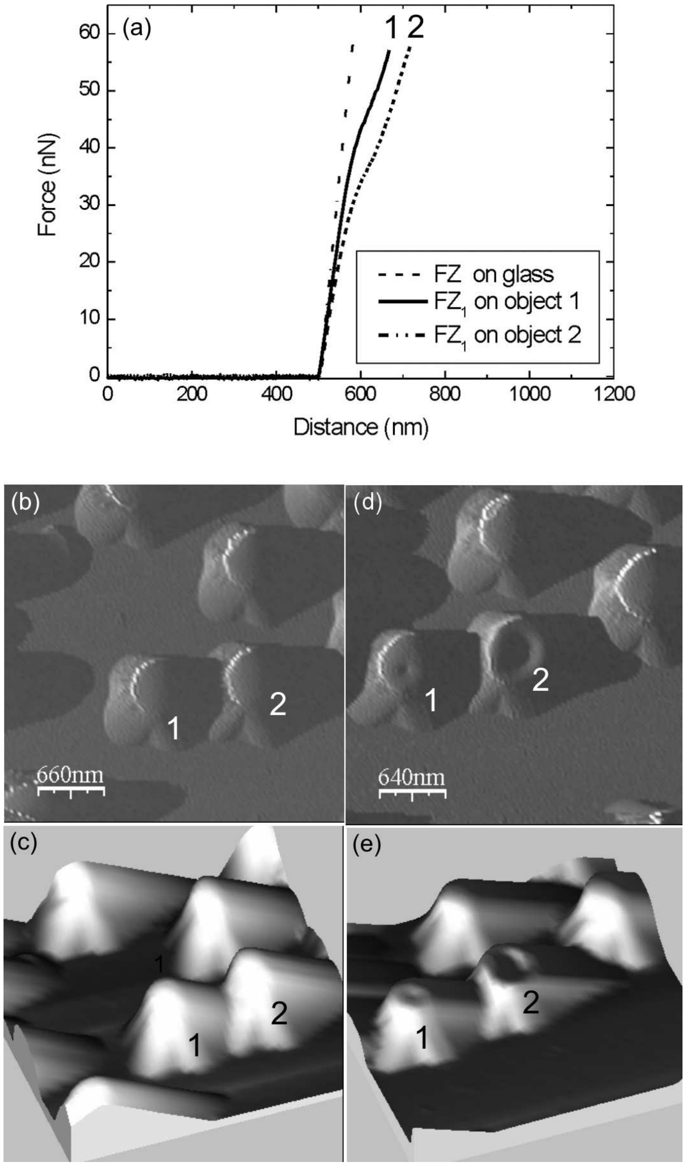

Figure 5.6: *(a) First forward FZ indentation curves performed on the objects 1 and 2 indicated in the SFM images.(b) Direct topographic SFM image of shells from sample Sc in water before indentation; (c) the same image in 3D representation. (d) SFM image of the objects after the FZ series and (e) the same image in 3D representation.*

By measuring the height of the objects before indentation, we found a difference of ≈ 10 % between the height of the softer and stiffer objects. Therefore, the differences in stiffness probably came from the bidispersity of the sample. In the quantitative investigations of the elastic response of the shells, we treated sample Sc as two distinct populations, Sc1 and Sc2.

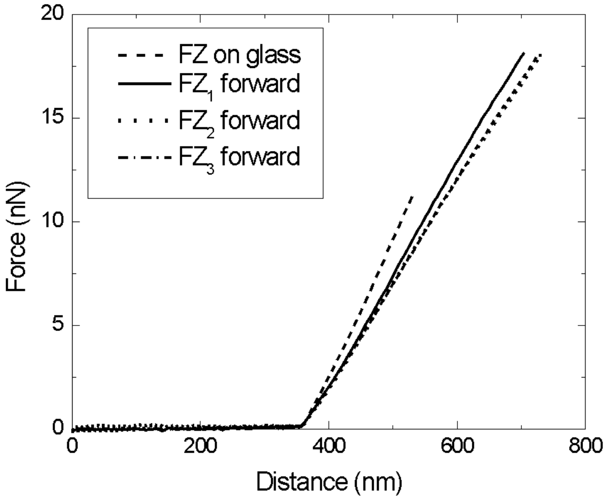

Figure 5.7: *Typical successive FZ indentation curves on a single shell from sample Sd; the most left dashed curve shows the cantilever on the glass surface.*

We also performed several experiments on bigger particles, sample Sd from Table 5.1, but with the same ratio d/R as sample Sb. Due to the limitations of the set-up concerning the scanning area and the imaging of bigger objects, we only measured a few particles. We used a cantilever with a spring constant of 0.07 N/m and the maximum force applied was ≈ 18 nN. We found elastic deformation of the shell as a result of the applied force, indicated by the linearity of the first FZ curve (Fig.5.7), similar with the case of smaller particles. Also, a slight softening of the structure after the first deformation was observed, indicated by the decrease of the slope for the second and third force-distance curves. The maximum indentation achieved was ≈ 50 nm., but no permanent deformation was identified after the FZ series.

5.3.2 DISCUSSION

The mechanics of thin-shells predict a linear elastic response for the indentation of a homogeneous spherical shell up to an indentation magnitude (Δz) on the order of the shell thickness (d) [71, 95], in which case, the applied force (F) is

$$F \sim \frac{Ed^2}{R}\Delta z \tag{5.1}$$

with E - Young's modulus and R - average radius of the shell. The linear response we obtained for our shells, up to forces of several newtons (first part of the FZ curves) indicates that they behave indeed as expected for such objects. Beyond this regime, nonlinear buckling is predicted because of the coupling of in-plane compression and out-of-plane bending. Moreover, the applied force is expected to be [95]

$$F \sim \frac{Ed^{5/2}}{R}(\Delta z)^{1/2} \tag{5.2}$$

for deformations larger than the shell thickness, which agrees well with the deviations from linearity observed in our measurements in the last part of the FZ curves.

The spring constant of a thin homogeneous shell of radius R can be related to the Young's modulus, E, of the shell material. The simplest model for the elastic response is to consider our object to be an elastic thin spherical shell undergoing small deformations. In that case,

$$F = k_{shell}\Delta z \tag{5.3}$$

with the spring constant

$$k_{shell} = \alpha E\frac{d^2}{R} \tag{5.4}$$

where α is a geometry-dependent proportionality factor, which depends on the Poisson ratio σ of the material and the geometric quantities d and R. [71] For our objects, the thin-shell approximation $d/R \ll 1$ is clearly applicable. Furthermore, assuming that the shell is composed of a linear elastic material with a Poisson ratio of 0.3, the value for the constant α we used was 2.25. [91,92]

In the case of deformations of closed capsules, the problem of the permeability/partial volume conservation is often encountered. [96] For an impermeable shell the volume is constrained. This leads to an additional restoring force which arises since the shell has to be stretched to keep the volume constrained when the spherical capsule is deformed. This contribution to the force is: [96]

$$F_{volume} \approx \frac{2\pi}{3}\frac{Ed}{R^2}E(\Delta z)^3 \tag{5.5}$$

Therefore, it does not affect the linear part of the FZ curves. Furthermore, it predicts a steepening of the FZ curves with displacement in z which was not observed in our experiments. On the contrary, we found a decrease in the slope of the FZ curves with increasing distance. This is an indication that on the time scale of the indentation ($\approx$ 1 s), the shell is fully permeable.

Spring constants for the shells can be obtained from the slopes of the forward FZ curves in the linear regime. The shell and cantilever can be considered as two harmonic springs in series. The spring constant of the shell (k_{shell}) is then related to the effective (measured, k_{eff}) spring constant, (the slope of the FZ curve), and k_c, the cantilever spring constant by:

$$k_{shell} = \frac{k_c k_{eff}}{k_c - k_{eff}} \tag{5.6}$$

Mean values of the spring constant distributions for each sample measured are shown in Table 5.2, and plotted in the histograms in Fig.5.8a. The values obtained for the spring constants show an increase of the object stiffness with increasing shell thickness. Although we measured only a few particles from sample Sd, the k value agrees quantitatively with the one obtained for sample Sb, in which the shells had the same d/R ratio.

Table 5.2: *Spring constants (k) for samples Sa, Sb, the two population found in sample Sc, Sc1 and Sc2, and sample Sd; threshold forces (F) up to which the shells respond linearly to the applied forces.*

Sample	k (N/m)	F (nN)
Sa	0.33 ± 0.04 (n=14)	10.6 ± 1.0
Sb	0.45 ± 0.04 (n=8)	15.0 ± 1.9
Sc1	1.04 ± 0.10 (n=9)	25.9 ± 1.7
Sc2	1.50 ± 0.10 (n=6)	25.9 ± 4.5
Sd	0.41 ± 0.02 (n=3)	17.1 ± 1.0

With the Eqn.5.4 and the measured k_{shell}, we can estimate Young's modulus of the shell material by taking the values of d and R obtained from SLS (Table 5.1). The E values calculated are plotted in the histogram in Fig.5.8b. Assuming that the shell material is the same in all three samples, we obtained a Young's modulus of 0.109 ± 0.027 GPa (n=37). There are several factors which are responsible for the spread in the E values. First of all, the polydispersity in particle size (determined by SLS) contributes to the spread in k values determined experimentally, as not all the particles from the same sample responded exactly in the same way to the applied force. Moreover, the size of the particle core was determined (with SLS) right before the encapsulation step and was used to determine the final size and polydispersity of the core-shell particles. Therefore there is an uncertainty in the shell thickness which arises from the polydispersity of the core. This will appear in the E values, in which the shell thickness is present as d^2. Furthermore, the value we used for the factor α was calculated for ratio's $d/R \approx 0.1$. This can also affect slightly the E values. Finally, we assume the same material for the shells in each case,

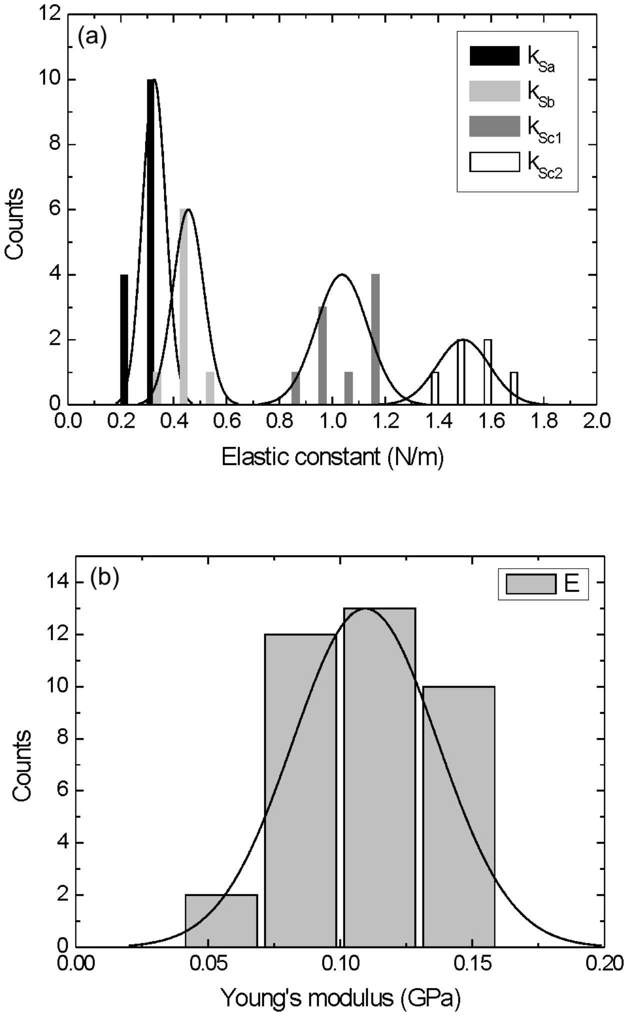

Figure 5.8: *(a) Histograms of measured spring constants (b) Histograms of calculated Young's moduli. The drawn lines are Gaussian fits.*

but the pores can be distributed differently over the shell for different shell thickness and can lead to differences in Young's modulus.

Taking into account the density of the shell material (≈ 1000 kg/m^3), this value for Young's modulus indicates that our shells are made of a material which is somewhere at the boundary between a stiff rubber and soft polymer (Fig.5.9). This is not unusual, considering that the shell represents in fact a cross-linked network in which the main components are dimethylsiloxane units, as we have shown in Chapter 3.

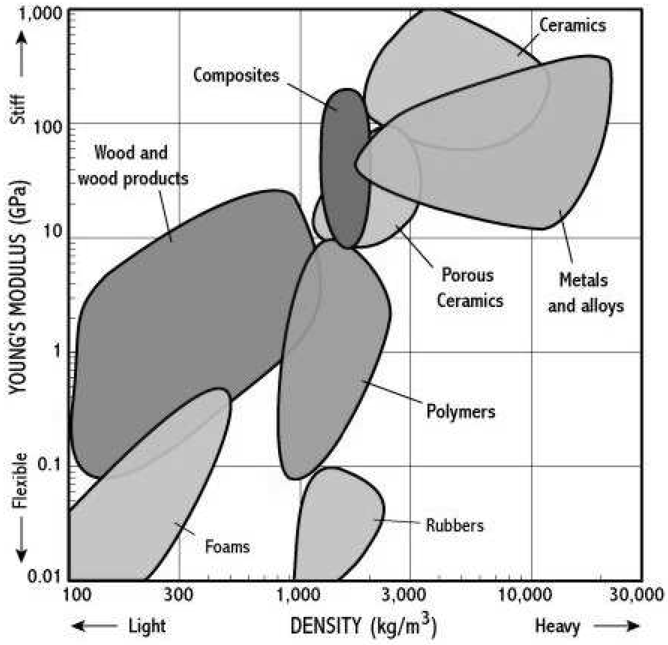

Figure 5.9: *Young's modulus as a function of the density for various materials. [97]*

5.4 Results and discussion: buckling

5.4.1 Study of buckling threshold

We discussed in section 3.3.4 (Chapter 3) the influence of drying on the three different types of hollow particles we synthesized. We concluded that the main factor which influences the particle behavior is the relative shell thickness (d/R). The deformation of the shells can be explained considering the same arguments used in literature for buckling of spherical shells. [98, 99] As the solvent trapped inside the shells begins to evaporate through the shells, solvent-air menisci grow hollow in the pores of the shell. This causes, for each pore, a global inwards capillary force. At larger scale, the effect is similar to an (maximum) external effective pressure

$$p_{eff} = \frac{\gamma}{a} \tag{5.7}$$

where γ is the solvent surface tension and a the typical diameter of the pores. Occurrence of buckling of thin spherical elastic shells is predicted by elasticity theory [71] to happen for a critical pressure

$$p_c = \frac{2E}{\sqrt{3(1-\sigma^2)}} \left(\frac{d}{R}\right)^2 \tag{5.8}$$

with E the Young modulus of the shell material, σ is the Poisson ratio, d shell thickness and R the average radius of the particle. When the effective pressure

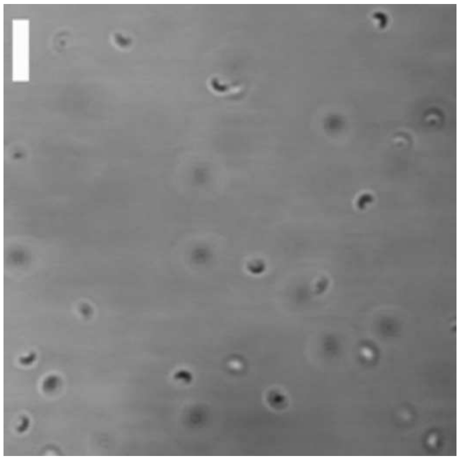

Figure 5.10: *Transmission optical microscopy image of a suspension of buckled colloidal silica/siloxane shells. Scale bar 5 μm.*

is realized through evaporation, it cannot be easily varied, as it is fixed by the solvent and the porosity of the shell. However, we can tune the macroscopic geometry in order to determine the critical relative thickness $(d/R)_c$ under which buckling occurs (R represents the average radius). From equations 5.7 and 5.8, the latter is expected to scale as:

$$\left(\frac{d}{R}\right)_c = \left(\frac{\sqrt{3(1-\sigma^2)}}{2}\right)^{1/2} \left(\frac{\gamma}{aE}\right)^{1/2} \tag{5.9}$$

According to the diagram presented in Fig.3.6 (Chapter 3), the relative thickness below which deformation occurs as a result of drying is: $(d/R_t)_{c,air} \approx 0.3$. Considering that for ethanol $\gamma = 22.4$ *mN/m* at 20°C, we obtain from Eqn.5.9 $aE = 0.21\ J/m^2$. With the Young modulus $E \approx 109$ MPa (as determined in section 5.3.2), the pore size can be approximated at $a \approx 1.9$ *nm*. This is in very good agreement with the permeability experiments presented in Chapter 3, from which we concluded that the diameter of the pores should be at least 1.1 nm (the longest diameter of the FITC molecule).

Buckling in solution was obtained, as mentioned in the experimental section, by mixing suspensions of oil-filled thin shells in water with the same volumes of ethanol. Surprisingly, we observed that the shells are all deformed in solution into a bowl-like shape (Fig.5.10). Since the particles in water did not show any deformation, the buckling must occur due to the presence of ethanol. This can be explained as follows: some of the low molecular weight PDMS from the oil droplets is dissolved in the exterior medium consisting of ethanol/water mixture, since ethanol is a good solvent for PDMS, while water is not. As a result, we should expect that there is an interface between the remaining oil and water/ethanol solvent in the pores. When the inner

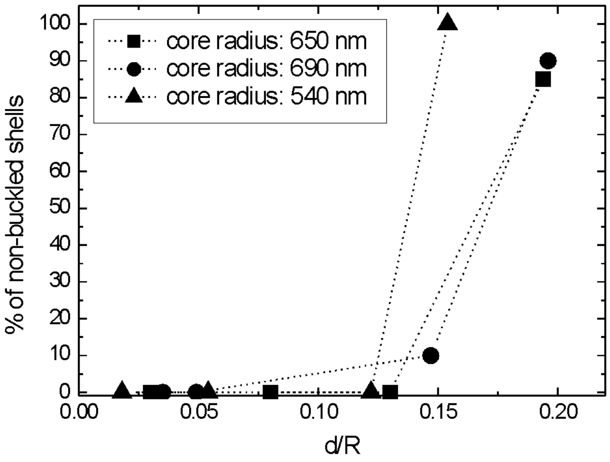

Figure 5.11: *Proportion of the shells keeping their spherical shape in solution after equivalent volume of ethanol have been added. Observations were performed on probes taken at different time during the shell growth. The symbols represent the three different samples used in the experiment, with different core-radius of the droplets used for encapsulation. Buckling clearly occurs under a relative shell thickness* $(d/R)_c \approx 0.17$.

oil dissolves into the external medium, one expects that a capillary force acts the same way as during drying, and Eqn.5.9 is expected to stay valid, with γ representing the oil/solvent interfacial tension.

Using optical microscopy, we determined the percentage of buckled shells. The results are presented in Fig.5.11, each point corresponds to 40 to 80 objects. The relative thickness below which buckling occurs was estimated at $(d/R)_{c,solution} = 0.17$. Using this and the value for the interfacial tension $\gamma_{oil/water} = 14$ mN/m (determined for the same type of synthesized-PDMS in water [70]), we obtained from Eqn.5.9, for $aE \approx 0.40$ J/m^2, which is in good agreement with the value obtained for the deformation induced by drying, considering all the assumptions we made. Furthermore, the value for the surface tension of PDMS we used was determined for PDMS in water and the presence of ethanol probably has an influence on this value.

In order to resolve the post-buckling structure by transmission optical microscopy, we used a sample of particles with radii between 3-6 μm. Once buckled in solution, they were found to hold a single depression with significant volume compared to that of the sphere. Moreover, it was not axisymmetric anymore. In one case (Fig.5.12) we did observe apparently similar objects, with a coffee-bean shape. This type of conformations were reported in literature for red blood cells and they were obtained both experimentally, [100] or using numerical simulations. [101, 102]

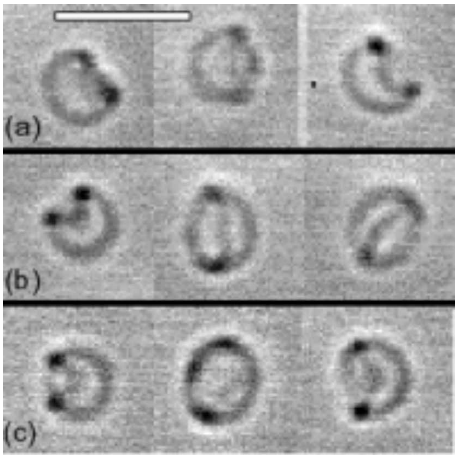

Figure 5.12: *Typical transmission optical microscopy images of particles from a suspension of colloidal spheres filled with oil, in a mixture of water and ethanol. Three different objects are displayed under three different views; they all show the same coffee-bean buckled shape, with an elongated depression. Scale bar 4 μm.*

In all other cases, the depression presented radial wrinkles, in a number varying from 4 to at least 8 (Fig.5.13), 7-8 being an upper limit that we could distinguish with these shell sizes, and count the wrinkles through optical microscopy. As the particles used for these experiments were not monodisperse enough in order to accurately determine their thin shell thicknesses (of the order of 5-20 nm) with light scattering, we could not differentiate the shell features that lead to different numbers of wrinkles. However, the fact that such structures can be obtained in solution is a novelty in itself. Comparable shapes obtained from hollow colloids were obtained from polystyrene shells filled with organic compounds through evaporation in air, [103, 104] but they were not as regular in shape. This may have been due to the fact that these particles were first dried before observation by electron microscopy.

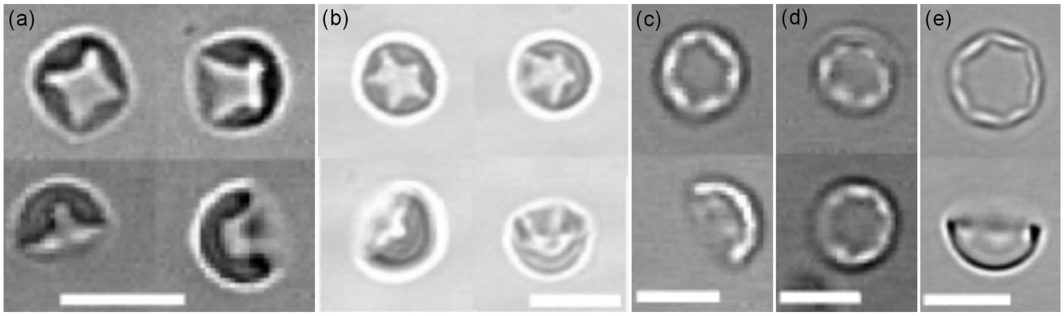

Figure 5.13: *Spherical shells buckled in solution, showing 4 to 8 wrinkles. Each sub-figure shows different transmission optical microscopy views of the same object. Scale bar 5 μm.*

Calculations of the elastic energy contained in the depressions at the surface of an elastic spherical shell [105], showed that conformations with a single depression (formed by inversion of a spherical cap) were more favorable than multiple depressions, for a significant relative volume change ($\Delta V/V > 0.7$, where $\Delta V/V = (V_0\text{-}V)/V_0$, V_0 - initial volume of the unstrained sphere.). Here we do observe a single depression on the shells, but with radial wrinkles. It is interesting to find out if some shell heterogeneity has to be invoked to explain such conformation, or if a model of elastic homogeneous spherical shells is sufficient to recover these non-trivial shapes. This will be done in the following section, using numerical simulations.

5.4.2 Simulations of elastic shells

The elastic energy stored in the deformation of a thin sheet of an isotropic and homogeneous material may be split into a bending and a stretching part [106] and we can write for the free energy

$$F = \int_{shellsurface} \left(\frac{1}{2} k (c - c_0)^2 + \frac{1}{2} A \left(\frac{\Delta S}{S} \right)^2 \right) dS \tag{5.10}$$

where

$$k = \frac{E d^3}{12(1-\sigma^2)} \tag{5.11}$$

is the bending constant [71], $A = Ed$ the stretching constant (E - Young's modulus of the material and d the shell thickness), and c_0 the spontaneous curvature of the shell (which is zero for a flat sheet, but $1/R$ for a spherical shell). As the surface integral scales like R^2 (R being the radius), a dimensionless parameter likely to drive the succession of configurations resulting from the balance between bending and stretching energy is

$$\left(\frac{k/A}{R^2} \right)^{1/2} = \frac{1}{\sqrt{12(1-\sigma^2)}} \frac{d}{R} \tag{5.12}$$

to which we will refer to as λ in the following discussions ($1/\lambda^2$ is known in the literature as Föppl-von Kármán number). It is interesting to note that this model shows that the conformations should be independent of E and finally depend only on the relative thickness d/R.

The simulated configurations presented in the following were obtained using the free software Surface Evolver [107], in which the elastic energy given by equation 5.10 is minimized in the space of conformations. The minimization was performed by alternating gradient, conjugate gradient and hessian methods. Such an approach was initiated by Tsapis et al. [99] and the same Surface Evolver routines were used in the present study.

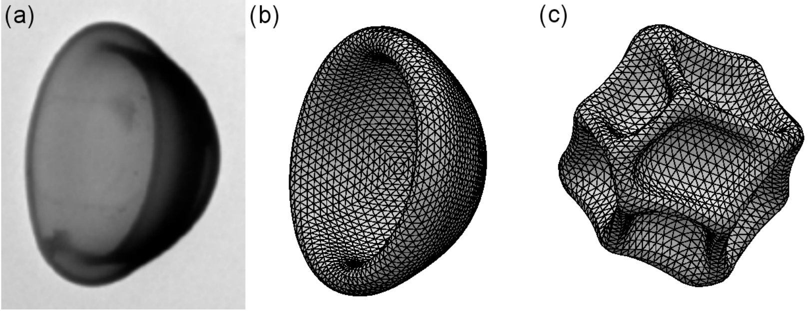

Figure 5.14: *(a) Capsule obtained from evaporation in air of a spherical shell of mean radius 870 nm, shell thickness 150 nm (TEM image). (b) Simulation obtained for a relative volume variation $\Delta V/V = 0.76$ performed with $\lambda = 0.049$; minimization was performed first with a zero curvature and then $c_0 = 1/R$. (c) The same λ and $\Delta V/V$, minimization directly performed with $c_0 = 1/R$. The elastic energy of this configuration is 26.3 times more important than for configuration b.*

The simulations results are characterized by the parameter λ which should scale in this infinitely thin surface model like the relative thickness d/R. We explored a discrete range of λ and the equilibrium conformations were examined by stepwise decreasing the inner volume. The entire process is very similar to what was done in [99], except for what concerns the spontaneous curvature c_0. As the shells are formed by templating the oil droplets, one can assume that they are unstrained in their initial state, hence the spontaneous curvature is expected to be $c_0 = 1/R$. But at each volume step, we first minimized with $c_0 = 0$ before changing to $c_0 = 1/R$ (which was the value used in [99]) and then minimizing again. Imposing a zero spontaneous curvature lowers the energy barrier for the merging of two different depressions at the surface of the sphere (merging happens through flattening of the high positive curvature ridge that separates the two depressions). This helps to get out of some local minima in

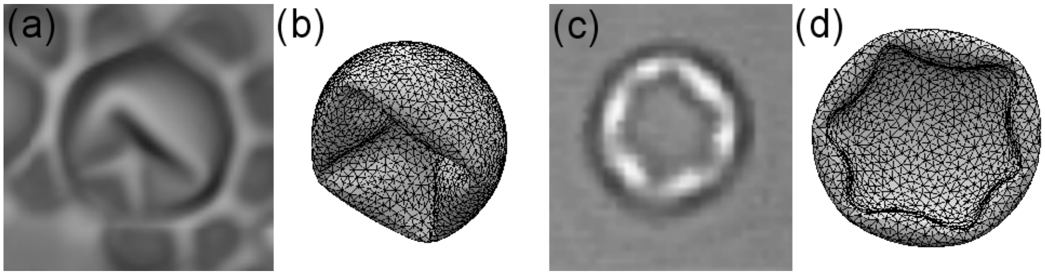

Figure 5.15: *(a) Dried shell ($d/R \approx 0.012$), transmission optical microscopy image, size 17 μm × 17 μm. (b) Simulation of a configuration with 4 wrinkles: $\Delta V/V = 0.36$ and $\lambda = 0.0116$. (c) Buckled shell in solution, transmission optical microscopy image. (d) Simulation of a configuration with 6 wrinkles: $\Delta V/V = 0.67$ and $\lambda = 0.015$.*

which the conformations are easily quenched, as is quite common in buckling problems.

As an example, Fig.5.14 shows the structures obtained for $\lambda = 0.049$ and $\Delta V/V = 0.76$. The configuration from Fig.5.14c was obtained by minimizing directly at $c_0 = 1/R$ and the one from Fig.5.14b by minimizing first at $c_0 = 0$ before changing to the desired value $1/R$. The elastic energy is decreased for the latter case by a factor ≈ 26. It was possible with this procedure to obtain axisymmetrical capsules for λ down to ≈ 0.039. Below this value, the axisymmetry is broken and the conformations do present radial wrinkles (Fig.5.15) This behavior is compatible with the observations reported in the previous section and in Chapter 3, showing that capsules were obtained for thick shells with d/R between 0.1 and 0.3, and wrinkles for the much thinner shells ($d/R = 0.012$ and below). For what concerns the thinnest shells with no axisymmetric conformations, the qualitative tendency shown by the simulations is that the number of wrinkles increases when (i) the relative shell thickness decreases or (ii) the relative volume change increases.

The simulations presented in this section reproduce the shapes obtained experimentally, described in section 5.4.1: axisymmetric capsules and innerly wrinkled bowls. Buckling in solution through osmotic pressures reported in literature [83] led to axisymmetric conformations with circular regions of very high curvature, which were not encountered in our simulations. Structures comparable with the wrinkled ones obtained from the thinnest shells have already been observed experimentally on millimetric half-spheres submitted to a localized force, [108] or numerically obtained by simulation of a sphere adhering to a flat surface. [109] We expect the number of ridges to depend on the shell characteristics (relative thickness) and the relative volume variation, but it has not been possible up to now to obtain a quantitative phase diagram linked to these parameters.

5.5 Conclusions

In this chapter we probed the elastic properties of hollow silica/siloxane shells and we found that they could be understood well with elasticity theory applied to a thin spherical shell. In the first part of the chapter we investigated the particles response to an applied point force and we found that up to a maximum force, the shells have a perfectly linear response and no remanent deformation occurs. The threshold force up to which the shells responded linearly is determined by the stiffness of the particles. Above this value, there are significant deviations from the linearity and the shells suffer irreversible buckling. From the linear region, we determined the spring constant and we found that the shells become stiffer with increasing relative shell thickness, in agreement with the findings from Chapter 3. Furthermore, we were able to extract quantitatively the material properties, i.e. Young's modulus. The value obtained for the latter, together with the considerations concerning the density of the shell material from section 3.3.7, suggest that we are dealing with a material with elastic properties, somewhere between those of a soft polymer and a stiff rubber.

In the second part of the chapter, the deformation of the particle is achieved by an original method consisting of the partially dissolution of the solvent initially contained in the shells. We have shown that the shapes observed after buckling are consistent with a model of elastic homogeneous thin spherical shells submitted to an isotropic external pressure. The numerical simulations evidenced a cross-over from an axisymmetric capsule to a shape with a wrinkled single depression, when the relative thickness of the shell is decreased. This result reproduces qualitatively the experimental observations. Hence, from a monodisperse enough population of colloids, it should be possible to obtain a monodisperse suspension of anisotropic objects for which geometric parameters are tunable from the characteristics of the initial spherical shell.

6 Assembly of microcellular structures from colloidal particles prepared by emulsion templating

In this chapter we study the materials that can be fabricated by the assembly of hollow shells prepared by emulsion templating into larger aggregates. When the shells are forced together they deform easily yielding microcellular materials reminiscent of foams. In the first part of the chapter we discuss the formation of clusters of hollow shells when they are pulled together by van der Waals forces after destabilization of the suspension. We show that the deformation of the shells upon cluster formation can be understood from a balance between adhesive van der Waals forces and repulsive elastic forces. In the second part we present 2D and 3D microcellular structures obtained from concentrated dispersions of oil droplets coated with solid silica/siloxane shells, by evaporation of both the solvent and the particle core. The shells become the cell walls in the porous structure. The 2D structures resemble two dimensional foams with well-defined pores. The average pore diameter is comparable with the size of the core. In the case of 3D structures, for very small relative shell thicknesses, the 3D foams show a structure of partially collapsed pores with very thin walls in between. On the contrary, for slightly larger relative shell thickness, the pores remain spherical in the 3D structure.

6.1 Introduction

Many materials have a cellular structure: an assembly of prismatic or polyhedral cells with solid edges and faces packed together to fill space. There are many examples of cellular structures in nature, among which cork, wood, sponge, bone or coral. Engineered foam structures are now made from polymers, metals, ceramics, and glasses. Their cellular structure gives them unique properties that are exploited in a variety of applications. [110] Their low weight makes them attractive for the cores of structural sandwich panels in various products. [111] In compression, cellular solids can withstand large strains, allowing them to adsorb the kinetic energy of an impact without generating high stresses. For this reason, they are often used in energy-absorption devices. [111, 112] Closed-cell foams are excellent materials for thermal insulation. Open-cell metallic foams are used for heat-exchange devices. [112–114] The interconnected porosity of open-cell foams is also exploited in their use as filters. [111, 115] Cellular solids can be found also in medical applications. Devices for tissue engineering comprise scaffolds with the appropriate chemistry and architecture to promote cell infiltration and colonization. [116, 117] There is intense interest in producing macroporous materials (which have pores larger than 50 nm) with a highly uniform pore size. Ordered macroporous materials with pore diameters comparable to optical wavelengths are predicted to have unique and highly useful optical properties, such as photonic bandgaps. [32, 34]

There are various methods to fabricate these porous materials, depending on the materials used, their structure or the size of the pores. We only mention here the emulsion templating technique, [118–120] as it has many common characteristics with the method we will describe in this chapter. The basic idea was in that case, to use sol-gel processing to deposit an inorganic material at the exterior of the droplets in a monodisperse emulsion. Subsequent drying and heat treatment yielded solid materials with spherical pores left behind by the emulsion droplets. The method took advantage of the fact that the oil droplets are both highly deformable and easily removable.

Our core-shell particles consisting of a liquid core (either oil or ethanol, after the core dissolution) and a solid, deformable shell (silica/siloxane) are ideal candidates for porous materials. First of all, the core can be easily removed by heating or evaporation. Secondly, as we have shown in the previous chapter, our shells exhibit highly elastic properties, which allows very high packing fractions. Moreover, we can control the core-size and shell thickness during synthesis, which means that we have control over the pore size. In addition, due to the fact that in our case the solid network of the structure originates from the particle shells, we can obtain fluorescent microcellular structures by using fluorescently labelled shells. In this chapter, we investigate the possibility of using our highly deformable particles obtained by emulsion templating, to prepare both small clusters and microcellular structures.

6.2 EXPERIMENTAL SECTION

6.2.1 MATERIALS

Dimethyldiethoxysilane (DMDES, $\geq$97.0 %) and tetraethoxysilane (TEOS, $\geq$98.0 %) were obtained from Fluka, rhodamine B-isothiocyanate (RITC) from Aldrich and ammonia (29.7 % w/w NH_3) and ethanol (absolute alcohol, analytical grade) from Merck. N,N-Dimethylformamide (DMF) was purchased from Biosolve. All chemicals were used as received. De-mineralized water was used in all described reactions and also for the cleaning of glassware.

6.2.2 SAMPLE PREPARATION

An overview of the samples used in the experiments presented in this chapter is given in Table 6.1. The particles with thin shells (samples $S_{4,f}$ - $S_{8,f}$ and $S_{10,f}$) were prepared using the method described in Chapter 2 for the microballoon-like particles. For these samples, we first prepared surfactant-free polydimethylsiloxane (PDMS) oil droplets in water using equal volumes of DMDES and ammonia (29.7 % w/w NH_3), which were varied between 1 - 4 % v/v. The total volume of emulsion was 25 mL (prepared in 50 mL glass vial) and it was prepared using a lab-minishaker for 4 minutes at 2500 rpm. The oil droplets were let to grow for $\approx$ 24 hours (samples $S_{4,f} - S_{6,f}$ and $S_{10,f}$), $\approx$ 48 hours (sample $S_{8,f}$) and $\approx$ 3 days (sample $S_{7,f}$), after which they were dialyzed against de-mineralized water for at least two days in order to remove the un-reacted DMDES. The droplets encapsulation in solid shells was

Table 6.1: *Size and polydispersity of coated oil droplets with solid shells used to prepare microcellular structures, as determined by SLS: R−core radius, d−shell thickness, δ−polydispersity and d/R_t−relative shell thickness, with R_t−total radius.*

Sample	DMDES (% v/v)	R (nm)	d (nm)	δ (%)	d/R_t
$S_{1,f}$	2	445	235	7	0.34
$S_{2,f}$	1	500	195	5	0.28
$S_{3,f}$	3	520	90	4	0.15
$S_{4,f}$	1	500	20	7	0.04
$S_{5,f}$	2	710	10	7	0.01
$S_{6,f}$	3	770	10	5	0.01
$S_{7,f}$	4	920	20	4	0.02
$S_{8,f}$	4	1015	20	4	0.02
$S_{9,f}$	3	740	165	4	0.18
$S_{10,f}$	4	915	10	6	0.01

achieved by adding ammonia (1.69 M final concentration) and TEOS (0.043 M final concentration) to the dialyzed emulsions, while mixing using a magnetic stirrer. TEOS was added in one step for sample $S_{4,f}$ and in 5 steps for the rest of the samples. The stirring was continued for ≈ 3 hours. ≈ 24 hours after the TEOS addition, samples were dialyzed against de-mineralized water to remove the ammonia.

Fluorescent particles were obtained following the procedure described in Section 3.3.8 (Chapter 3), by adding RITC dissolved in water (or ethanol, for sample $S_{5,f}$), to the suspension of particles (final RITC concentration ≈ 4.4×10^{-3} mg/mL). Samples $S_{1,f}$-$S_{3,f}$ and $S_{9,f}$ were prepared according to the method described in Chapter 2 for microcapsules. For $S_{1,f}$, $S_{2,f}$ and $S_{3,f}$, the surfactant-free emulsion droplets were prepared from 2 % v/v, 1 % v/v DMDES, and 3 % v/v DMDES respectively, in 400 mL total dispersion containing 10 % v/v ammonia (29.7 % w/w NH_3). The coating step started ≈ 15 hours after the emulsion preparation and was obtained as follows: 1.73 mL TEOS was first dissolved in 20 mL aqueous solution containing the same amount of ammonia as the emulsion and added during magnetic stirring together with 0.25 mL dye mixture containing RITC, prepared by the method described in Section 3.2.2 (Chapter 3). The shells were allowed to grow for ≈ 5 days, after which the particles were transferred to ethanol in order to remove the oil from the core. Sample $S_{9,f}$ was prepared by first synthesizing emulsions from 3 % v/v DMDES and 3 % v/v ammonia (in 25 mL dispersion); ≈ 24 hours after their preparations, 0.018 M TEOS was added to the emulsions during stirring. The shells were allowed to grow for ≈ 3 days, after which the particles were transferred to ethanol in order to remove the oil from the core.

We used several procedures to obtain foam-like materials. For the 2-dimensional structures, a TEM grid was dipped into the suspension of particles (≈ 2 % v/v), followed by drying. In this way, only a monolayer of particles were retained at the surface of the grid. Also, a thin layer of suspension of the same concentration was dried on a glass slide (22 mm in diameter) at ≈ 50 °C or 70 °C for 1.5 hours and 1 hour, respectively. Alternatively, concentrated dispersions of particles (≈ 20 % v/v) were spin-coated on a 22 mm diameter glass slide (thickness ≈ 0.15 mm), using a Spincoater Model P6700 from Specialty Coating Systems, Inc.. The total spin-coating time was 50 s; during the first 20 s, the speed was 600 rpm, followed by 30 s spinning at 2500 rpm. The 3-dimensional foams were obtained by drying a droplet of concentrated suspension of particles (≈ 20 % v/v) on a TEM grid, or using the same spin coating method as mention above, but with even more concentrated samples (≈ 40 % v/v).

6.2.3 Characterization

The size and polydispersity of the oil droplets and the thickness of the coating were determined with static light scattering (SLS), as described in Chapter 2. The foam-like structures were observed using an inverted Leica confocal scanning laser microscope (CSLM), type TCS-SP2, operated in transmission or fluorescence mode. The 543 nm line of a green He-Ne laser was used for excitation of the samples labeled with fluorescent dye (RITC). Transmission and scanning electron microscopy (TEM and SEM) were also used to study the small clusters of particles and the microcellular structures. The TEM images were taken with a Philips Tecnai 12 microscope with an accelerating voltage of 120 keV, and SEM images with a Philips XL 30 FEG scanning electron microscope.

6.3 Results and discussion

6.3.1 Small clusters of particles

Samples $S_{1,f}$, $S_{2,f}$ and $S_{3,f}$ were prepared as described in the experimental section. During and after the shell growth, the particles were kept in high ammonia concentration ($\approx$ 1.58 M). As a result, the double electrical layer is compressed so that the particles aggregate slowly in time. The van der Waals forces then pulls them together, forming clusters of particles. After removal of the oil from the core (by transferring the particles to ethanol), we obtained clusters formed from hollow particles. The particles contained in samples $S_{1,f}$ and $S_{2,f}$ were analyzed using TEM, after drying on the TEM grid (Fig.6.1). The clusters from sample $S_{3,f}$ were imaged in solution (ethanol), using confocal fluorescence microscopy (Fig.6.2). Due to the resolution of the confocal microscope, we were not able to determine accurately the deformation

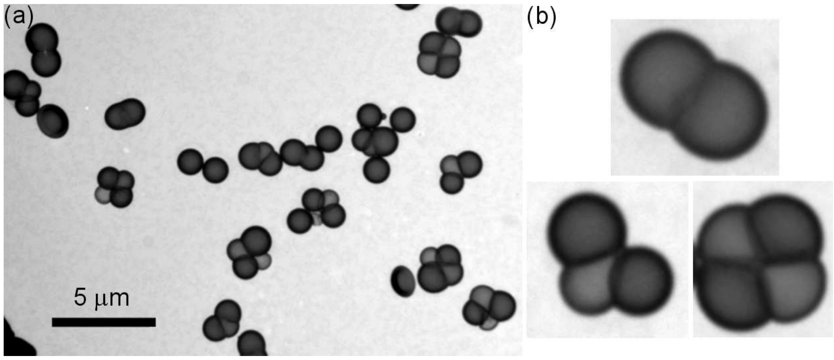

Figure 6.1: *(a) Transmission electron microscopy image of small clusters of particles from sample $S_{1,f}$ (Table 6.1) (b) higher magnification of clusters formed from two, three and four particles.*

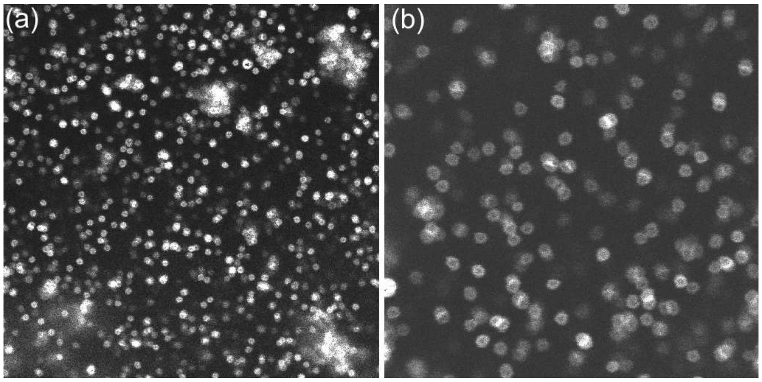

Figure 6.2: *Confocal microscope images (fluorescence mode) of small clusters of hollow particles in solution (ethanol), from sample $S_{3,f}$ (Table 6.1) Image sizes: (a) 74.6 μm × 74.6 μm and (b) 36 μm × 36 μm .*

of the particles within the clusters. However, the fact they are present in solution, shows that they are not pulled together due to drying. Therefore we used the TEM micrographs to investigate the clusters of hollow particles. Typical TEM images with examples of such clusters are shown in Fig.6.1.
The samples contained clusters of two, three and four particles, as well as single ones and a few bigger aggregates. It can be seen that the contact area between particles is always flat, somewhat similar to the shape of soap bubbles when they come together. In the latter case it is the minimization of the surface area that determines the final shape. In our case, it is expected that the shape is determined by an interplay between van der Waals forces, that driven the shells together, and the elastic forces that resist deformation from a spherical shape. We observed that when three particles form a cluster, they exhibit always the same angular shape, with the two particles at the sides never touching. This behavior is very different from the soap bubbles.

In the following, we will focus on the case of a cluster formed from two adhering shells. When a spherical elastic shell is in contact with a substrate, there are two regimes of deformation. In the small deformations regime, the deformation (H) is smaller than the shell thickness (d) and the shell deforms slightly from a sphere. For large deformations, $H > d$, a contact disc develops and the majority of the elastic energy is localized in the circular fold surrounding it (Fig.6.3). [121,122] In both cases, the deformation is due to the adhesion force between the shell and the substrate.The problem of two adhering shells is very similar; in this case, the van der Waals interaction between the particles leads to a considerable adhesion force to each other and consequently, to the deformation of the shells. The total deformation energy for the two shells, for each deformation regime is given by the result from [122], multiplied by two:

$$E_{def,small} \approx \frac{2Ed^2}{\sqrt{12}R} H^2 \tag{6.1}$$

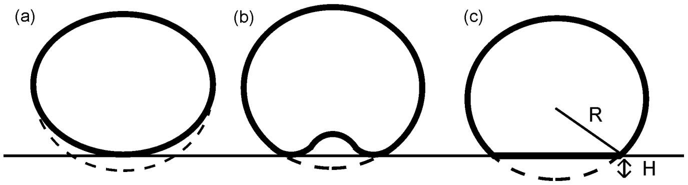

Figure 6.3: *Schematic representation of a shell in (a) small deformations regime, (b) large deformations regime with no adhesion and (c) large deformations regime with adhesion. .*

$$E_{def,large} \approx \frac{2Ed^{5/2}}{12^{3/4}R}H^{3/2} \tag{6.2}$$

with R - initial (average) radius of the shell, d - shell thickness, H - indentation and E - Young's modulus. Due to the the extent of the deformations that are occurring in our system, we treat our shells in the large deformation limit. The energy gain E_{adh} due to establishing the shell-shell contact can be described by a simple contact potential approach [122],

$$E_{adh} = -\pi R_{adh}^2 \gamma \tag{6.3}$$

where R_{adh} is the radius of the contact disc and γ is the (negative) energy gain per contact area (surface energy). For the case of a truncated sphere of radius R and indentation H,

$$R_{adh}^2 \approx 2RH \tag{6.4}$$

so that the energy becomes:

$$E_{adh} \approx -2\pi RH\gamma \tag{6.5}$$

As a result of the adhesion and elastic forces, the indentation H will adjust such that the total energy of the system is minimal:

$$\frac{\partial}{\partial H}(E_{adh} + E_{def}) = 0 \tag{6.6}$$

Using in this equation the expressions for the adhesion energy (Eqn.6.5) and for the deformation energy corresponding to large deformations (Eqn.6.2) one finds for the surface energy the following expression:

$$\gamma = \frac{3Eh^{5/2}H^{1/2}}{12^{3/4}2\pi R^2} \tag{6.7}$$

The radius R and thickness d have been measured with SLS as described in Chapter 2 and the value for the Young's modulus was determined in the previous Chapter (E = 0.109 ± 0.027 GPa). We determined the indentation H from the TEM images. The calculated values for the surface energy for

Table 6.2: *Surface energy for adhesion between two shells calculated in the large deformations regime (using Eqn.6.7) R− initial (average) radius of the shell (calculated as $R = R_c + d/2$, where R_c represents the core radius) and d− shell thickness (R_c and d determined with SLS), H− indentation (determined from TEM image analysis).*

Sample	R (nm)	d (nm)	H (nm)	γ (mJ/m^2)
$S_{1,f}$	562.5	235	336	271
$S_{2,f}$	695	195	384	174

particles from two different samples ($S_{1,f}$ and $S_{2,f}$) are given in Table 6.2. It is interesting to notice that the values obtained for the surface energy γ correspond to surface tensions which are only about 3 - 4 times larger than the typical values expected for the surface tensions of van der Waals solids. [123] The numbers we obtained are therefore reasonable estimates. Moreover, using the expression relating the surface energy γ to Hamaker constant A [123]

$$\gamma = \frac{A}{12\pi D_0^2} \tag{6.8}$$

where $D_0 = 0.165$ nm is the distance of closest approach [123], we can estimate for A values of $\approx 2.3\times10^{-19}$ J and $\approx 1.8\times10^{-19}$ J, respectively. Therefore, by measuring the deformation of the particles in contact, we can obtain information about the interaction force between them, as the deformation can be understood from a balance between van der Waals and elastic forces. For the case of three or four clusters, deformation of the shells which are in contact with at least two other shells is more pronounced, as expected due to the fact that the elastic energy has to balance the adhesion energy at the contact with the other shells.

We conclude that by tuning the interactions between our particles during the shell growth, we can obtain clusters of hollow shells of regular shapes. The deformation of the shells is possible due to their highly elastic properties.

6.3.2 2 -DIMENSIONAL FOAMS

We prepared 2D structures using the procedure described in the experimental section, from polydimethylsiloxane (PDMS) droplets coated with very thin solid shells dispersed in water. Details on these samples are given in Table 6.1. A layer of particles consisting of a liquid core and a solid shell was first deposited on a TEM grid or a glass slide. After drying, the low molecular oil from the core evaporated and as a result, a 2D structure of hollow, thin shells was obtained. Fig.6.4 shows a collection of electron microscopy images of 2D porous structures. The honeycomb structures are reminiscent of foams.

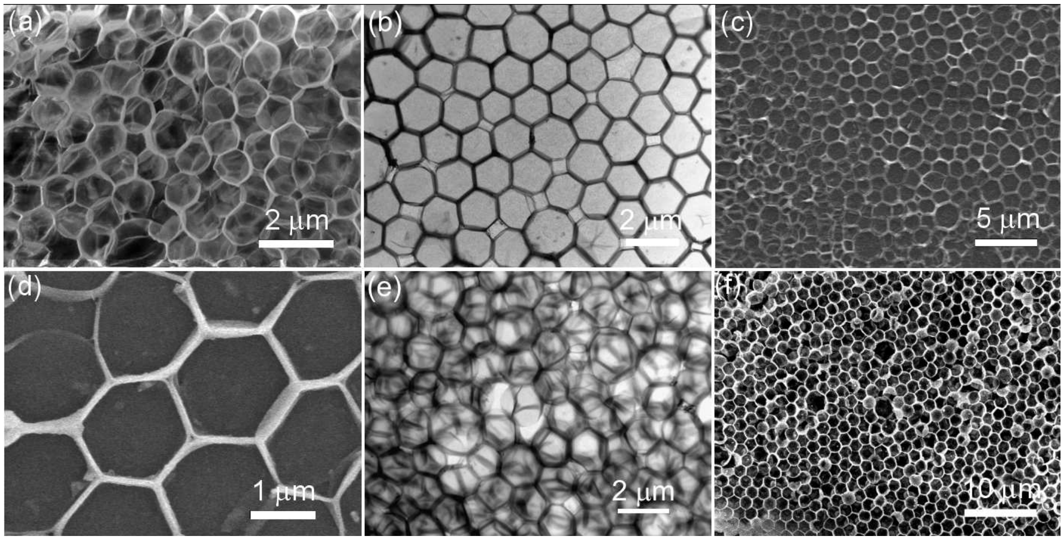

Figure 6.4: *Electron microscopy images of uniform macroporous silica/siloxane structures. They were obtained by drying a layer of particles from samples: (a)* $S_{4,f}$ *(SEM image), (b)* $S_{5,f}$ *(TEM image), (c)* $S_{5,f}$ *(SEM image), (d)* $S_{6,f}$ *(SEM image), (e)* $S_{5,f}$ *(TEM image) and (f)* $S_{7,f}$ *(SEM image). The size and polydispersity of the particles is given in Table 6.1.*

The 2D cellular structures have well-defined pores with sizes comparable with the size of the particles core. The average pore diameter was ≈ 1.47 μm for the foam shown in Fig.6.4b, ≈ 1.47 μm for the structure presented in Fig.6.4d and ≈ 1.63 μm for the one in Fig.6.4f. These values are between 3 and 11 % smaller compared with the initial core radius of the particles due to shrinkage which occurred as a result of drying. However, the size of the pores is large enough to consider these materials as macroporous. The structure consists of a network of polyhedral cells, resulting from the evaporation of the oil. The walls of the cells are in fact the solid shells which originally coated the oil droplets. The total pore area in these 2D structures represents $\approx 70-75$ % of the total surface.

We have shown in Chapter 3 that the shell material is composed of a cross-linked silica/siloxane network. Therefore, we consider the cellular materials we obtained, to be silica/siloxane foams. Moreover, as we have shown in Chapter 5, the shell material exhibits highly elastic properties and as a result a high deformability, which allows the structure to sustain the large stresses which appear during drying.

As can be seen in Fig.6.4, the large pores are separated by thin solid walls. The cells are highly uniform in size and exhibit ordering in a uniform lattice. When the particles used were highly monodisperse, the ordering consists of hexagonal domains, resembling a honeycomb structure (Fig.6.4 d, f). The polydispersity of the particles influences directly the ordering of the pores; for

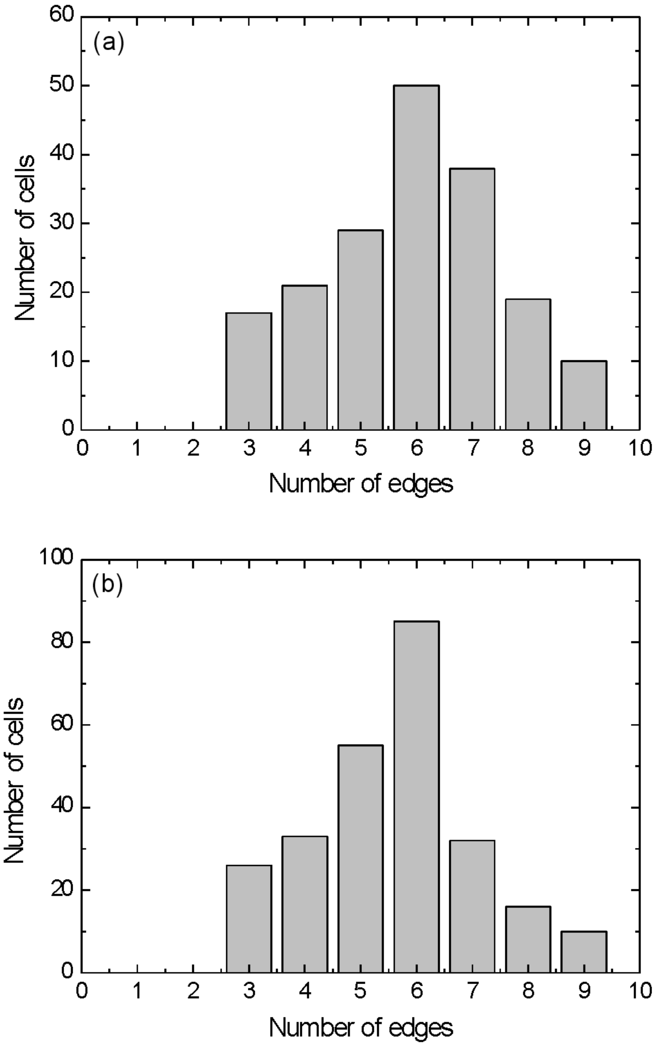

Figure 6.5: *Distribution of number of edges corresponding to a cell for the 2 - dimensional foams shown in (a) Fig.6.4b and (b) Fig.6.4f.*

slightly higher polydispersities, the pore lattice shows deviations from hexagonal ordering (Fig.6.4 b, c). In some cases, we obtained an open-pored layer of silica/siloxane foam (Fig.6.4 b-d, f). Sometimes it is still visible that the material consists of packing of spherical shells (Fig.6.4a, d).

We determined the type of polygonal cells in these 2D structures. Two examples of the distribution of the polygonal cells corresponding to the foams shown in Fig.6.4b, f are shown in Fig.6.5. For the first case (Fig.6.5a), we found $\approx$ 27.7 % hexagonal cells, $\approx$ 21.2 % heptagonal, $\approx$ 16.3 % pentagonal and $\approx$ 11.9 % tetragonal. The rest of the cells consisted of polygons with 3, 8 or 9 edges. In the second case (Fig.6.5b), the percentage of hexagonal polygons was slightly higher, $\approx$ 33.5 %. The other dominant types of polygons

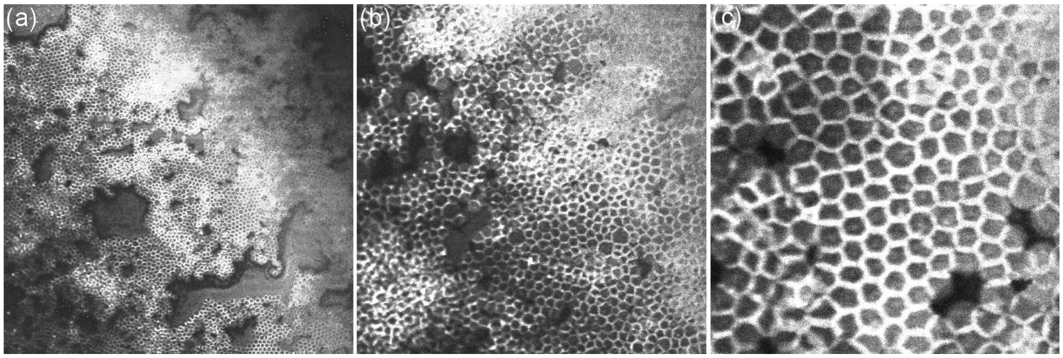

Figure 6.6: *Confocal microscopy images (fluorescence mode) of 2-dimensional fluorescent silica/siloxane foam obtained by drying concentrated suspensions of particles from sample $S_{8,f}$ (Table 6.1) on a glass slide, in the oven (air atmosphere), at 50 °C, for 1.5 h. The size of the images is as follows: (a) 150 $\mu m \times$ 150 μm, (b) 65 $\mu m \times$ 65 μm and (c) 25 $\mu m \times$ 25 μm.*

were pentagons ($\approx$ 21.8 %), tetragons ($\approx$ 13.3 %) and heptagons ($\approx$ 12.8 %). Again, the rest of the cells had 3, 8 or 9 edges.

Hexagonal cells are characteristic for a perfect 2D honeycomb structure. [124] In real cases, it is not surprising to find cells with different number of edges, which can appear due to several factors. Among these, polydispersity of the particles used to prepare the 2D foams, plays an important role. The difference in polydispersity between the particles used to prepared the 2D foams analyzed above can be, therefore, responsible for the difference in the percentage of hexagonal cells found in these structures. Another factor, equally important, is the relative shell thickness, which will influence the deformability of the particles. Moreover, the particles used to prepare the first structure analyzed ($S_{5,f}$ from Table 6.1) are able to deform more than those used for the second structure analyzed ($S_{7,f}$), due to the fact that their relative shell thickness is $\approx$ 2 times smaller than of the particles used for the second one. However, the difference between the two structures remains relatively small.

We have shown in Chapter 3 that our particles can be labelled with a fluorescent dye (RITC), in order to image them with confocal microscopy. We used the same procedure (see experimental section) for particles used to prepare macroporous structures. The RITC dye was first adsorbed at the surface of the particles while they were in suspension and it remained there after drying. Consequently, fluorescent silica/siloxane foam structures can be obtained and analyzed with confocal microscopy (Fig.6.6).

So far we only showed examples of 2D foams prepared from oil droplets coated with very thin shells. The microcellular structures can be prepared also from particles with thicker shells, as long as the relative shell thickness is small enough that capillary forces during drying can still deform them. As an illustration, we made 2D structures from suspensions of particles in ethanol, with thicker shells, from which the oil from the core was already removed (sample $S_{9,f}$). We used again RITC dissolved in the solvent (see experimental section) to fluorescently label the shells. Fig.6.7 shows a fluorescent 2D macroporous structure obtained from a suspension of hollow shells in ethanol, obtained by spin coating. The pores are very uniform in size and show a high degree of ordering. However, the pore lattice exhibits lattice defects, such as vacancies and dislocations, usually seen in sphere packing. The distribution of polygonal cells in the 2D structures shown in Fig.6.6 and Fig.6.7 is presented in Fig.6.8. For the first case (2D foams from Fig.6.6), we considered ≈ 400 cells in the analysis. We found ≈ 26 % hexagonal cells, ≈ 27 % pentagonal, ≈ 19.5 % tetragonal and ≈ 14 % heptagonal. The rest of the cells consisted of polygons with 3, 8 or 9 edges.

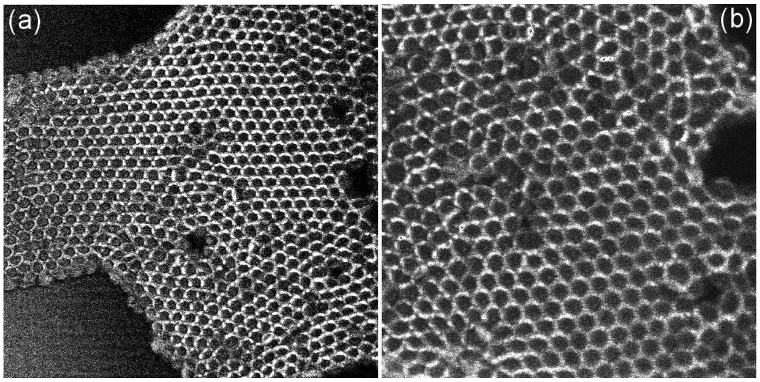

Figure 6.7: *Confocal microscopy images (fluorescence mode) of 2-dimensional foams obtained by spin-coating concentrated suspensions of particles from sample $S_{9,f}$ (Table 6.1) on a 22 mm diameter glass slide, as described in the experimental section. The size of the images is as follows: (a) 48 μm × 48 μm and (b) 33 μm × 33 μm.*

We considered ≈ 450 cells in the analysis of the 2D foams from Fig.6.7. In this case, most of the cells were found to be hexagonal (≈ 74.5 %). However, we also found a small percentage of pentagonal cells (≈ 14 %) and cells with 3, 4 or 7 edges (≈ 10.7 % in total). This time, the difference between the two structures is considerably larger than for the previous two structures discussed (Fig.6.5) as can be seen both from the confocal images (Fig.6.6 and Fig.6.7) and the cells distribution (Fig.6.8).

By comparing the types of cells found in all the 2D foams analyzed, we can conclude the following: the number of edges/cell exhibits a gaussian distribution, with the maximum corresponding to a hexagonal cell (except for structure from Fig.6.6, in which case the number of pentagonal cells is slightly higher). The percentages of other polygonal structures found showed only small differences between different structures, except for the structure presented in Fig.6.7 prepared from sample $S_{9,f}$. In that case, most of the cells were hexagonal, with only a small number of different polygons. We already

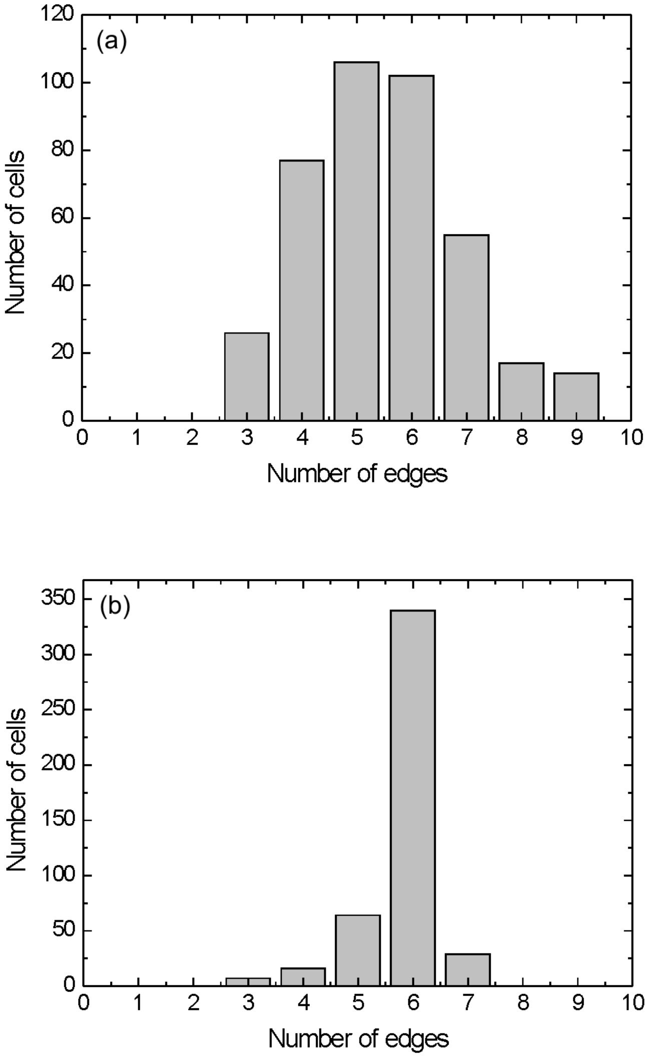

Figure 6.8: *Distribution of number of edges corresponding to a cell for the 2 - dimensional foams shown in (a) Fig.6.6 and (b) Fig.6.7.*

mentioned the polydispersity and the relative shell thickness of the initial particles as possible factors which might influence the final 2D structures. In addition, other factors need to be considered, such as the preparation method and the content of the particle core, which will influence the drying process and as a consequence, the final structure. For the foam presented in Fig.6.4 and in Fig.6.6, the particles still contained oil in the core and they were dispersed in water when the structure was prepared. On the contrary, the foam shown in Fig.6.7 was prepared from hollow particles (filled with ethanol) suspended in ethanol. Probably the evaporation of both the solvent and the particles core took place much faster for the latter case. From this and from the fact that the relative shell thickness was considerably larger for the particles used for the latter structure, we conclude that highly-ordered, 2D macroporous structures can be obtained by spin-coating of suspensions of monodisperse hollow shells in ethanol, with relative shell thicknesses for which the particles can still deform, but their deformation corresponds to the region between microbaloons and microcapsules (see Section 3.3.4 of Chapter 3).

It will be interesting to determine conditions under which spin coating will lead to large regions of contiguous cells. This can be optimized by varying parameters such as particle concentration, spinning speed and duration, as well as the temperature at which the foam is dried.

6.3.3 3 -DIMENSIONAL FOAMS

We obtained 3D macroporous structures from the same type of liquid-core solid-shell particles as described in the experimental section. 3D silica/siloxane foams were prepared by drying (in air, at room temperature), of concentrated aqueous dispersions of such particles on a TEM grid. A structure obtained from sample $S_{5,f}$ (Table 6.1) is shown in Fig.6.9. The total thickness of the structure was ≈ 13 μm, and the pores diameter ≈ 0.95 μm. Although we used the same particles as for the 2D foam shown in Fig.6.4b, c, the cells for the 3D structure are ≈ 25 % smaller. Moreover, the 3D foam appears to contain more solid material per volume, which might be an indication that the 3D structure is much more compressed. Based on the relative shell thickness and cell shrinkage we estimate that the foam has a cell volume fraction of ≈ 93 %.

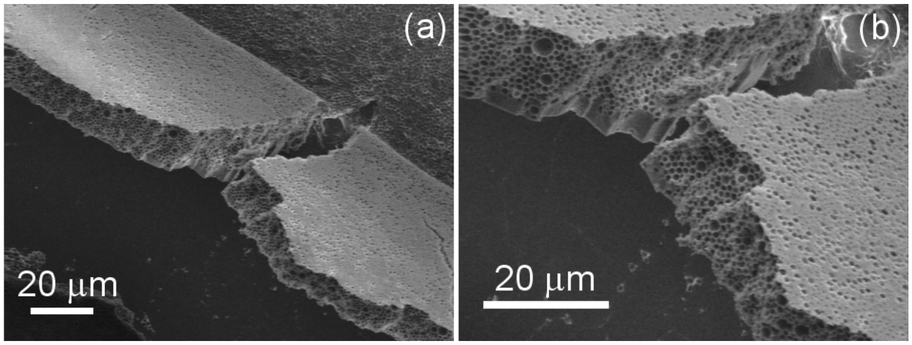

Figure 6.9: *SEM micrographs of a 3D macroporous silica/siloxane foam (prepared by drying of a concentrated droplet from sample $S_{5,f}$, Table 6.1).*

Alternatively, we used spin-coating (see Experimental section) to prepare thick microcellular films. A concentrated dispersion of silica/siloxane-coated droplets (sample $S_{10,f}$) was spin-coated on a 22 mm diameter glass slide and dried in air. We used relatively large particles (core-radius 915 nm) with a very thin shell (10 nm) in order to obtain a very porous material. Due to this thin shell relative to the particle radius, the particles do not maintain their spherical shape in the resulting structure (shown in Fig.6.10), they partially collapse because of drying. As a result, the materials obtained this way do not exhibit an ordered structure. However, they consist of a very thin solid network, with large open pores "filled" with air. Moreover, the low density of the silica/siloxane shells ($\approx$ 1000 kg/m^3), combined with the large amount of air in our structure due to the evaporation of the oil from the particles core, lead to a very low density for the material we obtained. These properties are common for aerogels structures, [125] and mesostructured cellular foams. [126, 127] In Fig.6.10c is even visible the strut-like structure, which is reminiscent of aerogels and mesostructured cellular foams (Fig.6.11).

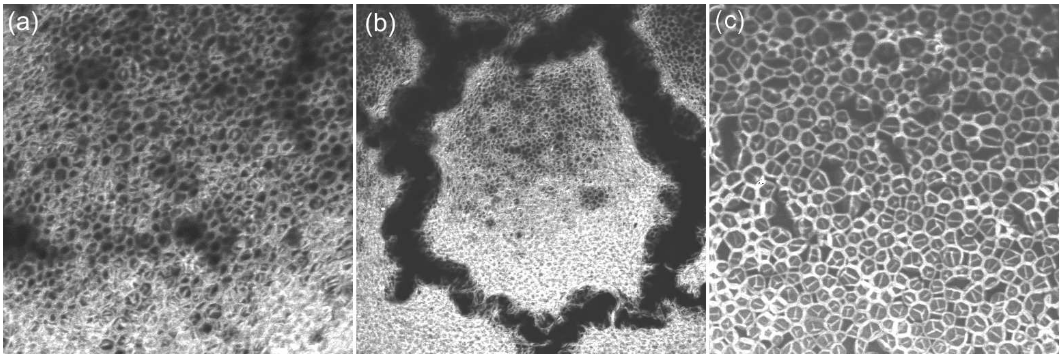

Figure 6.10: *Confocal microscopy images (fluorescence mode)of a macroporous structure obtained by spin-coating concentrated suspensions of particles from sample $S_{10,f}$ (Table 6.1) on a 22 mm glass slide, as described in the experimental section. The size of the images is as follows: (a) 80 μm × 80 μm, (b) 158.7 μm × 158.7 μm, and (c) 67 μm × 67 μm.*

The presence of the fluorescent dye RITC at the surface of our particles allows us to investigate the inner structure of the 3D silica/siloxane foams using confocal fluorescence microscopy. For this purpose, we first prepared a 3D foam structure from a dispersion of particles (sample $S_{10,f}$) containing RITC, following the spin-coating procedure described in the Experimental section. After the dried-foam structure was obtained, a droplet of DMF was put into contact with it and due to capillary forces, the DMF was absorbed into the porous structure. We chose DMF in order to match the refractive index of the silica/siloxane shells so that light scattering is minimized, allowing us to examine the structure in the bulk. The 3D structure had a total thickness of $\approx$ 38 μm, as determined by scanning through the height of the sample. The structure consisted of open-pored layers in which ordering was present only at very short range. Also we identified the presence of large voids which were probably caused by drying of non-uniformly distributed layers of particles. In Fig.6.12 we show three x-y slices situated at different heights in the sample.

Although the 3D structures of fluorescent silica/siloxane foams we obtained do not show long range ordering, they remain interesting materials, with pro-

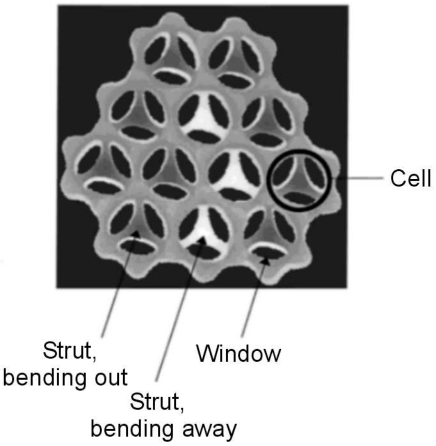

Figure 6.11: *Schematic cross section of the strut-like structure exhibited by mesostructured cellular foams. [127] The gray-shaded areas represent the solid framework and the struts (left arrows), the circular arrays represent the spherical cells (black circle) and the black areas between the cells (right arrow) represent the windows.*

perties characteristic for mesocellular foam structures. Long range ordering could be achieved by using particles with slightly larger relative shell thicknesses and lower polydispersities.

6.3.4 CRYSTALS

Several attempts were made in order to fabricate crystals of silica particles with hollow spheres incorporated as defects. In the first experiments [128],

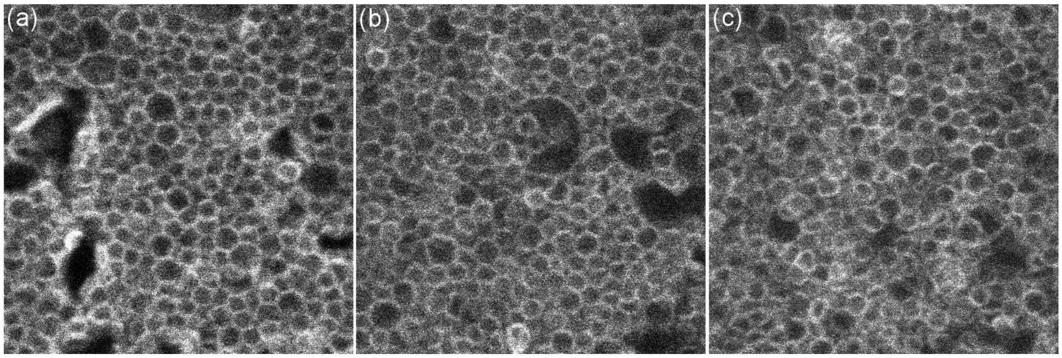

Figure 6.12: *Confocal microscopy images (fluorescence mode)showing three x-y slices obtained by scanning through the height of a 3D foam obtained by spin-coating of a concentrated suspension of particles from sample $S_{10,f}$ (Table 6.1) The size of the images is 29.7 μm × 29.7 μm. The x-y scans are situated at (a) 2 μm, (b) 18 μm and (c) 27.5 μm respectively, from the glass slide.*

such crystals were obtained by sedimentation in an electric field perpendicular to gravity. The results indicated that the shells can be incorporated in these crystals without disturbing the crystal lattice, but the difference in mass density between the two types of spheres caused a non-uniformity in the distribution of the hollow shells which were concentrated in the upper part of the crystal. Moreover, the presence of dimethyl sulfoxide (DMSO) as solvent in these experiments caused slight aggregation of the hollow shells.

Alternatively, mechanical shearing between two glass slides [129] was applied to induce crystallization of suspensions containing silica particles (1.2 μm in diameter, labeled with fluorescein isothiocyanate, FITC) and hollow spheres (1.3 μm, labeled with rhodamine B-isothiocyanate, RITC) in ethanol. This method yielded better results regarding the number of defects incorporated in the crystal, but still not enough to affect the transmission of light through the crystal.

Preliminary investigations [130] showed that even better incorporation of the defects can be obtained by using by spin coating viscous dispersions of silica and hollow spheres (the same sizes as for the mechanical shearing). The dispersions were prepared by suspending silica particles and hollow spheres in a mixture of a monomer (ethoxylated trimethylolpropane triacrylate) and a photoinitiator (2-hydroxy methylpropriophenone). The crystalline film obtained after spin-coating was frozen-in using UV-light. An example of hollow shells incorporated in a crystal of silica particles using this method is shown in Fig.6.13. The silica particles with a fluorescent core containing FITC (depicted in small white spheres) form a hexagonal crystalline structure which accommodates the hollow shells containing RITC (depicted in larger, grey spheres).

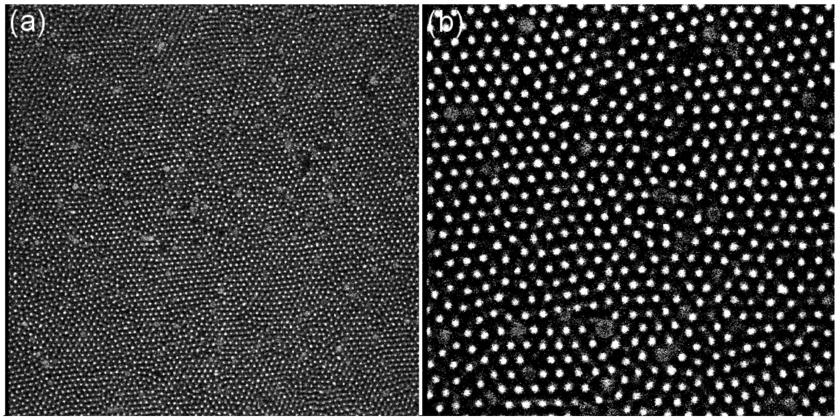

Figure 6.13: *Superimposed confocal microscopy images (taken in fluorescence mode, λ = 488 nm for FITC and λ = 543nm for RITC) showing a xyz scan through a crystal of silica particles (small white spheres) containing hollow shells(larger, grey spheres). The size of the images is (a) 100 μm × 100 μm and (b) 35 μm × 35 μm. The images were taken after polymerization of the monomer.*

The hollow shells do not disturb the ordering of the silica particles, but some of them collapsed after the polymerization of the monomer, due to their relative shell thickness. These preliminary investigations show that our hollow shells can be used to create dielectric defects in photonic crystals, but the fabrication method needs to be optimized. This can be done by using hollow shells with exactly the same diameter as the silica particles and with larger relative shell thickness in order to prevent them from collapsing after drying.

6.4 Conclusions

In this chapter, we investigated the possibility of making microcellular structures based on highly deformable hollow colloidal particles. In the first part of the chapter we showed that due to the high deformability of our shells and in the presence of high ammonia concentrations, small clusters of hollow particles of regular shapes can be formed. Assuming the shells to be in the large deformation regime, we determined for the surface energy at contact of two shells values which are only a few times larger than typical values expected for surface energies of van der Waals solids. By starting with very monodisperse emulsion droplets, one could obtain very regular clusters of particles. The different types of clusters could then be separated with a density gradient centrifugation method used for separation of clusters of microspheres. [131] Such colloidal clusters have recently received a lot of attention.

In the second part of the chapter, we discussed methods to prepare silica/siloxane macroporous structures using both PDMS droplets coated with very thin shells dispersed in water and hollow shells dispersed in ethanol. We obtained 2D microcellular structures with well-defined pores with sizes comparable with the size of the particles core. These structures consist of a network of pores in the shape of polyhedral cells, which occupy ≈ 75 % of the total surface of the 2D foam. Alternatively, we were able to obtain 3D silica/siloxane solid foams. Depending on the relative shell thickness and on the preparation method, the pores in the 3D structures maintained their spherical shape, or formed polygonal pores. Due to the fact that the molecules of a fluorescent dye (RITC) can be adsorbed at the surface of the particles, we obtained fluorescent 2D and 3D microcellular structures which can be studied with confocal microscopy. Since the size of the core and the shell thickness can be controlled during the particle synthesis, as we have shown in Chapter 3, our method for the preparation of microcellular structures offers control over the pore size and over the silica/siloxane layer. Due to the low density of the silica/siloxane material of the shell combined with the presence of pores, these materials have a very low density and high porosity. Preliminary investigations show promising results in using the hollow shells as dielectric defects in photonic crystals.

REFERENCES

[1] D. Wilkox, M. Berg, T. Bernat, D. Kellerman, and J. C. Jr., *Hollow and Solid Spheres and Microspheres: Science and Technology Associated with Their Fabrication and Application*, volume 372, Materials Research Society Proceedings: Pittsburgh, 1995.

[2] R. Partch, *Materials Synthesis and Characterization*, Plenum: New York, 1997.

[3] F. Caruso, *Nanoengineering of Particle Surfaces*, Adv. Mater. **13**, 11 (2001).

[4] A. van Blaaderen, *Materials Science: colloids get complex*, Nature **439**, 545 (2006).

[5] W. Stöber, A. Fink, and E. Bohn, *Controlled Growth of Monodisperse Silica Spheres in the Micron Size Range*, J. Colloid Interface Sci. **26**, 62 (1968).

[6] A. V. Helden, J. Jansen, and A. Vrij, *Preparation and characterization of spherical monodisperse silica dispersions in nonaqueous solvents*, J. Colloid Interface Sci. **81**, 354 (1981).

[7] A. Philipse, *Quantitative aspects of the growth of (charged) silica spheres*, Colloid. Polym. Sci **266**, 1174 (1988).

[8] A. van Blaaderen, J. van Geest, and A. Vrij, *Monodisperse Colloidal Silica Spheres from Tetraalkoxysilanes: Particle Formation and Growth Mechanism*, J. Colloid Interface Sci. **154**, 481 (1992).

[9] A. Philipse and A. Vrij, *Preparation and Propertis of Nonaqueous Model Dispersions of Chemically Modified, Charged Silica Spheres*, J. Colloid Interface Sci. **128**, 121 (1989).

[10] A. van Blaaderen and A. Vrij, *Synthesis and Characterization of Monodisperse Colloidal Organo-silica Spheres*, J. Colloid Interface Sci. **156**, 1 (1993).

[11] A. van Blaaderen and A. Vrij, *Synthesis and Characterization of Colloidal Dispersions of Fluorescent, Monodisperse Silica Spheres*, Langmuir **8**, 2921 (1992).

[12] G. Bogush, M. Tracy, and C. Zukoski-IV, *Preparation of Monodisperse Silica Particles: Control of Size and Mass Fraction*, J. Non-Cryst. Solids **104**, 95 (1988).

[13] G. Bogush and C. Zukoski-IV, *Studies of the Kinetics of the Precipitation of Uniform Silica Particles through the Hydrolysis and Condensation of Silicon Alkoxides*, J. Colloid Interface Sci. **142**, 1 (1991).

[14] G. Bogush and C. Zukoski-IV, *Uniform Silica Particles Precipitation: An Aggregative Growth Model*, J. Colloid Interface Sci. **142**, 19 (1991).

[15] T. J. Barder and P. D. DuBois, *Process for forming highly uniform silica spheres*, U.S. Patent , 4983369 (1991).

[16] C. Graf, W. Schärtl, K. Fischer, N. Hugenberg, and M. Schmidt, *Dye-Labeled Poly(organosiloxane) Microgels with Core-Shell Architecture*, Langmuir **15**, 6170 (1999).

[17] F. Baumann, B. Deubzer, M. Geck, and J. Dauth, *Elastomeric Organosilicon Micronetworks*, Macromolecules **30**, 7568 (1997).

[18] F. Baumann, B. Deubzer, M. Geck, J. Dauth, and M. Schmidt, Macromolecules **30**, 7568 (1997).

[19] J. Choi, C. Kim, and D. Kim, *Formation and Characterization of Monodisperse, Spherical Organo-Silica Powders from Organo-Alkoxysilane-Water System*, J. Am. Ceram. Soc. **81**, 1184 (1998).

[20] I.-S. Seog and C. Kim, *Preparation of monodispersed spherical silicon carbide by the sol-gel method*, J. Mater. Sci. **28**, 3277 (1993).

[21] T. Matsumoto, Y. Takayama, H. Onoda, and K. Kojima, *Synthesis of Rhodamine B-Doped and Monodispersed Spherical Particles of Polyorganosiloxane Using a W/O Emulsion*, J. Am. Ceram. Soc. **88**, 3458 (2005).

[22] T. M. Obey and B. Vincent, *Novel Monodisperse Silicone Oil/Water Emulsions*, J. Colloid Interface Sci. **163**, 454 (1994).

[23] M. I. Goller, T. M. Obey, D. O. H. Teare, B. Vincent, and M. R. Wegener, *Inorganic silicone oil microgels*, Colloids Surf. A **123-124**, 183 (1997).

[24] M. Goller and B. Vincent, *Silica encapsulation of liquid PDMS droplets*, Colloids Surf. A **142**, 281 (1998).

[25] F. Caruso, R. Caruso, and H. Möhwald, *Nanoengineering of Inorganic and Hybrid Hollow Spheres by Colloidal Templating*, Science **282**, 1111 (1998).

[26] C. Fowler, D. Khushalani, and S. Mann, *Interfacial synthesis of hollow microspheres of mesostructured silica*, Chem. Commun. , 2028 (2001).

[27] I. Gill and A. Ballesteros, *Encapsulation of Biologicals within Silicate, Siloxane, and Hybrid Sol-Gel Polymers: An Efficient and Generic Approach*, J. Am. Chem. Soc. **120**, 8587 (1998).

[28] J. Jang and K. Lee, *Facile fabrication of hollow polystyrene nanocapsules by microemulsion polymerization*, Chem. Commun. , 1098 (2002).

[29] X. Wang, W. Yang, Y. Wang, S. Fu, and Z. Gao, *Fabrication of hollow zeolite spheres*, Chem. Commun. , 2161 (2000).

[30] C. Morris, M. Anderson, R. Stroud, C. Merzbacher, and D. Rolison, *Silica sol as a nanoglue: Flexible synthesis of composite aerogels*, Science **284**, 622 (1999).

[31] W. Meier, *Polymer nanocapsules*, Chem. Soc. Rev. **29**, 295 (2000).

[32] J. Joannopoulos, R. Meade, and J. Winn, *Photonic crystals*, Princeton University Press: Princeton, 1995.

[33] X. Xu and S. A. Asher, *Synthesis and Utilization of Monodisperse Hollow Polymeric Particles in Photonic Crystals*, J. Am. Chem. Soc. **126**, 7940 (2004).

[34] J. Joannopoulos, P. Villeneuve, and F. Shanhui, *Photonic crystals: putting a new twist on light*, Nature **386**, 143 (1997).

[35] I. Tissot, J. Reymond, F. Lefebvre, and E. Bourgeat-Lami, *SiOH-Functionalized Polystyrene Latexex. A step toward the Synthesis of Hollow Silica Nanoparticles*, Chem. Mater. **14**, 1325 (2002).

[36] S. Schacht, Q. Hou, I. Voigt-Martin, G. D. Stucky, and F. Schuth, *Oil-Water Interface Templating of Mesoporous Macroscale Structures*, Science **273**, 768 (1996).

[37] P. Bruinsma, A. Kim, J. Liu, and S. Baskaran, *Mesoporous Silica Synthesized by Solvent evaporation: Spun Fibers and Spray-Dried Hollow Spheres*, Chem. Mater. **9**, 2507 (1997).

[38] M. Iida, T. Sasaki, and M. Watanabe, *Titanium Dioxide Hollow Microspheres with an Extremely Thin Shell*, Chem. Mater. **10**, 3780 (1998).

[39] Y. Lu, H. Fan, A. Stump, T. Ward, T. Rieker, and C. Brinker, *Aerosol-assisted self-assembly of mesostructured spherical nanoparticles*, Nature **398**, 223 (1999).

[40] O. Emmerich, N. Hugenberg, M. Schmidt, S. S. Sheiko, F. Baumann, B. Deubzer, J. Weis, and J. Ebenhoch, *Molecular Boxes Based on Hollow Organosilicon Micronetworks*, Adv. Mater. **11**, 1299 (1999).

[41] A. Imhof, *Preparation and Characterization of Titania-Coated Polystyrene Spheres and Hollow Titania Shells*, Langmuir **17**, 3579 (2001).

[42] C. Graf and A. van Blaaderen, *Metallodielectric Colloidal Core-Shell Particles for Photonic Applications*, Langmuir **18**, 524 (2002).

[43] S. M. Marinakos, J. P. Novak, I. L. C. Brousseau, A. B. House, E. M. Edeki, J. C. Feldhaus, and D. L. Feldheim, *Gold Particles as Templates for the Synthesis of Hollow polymer Capsules. Control of Capsule Dimensions and Guest Encapsulation*, J. Am. Chem. Soc. **121**, 8518 (1999).

[44] C. Pathak, A. Sawhney, and J. Hubbell, *Rapid photopolymerization of immunoprotective gels in contact with cells and tissue*, J. Am. Chem. Soc. **114**, 8311 (1992).

[45] R. Langer, *New methods for drug delivery*, Science **249**, 1527 (1990).

[46] N. Peppas and R. Langer, *New challenges in biomaterials*, Science **263**, 1715 (1994).

[47] H. Feilchenfeld, G. Chumanov, and T. Cotton, *Photoreduction of Methylviologen Adsorbed on Silver*, J. Phys. Chem. **100**, 4937 (1996).

[48] F. Caruso, H. Lichtenfeld, M. Giersig, and H. Möhwald, *Electrostatic Self-Assembly of Silica Nanoparticle-Polyelectrolyte Multilayers on Polystyrene Latex Particles*, J. Am. Chem. Soc. **120**, 8523 (1998).

[49] Y. Yin, Y. Lu, B. Gates, and Y. Xia, *Synthesis and Characterization of Mesoscopic Hollow Spheres of Ceramic Materials with Functionalized Interior Surfaces*, Chem. Mater. **13**, 1146 (2001).

[50] L. Zha, Y. Zhang, W. Yang, and S. Fu, *Monodisperse Temperature-Sensitive Microcontainers*, Adv. Mater. **14**, 1090 (2002).

[51] T. K. Mandal, M. S. Fleming, and D. R. Walt, *Production of Hollow Polymeric Hollow Microspheres by Surface-Confined Living Radical Polymerization on silica Templates*, Chem. Mater. **12**, 3481 (2000).

[52] K. Velikov and A. van Blaaderen, *Synthesis and Characterization of Monodisperse core-Shell Colloidal Spheres of Zinc Sulfide and Silica*, Langmuir **17**, 4779 (2001).

[53] J. M. Jafelicci, M. R. Davolos, F. J. dos Santos, and S. J. de Andrade, *Hollow silica particles from microemulsions*, J. Non-cryst. Solids **247**, 98 (1999).

[54] J.-H. Park, C. Oh, S.-I. Shin, S.-K. Moon, and S.-G. Oh, *Preparation of hollow silica microspheres in W/O emulsions with polymers*, J. Colloid Interface Sci. **266**, 107 (2003).

[55] J. Cornelissen, E. Connor, H.-C. Kim, V. Lee, T. Magibitang, P. Rice, W. Volksen, L. Sundberg, and R. Miller, *Versatile synthesis of nanometer sized hollow silica spheres*, Chem. Commun. , 1010 (2003).

[56] D. Hubert, M. Jung, P. Frederik, P. Bomans, J. Meuldijk, and A. German, *Vesicle-Directed Growth of Silica*, Adv. Mater. **12**, 1286 (2000).

[57] C. McKelvey, E. Kaler, J. Zasadzinski, B. Coldren, and H.-T. Jung, *Templating Hollow Polymeric Spheres from Cationic equilibrium Vesicles: Synthesis and Characterization*, Langmuir **16**, 8285 (2000).

[58] H.-P. Hentze, S. R. Raghavan, C. A. McKelvey, and E. W. Kaler, *Silica Hollow Spheres by Templating of Cationic Vesicles*, Langmuir **19**, 1069 (2003).

[59] M. Sauer, D. Streich, and W. Meier, *pH-Sensitive Nanocontainers*, Adv. Mater. **13**, 1649 (2001).

[60] Q. Sun, P. Kooyman, J. Grossmann, P. Bomans, P. Frederik, P. M. Magusin, T. Beelen, R. van Santen, and N. Sommerdijk, *The Formation of Well-Defined Hollow Silica Spheres with Multilamellar Shell Structure*, Adv. Mater. **15**, 1097 (2003).

[61] L. M. Liz-Marzan, M. Giersig, and P. Mulvaney, *Synthesis of Nanosized Gold-Silica Core-Shell Particles*, Langmuir **12**, 4329 (1996).

[62] K. Kamata, Y. Lu, and Y. Xia, *Synthesis and Characterization of Monodisperse Core-Shell Spherical Colloids with Movable Cores*, J. Am. Chem. Soc. **125**, 2384 (2003).

[63] H. Sertchook, H. Elimelech, and D. Avnir, *Composite Particles of Silica/Poly(dimethylsiloxane)*, Chem. Mater. **17**, 4711 (2005).

[64] C.I.Zoldesi and A.Imhof, *Synthesis of monodisperse colloidal spheres, capsules and microballoons by emulsion templating*, Adv.Mater. **17**, 924 (2005).

[65] C. Bohren and D. Huffman, *Absorption and scattering of light by small particles*, John Wiley and Sons: New York, 1983.

[66] A. Smith, *The Analytical Chemistry of Silicones*, Wiley-Interscience: New York, 1991.

[67] C.I.Zoldesi, C. van Walree, and A.Imhof, *Deformable hollow hybrid silica/siloxane colloids by emulsion templating*, Langmuir **22**, 4343 (2006).

[68] G. Engelhardt and H. Jancke, *Uber die 1H-, 13C- und 29Si-NMR chemischen verschiebungen einiger linearer, verzweigter und cyclischer methylsiloxan-verbindungen*, J. Organometal. Chem. **28**, 293 (1971).

[69] S. Rankin and A. McCormick, *29Si NMR study of base-catalyzed polymerization of dimethyldiethoxysilane*, Magn. Reson. Chem. **37**, 27 (1999).

[70] B. Neumann, B. Vincent, R. Krustev, and H.-J. Muller, *Stability of Various Silicone Oil/Water Emulsion Films as a Function of Surfactant and Salt Concentration*, Langmuir **20**, 4336 (2004).

[71] L. Landau and E. Lifshitz, *Course of Theoretical Physics ,Vol.7, Theory of Elasticity*, Butterworth-Heinemann: Oxford, 3rd edition, 1997.

[72] A. Pogorelov, *Bending of Surface and Stability of Shells*, American Mathematical Society, 1988.

[73] J. Brus and J. Dybal, *Copolymerization of tetraethoxysilane and dimethyl(diethoxy)silane studied by 29Si NMR and ab initio calculations of 29Si chemical shifts*, Polymer **40**, 6933 (1999).

[74] J. Brus and J. Dybal, *Solid-state NMR study of structure, size and dynamics of domanis in hybrid siloxane networks*, Polymer **41**, 5269 (2000).

[75] N. Verhaegh and A. van Blaaderen, *Dispersions of Rhodamine-Labeled Silica Spheres: Synthesis, Characterization, and Fluorescence Confocal Scanning Laser Microscopy*, Langmuir **10**, 1427 (1994).

[76] D. Evans and H. Wennerstrom, *The colloidal domain - where physics, chemistry biology, and technology meet*, Wiley-VCH: New York, 2nd edition, 1999.

[77] R. Hunter, *Foundations of Colloid Science*, Oxford University Press, 1986.

[78] H. Onori and A. Santucci, *Dynamical and structural properties of water/alcohol mixtures*, J. Mol. Liq. **69**, 161 (1996).

[79] K. Anderson, T. Obey, and B. Vincent, *Surfactant-Stabilized Silicone Oil in Water Emulsions*, Langmuir **10**, 2493 (1994).

[80] S. Oh and D. Shah, *Effect of Counterions on the Interfacial Tension and Emulsion Droplet Size in the Oil/Water/Dodecyl Sulfate System*, J. Phys. Chem. **97**, 284 (1993).

[81] C.-E. Lin, *Determination of critical micelle concentration of surfactants by capillary electrophoresis*, J. Chromatogr. A **1037**, 467 (2004).

[82] M. Li, Y. Rharbi, X. Huang, and M. Winnik, *Small Variations in the Composition and Properties of Triton X-100*, J.Colloid Interface Sci. **230**, 135 (2000).

[83] C. Gao, E. Donath, S. Moya, V. Dudnik, and H. Möhwald, *Elasticity of hollow polyelectrolyte capsules prepared by the layer-by-layer technique*, Eur. Phys. J. E **5**, 21 (2001).

[84] O. Vinogradova, *Mechanical properties of polyelectrolyte multilayer microcapsules*, J. Phys.: Condens. Matter **16**, R1105 (2004).

[85] O. Vinogradova, D. Andrienko, V. Lulevich, S. Nordschild, and G. Sukhorukov, *Young's modulus of Polyelectrolyte Multilayers from Microcapsule Swelling*, Macromolecules **37**, 1113 (2004).

[86] O. Lebedeva, B.-S. Kim, and O. Vinogradova, *Mechanical Properties of Polyelectrolyte-Filled Multilayer Microcapsules Studied by Atomic Force and Confocal Microscopy*, Langmuir **20**, 10685 (2004).

[87] V. Lulevich, D. Andrienko, and O. Vinogradova, *Elasticity of polyelectrolyte multilayer microcapsules*, J. Chem. Phys. **120**, 3822 (2004).

[88] S. Leporatti, A. Voigt, R. Mitlohner, G. Sukhorukov, E. Donath, and H. Möhwald, *Scanning Force Microscopy Investigation of Polyelectrolyte Nano- and Microcapsule Wall Texture*, Langmuir **16**, 4059 (2000).

[89] S. Leporatti, C. Gao, A. Voigt, E. Donath, and H. Möhwald, *Shrinking of ultrathin polyelectrolyte multilayer capsules upon annealing: A confocal laser scanning microscopy and scanning force microscopy study*, Eur. Phys. J. E **5**, 13 (2001).

[90] F. Dubreuil, N. Elsner, and A. Fery, *Elastic properties of polyelectrolyte capsules studied by atomic-force microscopy an RICM*, Eur. Phys. J. E **12**, 215 (2003).

[91] I. Ivanovska, P. de Pablo, B. Ibarra, G. Sgalari, F. MacKintosh, J. Carrasccosa, C. Schmidt, and G. Wuite, *Bacteriophage capsids: Tough nanoshells with complex elastic properties*, Proc.Natl.Acad.Sci.USA **101**, 7600 (2004).

[92] J. Michel, I. Ivanovska, M. Gibbons, W. Klug, C. Knobler, G. Wuite, and C. Schmidt, *Nanoindentation studies of full and empty viral capsids and the effect of capsid protein mutations on elasticity and strength*, Proc.Natl.Acad.Sci.USA **103**, 6184 (2006).

[93] C. Quilliet, C. Zoldesi, C. Riera, A. Imhof, and A. van Blaaderen, *Anisotropic colloids through buckling in solution*, in preparation (2006).

[94] P. de Pablo, J. Colchero, J. Gomez-Herrero, and A. Baro, *Jumping mode scanning force microscopy*, Appl. Phys. Lett. **73**, 3300 (1998).

[95] L. Pauchard, Y. Pomeau, and S. Rica, *Déformation des coques élastiques*, C.R. Acad. Sci., Ser.IIb **324**, 411 (1997).

[96] A. Fery, F. Dubreuil, and H. Möhwald, *Mechanics of artificial microcapsules*, New journal of Physics **6**, 18 (2004).

[97] M. Ashby, *Materials selection in mechanical design*, Elsevier, 2nd edition, 1999.

[98] L. Pauchard and Y. Couder, *Invagination during the collapse of an inhomogeneous spheroidal shell*, Europhys. Lett. **66**, 667 (2004).

[99] N. Tsapis, E. Dufresne, S. Sinha, C. Riera, J. Hutchinson, L. Mahadevan, and D. Weitz, *Onset of Buckling in Drying Droplets of Colloidal Suspensions*, Phys. Rev. Lett. **94**, 018302 (2005).

[100] M. Bessis, *Cytology of the Blood and Blood-Forming Organs*, Grune and Stratton: New York, 1956.

[101] G. Lim, M. Wortis, and R. Mukhopadhyay, *Stomatocyte-dyscocyte-echinocyte sequence of the huma red blood cell: Evidence for the bilayer-couple hypothesis from membrane mechanics*, Proc.Natl.Acad.Sci.USA **99**, 16766 (2002).

[102] R. Mukhopadhyay, G. Lim, and M. Wortis, *Echinocyte Shapes: bending, Stretching, and Shear Determine Spicule Shape and Spacing*, Biophys. J. **82**, 1756 (2002).

[103] M. Okubo, H. Minami, and K. Morikawa, *Production of micron-sized, monodisperse, transformable rugby-ball-like-shaped polymer particles*, Colloid. Polym. Sci. **279**, 931 (2001).

[104] M. Okubo, H. Minami, and K. Morikawa, *Influence of shell strenght on shape transformation of micron-sized, monodisperse, hollow polymer particles*, Colloid Polym. Sci. **281**, 214 (2003).

[105] C. Quilliet, *Despressions at the surface of an elastic spherical shell submitted to external pressure*, submitted (2006).

[106] M. Amar and Y. Pomeau, *Crumpled Paper*, Proc. R. Soc. Lond. A **453**, 729 (1997).

[107] K. Brakke, *The Surface Evolver*, Exp. Math **1**, 141 (1992).

[108] L. Pauchard and S. Rica, *Contat and compression of elastic spherical shells: the physics of a 'ping-pong'ball*, Philos. Mag. B **78**, 225 (1998).

[109] S. Komura, K. Tamura, and T. Kato, *Buckling of spherical shells adhering onto a rigid substrate*, Eur. Phys. J. E **18**, 343 (2005).

[110] L. Gibson, *Cellular Solids*, MRS Bulletin **April**, 270 (2003).

[111] D. Green and P. Colombo, *Cellular Ceramics: Intriguing Structures, Novel Properties, and Innovative Applications*, MRS Bulletin **April**, 296 (2003).

[112] J. Banhart, M. Ashby, and N. Fleck, *Metal Foams and Porous Metal Structures*, MIT-Verlag: Bremen, 1999.

[113] L. Gibson and M. Ashby, *Cellular Solids: Structure and Properties*, Cambridge University Press: Cambridge, 2nd edition, 1997.

[114] J. Banhart, *Aluminum Foams: On the Road to Real Applications*, MRS Bulletin **April**, 290 (2003).

[115] B. Leyda, *Applications for Open-Cell Metallic Foams*, MRS Bulletin **April**, 292 (2003).

[116] J. Karp, P. Dalton, and M. Shoichet, *Scaffolds for Tissue Engineering*, MRS Bulletin **April**, 301 (2003).

[117] F. Cahn, *Clinical Use of Porous Scaffolds for Tissue Engineering of Skin*, MRS Bulletin **April**, 302 (2003).

[118] A. Imhof and D. Pine, *Ordered macroporous materials by emulsion templating*, Nature **389**, 948 (1997).

[119] A. Imhof and D. Pine, *Uniform Macroporous Ceramics and and Plastics by Emulsion Templating*, Adv. Mater. **10**, 697 (1998).

[120] A. Imhof and D. Pine, *Preparation of Titania Foams*, Adv. Mater. **11**, 311 (1999).

[121] U. Schwarz, S. Komura, and S. Safran, *Deformation and tribology of multi-walled hollow nanoparticles*, Europhys. Lett. **50**, 762 (2000).

[122] N. Elsner, F. Dubreuil, and A. Fery, *Tuning of microcapsule adhesion by varying the capsule-wall thickness*, Phys. Rev. E **69**, 031802 (2004).

[123] J. Israelachvili, *Intermolecular and Surface Forces*, Academic Press, Harcourt Brace and Company, 2nd edition, 1991.

[124] D. Weaire and S. Hutzler, *The Physics of Foams*, Oxford University Press, USA: Oxford, 1999.

[125] N. Husing and U. Schubert, *Aerogels-Airy Materials: Chemistry, Structure, and Properties*, Angew. Chem. Int. Ed. **37**, 22 (1998).

[126] P. Schmidt-Winkel, W. L. Jr., D. Zhao, P. Yang, B. Chmelka, and G. Stucky, *Mesocellular Siliceous Foams with Uniformly Sized Cells and Windows*, J. Am. Chem. Soc. **121**, 254 (1999).

[127] P. Schmidt-Winkel, W. L. Jr., P. Yang, D. Margolese, J. Lettow, J. Ying, and G. Stucky, *Microemulsion Templating of Siliceous Mesostructured Cellular Foams with Well-Defined Ultralarge Mesopores*, Chem. Mater. **12**, 686 (2000).

[128] B. Droop, *Point Defects in Colloidal Photonic Crystals*, Internal report, Soft Condensed Matter Group, Utrecht University (2006).

[129] R. van 't Hoog, *Doping colloidal photonic crystals with dielectric defects*, Internal report, Soft Condensed Matter Group, Utrecht University (2006).

[130] Y. L. Wu, *Private communications.*

[131] V. Manoharan, M. Elsesser, and D. Pine, *Dense Packing and Symmetry in Small Clusters of Microspheres*, Science **301**, 483 (2003).

SUMMARY

Particles with a size ranging from several nanometers up to several micrometers, generally known as colloids, have gained increasing interest due to their wide range of applications. Colloidal particles can be tuned in size, shape and chemical composition. They exhibit similar phase behavior as atoms and molecules and therefore they have become an important model system to study, from a scientific point of view. Colloids are also very important from a technological point of view. They find applications in various areas, from encapsulation of products to development of advanced materials. A distinct class of colloids is represented by the hollow particles, which are of interest in the fields of medicine, pharmaceutics and materials science.

The work described in this thesis can be roughly divided in three main parts: synthesis of a new type of hollow colloidal particles, with an elastically deformable shell, their characterization and materials obtained from assembly of such colloids. In the first part we focused on developing a new method to prepare micrometer-sized hollow particles. Our approach is introduced in Chapter 2 and is based on an emulsion templating technique in which monodisperse silicone oil-in-water emulsion droplets, surfactant free, were used as templates for the encapsulation with solid shells. Monodisperse PDMS oil droplets were prepared by hydrolysis and polymerization of dimethylsiloxane monomer, and incorporated in a solid shell using tetraethoxysilane. After the encapsulation, the droplets consisting of low molecular weight silicone oil were easily removed by dissolution in ethanol. We showed that emulsion templating can be successfully used to prepare monodisperse, micrometer-sized hollow particles, with variable shell thicknesses, from 5 - 300 nm, in a simple two-step process. Using this method, we synthesized three different types of hollow particles, with different properties, simply by tuning the ratio between the shell thickness and the particle radius. They were designated as microspheres, microcapsules and microballoons, based on the way they collapse upon drying. The microspheres remain un-deformed as a result of drying; the microcapsules, more flexible and deformable, collapse, forming hemispherical, double-walled caps, while the microballoons have a crumpled appearance.

In Chapter 4, we extended our encapsulation method to surfactant-stabilized emulsion droplets. We have shown that both surfactants used (SDS, an anionic and Triton X-100, a non-ionic surfactant), cause a decrease in the average radius of the droplets, but they are effective in different concentration ranges due to their different critical micelle concentration. Moreover, in both cases, we found a linear dependence of the droplet radius on the logarithm of surfactant concentration, indicating that the surfactant mainly influences the oil droplets through a reduction in interfacial tension of the oil/water interface. The surfactant-stabilized oil droplets can be also used as templates for encapsulation with solid shells. When Triton X-100 was used to stabilize the droplets, we obtained hollow particles of different shell thicknesses, in one growth step, similar as for the surfactant free emulsions. However, in the case of SDS-stabilized emulsions, we only obtained relatively thin shells, due to the fact that, although we were not able to detect it, probably SDS was still present on the surface of the shells and its higher surface charge, possibly in addition to surface wetting properties, prevented the growth of silica monomers and small oligomers to take place. Preliminary experiments showed that our coating procedure can be extended also to other types of oil droplets stabilized by surfactants.

The second part of the thesis is focused on particle characterization, from physical and chemical point of view. In Chapter 3, both the emulsion droplets used as templates and the resulting hollow shells were investigated in detail. Because of the slow reaction, the PDMS oil droplets obtained from hydrolysis and polymerization of dimethylsiloxane monomer are excellent templates for encapsulation with solid shells using tetraethoxysilane. We found that the shell formation is a copolymerization between the monomer used to prepare the oil droplets (DMDES) and tetraethoxysilane. The condensation of DMDES limits the rate of growth for both the oil droplets and the shell. The shells consist mainly of dimethylsiloxane units cross-linked with tetra-functional silicate units. The properties of the shells resemble more closely those of silicone rubber than of silica. We also showed that the shells are permeable to small molecules, which makes them interesting as encapsulation agents. Moreover, fluorescent dye molecules can be either incorporated into the shell material, or adsorbed at the surface. This is important for their use in making ordered structures which can be studied by confocal microscopy. For the type of silica/siloxane shells prepared, the deformability of the particles depends only on the ratio between the shell thickness and the particle radius. Due to the specific reaction kinetics, the ratio can be influenced either by varying the time between the preparation of the emulsions and the start of the coating step, or by choosing different times for ending the encapsulation reaction.

Special emphasis was put on the elastic properties of the hollow shells, in Chapter 5. We found that they could be understood well with elasticity theory applied to a thin spherical shell. The elastic properties were probed by nanoindentation measurements, in which point forces were applied to particles supported on a flat surface using a Scanning Force Microscope. We showed that the shells have a linear response up to forces of several nN, with an elastic constant depending on the shell thickness, for a given size of the template. In the linear region, the particle deformation is reversible. However, permanent deformations were induced after probing the shells repetitively, or beyond the linear regime. The value for the Young's modulus obtained from the indentation measurements, combined with the density of the shell material determined in Chapter 3, indicates that our material is situated somewhere at the boundary between soft polymers and stiff rubbers. Additionally, the deformation of the particles was achieved by an original method consisting of the partial dissolution of the solvent initially contained in the shells. We have shown in Chapter 5 that the shapes observed after buckling are consistent with a model of elastic homogenous thin spherical shells submitted to an isotropic external pressure. These particles could find applications in studies of monodisperse non-spherical colloids.

The last part of the thesis is focused on preliminary investigations of materials that can be fabricated by the assembly of hollow shells into larger aggregates. We showed in Chapter 6 that the particles' deformability makes it possible to prepare new types of regularly deformed particles, bubble-like clusters and solid microcellular foams. The deformation of the shells upon cluster formation could be understood from a balance between adhesive van der Waals forces, and repulsive elastic forces. In Chapter 6 we also discussed methods to prepare silica/siloxane macroporous structures based on PDMS droplets coated with very thin shells (a few nm) and hollow shells. We obtained 2D microcellular structures with well-defined pores, with sizes comparable with the size of particles core, which resemble two dimensional foams. Alternatively, we were able to obtain 3D silica/siloxane solid foams, with pores which maintained their spherical shape, or formed polygonal cells, depending on the relative shell thickness and the preparation method. Due to the low density of the silica/siloxane material of the shell combined with the presence of the pores, these materials have a very low density and high porosity. Both 2D foams and 3D structures were obtained also using fluorescently labeled particles, which made possible their investigation using confocal microscopy. Additionally, preliminary investigations showed promising results in using the fluorescently labeled hollow shells as dielectric defects in photonic crystals, but the fabrication method needs to be optimized. This can be done by using hollow shells with exactly the same diameter as the silica particles and with larger relative shell thickness in order to prevent them from collapsing after drying.

SAMENVATTING

Colloïdale deeltjes, met een grootte van enkele nanometers tot enkele micrometers, worden steeds belangrijker vanwege hun diverse toepassingen. Het is mogelijk om colloïdale deeltjes te maken met verschillende groottes, vormen en chemische samenstellingen. Colloïden gedragen zich thermodynamisch net als atomen en moleculen. Daarom worden ze gebruikt als modelsysteem. Ze zijn ook van groot belang voor technologische applicaties. Ze worden gebruikt in verschillende gebieden, bijvoorbeeld voor het inkapselen van producten en voor de ontwikkeling van geavanceerde materialen. Holle colloïdale deeltjes zijn een afzonderlijke categorie met toepassingen in de geneeskunde, farmacie en materiaalkunde.

Het onderzoek beschreven in dit proefschrift kan verdeeld worden in drie delen: de synthese van een nieuwe soort holle colloïdale deeltjes, met een schil die flexibel en elastisch is, de karakterisering van de deeltjes en de fabricatie van materialen door zelf-assemblage van dit soort colloïden. In deel één hebben we ons geconcentreerd op de ontwikkeling van een nieuwe methode om holle deeltjes met een grootte van $\sim$ micrometer te verkrijgen. Hoofdstuk 2 introduceert onze aanpak, die gebaseerd is op het gebruik van een mal. In deze methode, wordt de mal gevormd door monodisperse, siliconenolie-in-water emulsiedruppels, die zonder surfactant zijn gemaakt. De oliedruppels worden in een solide schil ingekapseld. De monodisperse PDMS, (polydimethylsiloxaan) oliedruppels zijn gemaakt door middel van de hydrolyse en polymerisatie van dimethylsiloxaanmonomeer en worden ingekapseld in een vaste schil door gebruik te maken van tetraethoxysilaan. Na de inkapseling, worden die druppels makkelijk verwijderd door ze op te lossen in ethanol. Dit gebeurt omdat de druppels bestaan uit een siliconenolie met een laag molair gewicht silicon, dat oplosbaar is in ethanol.

We laten zien dat deze methode succesvol gebruikt kan worden om monodisperse, holle deeltjes met een diameter van 5 tot 300 nanometer te maken, met een variabele schil dikte. Met behulp van deze methode, en door aanpassing van de dikte van de schil en de straal van de deeltje, hebben we drie soorten deeltjes gemaakt. We hebben ze microbollen, microcapsules and microbalonnen genoemd, vanwege hun manier van inklappen als ze droog worden. De microbollen blijven in dezelfde vorm, zonder zich te deformeren; de microcapsules zijn flexibeler, ze vormen een soort van hemisferische capsules, en de microbalonnen zien er verfrommeld uit.

Onze inkapselingsmethode wordt in hoofdstuk 4 uitgebreid naar emulsies die door een surfactant gestabiliseerd zijn. We hebben twee surfactanten gebruikt: SDS, dat anionisch is, en Triton X-100, dat non-ionisch is. Beide veroorzaken een reductie in de gemiddelde straal van de druppels, maar ze zijn effectief bij andere concentraties. Dit komt door hun verschillende kritische concentraties voor micelvorming. Bovendien hebben we voor beide surfactanten een lineaire afhankelijkheid tussen de straal van de druppel en de logaritme van de concentratie van de surfactant gevonden. Deze afhankelijkheid is een indicatie dat de surfactanten invloed hebben op de oliedruppels via een reductie van de grensvlakspanning van het olie-watergrensvlak.

De surfactant-gestabiliseerde oliedruppels kunnen ook voor inkapseling met een solide schil gebruikt worden. Voor de Triton X-100 gestabiliseerde druppels, hebben we holle deeltjes met verschillende diktes van de schil gemaakt, in één stap, net als voor de emulsies zonder surfactant. Echter, in het geval van SDS gestabiliseerde druppels, hebben we slechts een dunne schil gekregen. Hoewel we de SDS niet hebben waargenomen, is het mogelijk dat SDS aanwezig is aan het oppervlak van de druppels. De hogere oppervlaktelading vas SDS, in combinatie met de oppervlaktebevochtiging, voorkomen de groei van de silica monomeren en de kleine oligomeren. Daarnaast tonen enkele zeer recente experimenten aan dat onze inkapselingsmethode ook naar andere soorten olie druppels, gestabiliseerd door surfactanten, uitgebreid kan worden.

In deel twee van dit proefschrift presenteren we de karakterisatie van onze holle colloïden. Zowel de emulsiedruppels als de holle deeltjes worden in hoofdstuk 3 in detail bestudeerd. Vanwege hun lage reactiesnelheid zijn de PDMS druppels zeer geschikt als templates voor inkapseling met behulp van tetraethoxysilaan. De schil rond de druppels is gevormd door een copolymerisatie tussen het monomeer dat voor de oliedruppels gebruikt is en de tetraethoxysilaan. De condensatie van DMDES beperkt de snelheid waarmee zowel de olie druppels als de schil groeien. De schillen bestaan voornamelijk uit een netwerk van dimethylsiloxaan eenheden en vierwaardig gefunctionaliseerde sillicaat eenheden. De eigenschappen van onze schillen lijken meer op die van een rubberachtig materiaal dan op die van silica. We tonen ook aan dat de schillen voor kleine moleculen permeabel zijn. Daarmee zijn ze interessant als opslageenheden. Daarnaast laten we zien dat fluorescente moleculen in de schil ingebouwd kunnen worden of op het oppervlak van de schil geadsorbeerd kunnen worden. Verschillende structuren kunnen door fluorescente schillen gevormd worden en ze kunnen met een confocale microscoop bestudeerd worden.

In het geval van onze silica/siloxaan schillen hangt de deformatie slechts af van de verhouding tussen de dikte van de schil en de straal van de deeltjes. We kunnen deze verhouding op twee manieren beïnvloeden: door de tijd tussen de bereiding van de emulsies en het begin van de inkapselingstap te variëren, of door de inkapselingsreactie na verschillende tijden te stoppen.

In hoofdstuk 5 hebben de elastische eigenschappen van de holle schillen bijzondere aandacht gekregen. We komen tot de conclusie dat ze door de theorie van elasticiteit toegepast aan een dunne sferische schil goed begrepen kunnen worden. We hebben deformatiemetingen met behulp van een "Scanning Force Microscoop" (SFM) gedaan. Bij deze metingen wordt een kracht op een enkel punt van de schil uitgeoefend. We laten zien dat de schillen op een lineaire manier op krachten tot enkele nN reageren. Daarnaast hangt de elastische constante af van de dikte van de schil voor ee gegeven grootte van de oliedruppel. Binnen het lineaire domein ondergaan de deeltjes een reversibele deformatie. Desondanks zijn buiten het lineaire domein ook permanente deformaties te zien. Permanente deformaties kunnen ook door herhaalde uitoefening van krachten worden veroorzaakt. Vervolgens hebben we uit de metingen de Youngs modulus bepaald. De uitkomst, samen met de dichtheid van het schilmateriaal die we in hoofdstuk 3 hebben berekend, wijzen erop dat ons materiaal tussen zachte polymeren en stijve rubbers gesitueerd is.

Daarnaast is in hoofdstuk 5 een originele methode voor de deformatie van de deeltjes beschreven. In deze methode wordt de inhoud van de deeltjes gedeeltelijk opgelost, wat leidt tot het inklappen van de deeltjes. De vormen na het inklappen zijn verenigbaar met een model van een sferische schil die elastisch, homogeen en dun is, en die aan een isotrope en externe druk blootgesteld worden. Deze deeltjes kunnen toegepast worden als modelsystemen met monodisperse colloïden die geen sferische vorm hebben.

Tenslotte laten we onze zeer recente resultaten zien wat betreft de fabricatie van materialen door zelf-assemblage van de holle schillen. In hoofdstuk 6 tonen we aan dat de deformatie leidt tot nieuwe soorten van ordelijk gedeformeerde deeltjes. Dit kunnen kleine clusters zijn of micro-cellulaire structuren die op schuim lijken. We verklaren de deformatie van de schillen in de cluster structuur door middel van een balans tussen de attractieve van der Waals krachten en de repulsieve elastische krachten. In ditzelfde hoofdstuk 6 presenteren we ook enkele methoden die tot poreuze "silica/siloxaan" structuren leiden. Om deze structuren te vormen hebben we zowel PDMS druppels ingekapseld in een dunne schil als holle schillen gebruikt. We hebben 2D micro-cellulaire structuren gekregen die goed gedefinieerde poriën hebben. De grootte van de poriën is vergelijkbaar met de grootte van de kern van de deeltjes. Eveneens laten we "silica/siloxaan" 3D solide schuimen zien. In dit geval hebben de poriën een sferische vorm, net als de schillen, of ze vormen veelhoekige cellen, afhankelijk van de relatieve dikte van de schil en de methode die gebruikt is. De lage dichtheid van de schil, samen met de aanwezigheid van de poriën, bepaalt de lage dichtheid en hoge poreusheid van deze micro-cellulaire structuren. Zowel de 2D als de 3D structuren kunnen ook fluorescent gemaakt worden door gebruik te maken van fluorescente deeltjes. Daardoor kunnen ze met confocale microscopie bestudeerd worden. Daarnaast beschrijven we enkele recente experimenten waarin de holle, fluorescente schillen als diëlektrische defecten in fotonische kristallen gebruikt worden. Deze methode kan nog geoptimaliseerd worden, bijvoorbeeld door gebruik te maken van holle deeltjes met dezelfde diameter als de silica deeltjes en/of met relatief dikkere schil, zodat ze niet inklappen.

PUBLICATIONS

Publications related to the work described in this thesis:

- *Synthesis of monodisperse colloidal spheres, capsules and microballoons by emulsion templating*; Advanced Materials, **17**, 924 (2005); C.I. ZOLDESI AND A. IMHOF. (Chapter 2)

- *Deformable hollow hybrid silica/siloxane colloids by emulsion templating*; Langmuir, **22**, 4343 (2006); C.I. ZOLDESI, C. VAN WALREE AND A. IMHOF. (Chapter 3)

- *Hollow colloidal particles by surfactant-stabilized emulsion templating*; In preparation (2006); C.I. ZOLDESI, P. STEEGSTRA AND A. IMHOF. (Chapter 4)

- *Elastic properties of hollow colloidal particles*; In preparation (2006); C.I. ZOLDESI, I.L. IVANOVSKA, G.J.L. WUITE AND A. IMHOF. (Chapter 5)

- *Anisotropic colloids through buckling in solution*; In preparation (2006); C. QUILLIET, C.I. ZOLDESI, C. RIERA, A. IMHOF AND A. VAN BLAADEREN. (Chapter 5)

- *Solid silica/siloxane microcellular structures* ; In preparation (2006); C.I. ZOLDESI AND A. IMHOF. (Chapter 6)

Other publications:

- *EPR investigations of the* Fe_2O_3-Bi_2O_3-PbO-As_2O_3 *glass system*; Studia University Babes-Bolyai.Physica **1**(2001); M. PETEANU, C. BORSA AND I. ARDELEAN

- *The influence of melting temperature on iron ion distribution in* Bi_2O_3-PbO-As_2O_3 *glass matrix, studied by EPR*; Modern Physics Letters B, **14**, 785 (2000); I. ARDELEAN, M. PETEANU, V. SIMON, C. BORSA, F. CIORCAS AND V. IONCU

- *Spectroscopic and photoacoustic investigation of x($V_2O_5 \cdot CuO$)(1-x)[3 $Bi_2O_3 \cdot K_2O$] glasses*; Journal of Molecular Structure, **482-483**, 675 (1999); I. Bratu, I. Ardelean, A. Barbu, D. Maniu and C. Borsa

- *Spectroscopic investigations of x($V_2O_5 \cdot CuO$)(1-x)[3 $Bi_2O_3 \cdot K_2O$] glasses*; Balkan Physics Letters, **5**, 199 (1997); D. Maniu, I. Ardelean, I. Bratu, R. Grecu, O. Cozar, T. Iliescu and C. Borsa

ACKNOWLEDGEMENTS

There are many people who contributed directly or indirectly, to the work described in this thesis. I am grateful to all of you!

Most of all, I would like to acknowledge my supervisor, Arnout Imhof, who made everything possible from the very beginning up to the very end. Thank you for the interesting and challenging research subject, many fruitful discussions, your guidance and patience with which you've read over and over again all my manuscripts. I enjoyed very much working with you and it was a privilege to have you as supervisor. My gratitude goes also to my promotor, Alfons van Blaaderen, for giving me the opportunity to work in a very competitive group, in an extremely stimulating atmosphere. Thank you for your support, valuable suggestions and interest in my research.

During my years in Utrecht, I collaborated with many people both from my own group and outside of it. Especially I would like to thank my colleague Carlos van Kats for introducing me to the world of fluorescence, for all the SEM work we did together and for many interesting discussions we had over the years, both in English and Dutch. Many thanks also to Dannis 't Hart for the help with some of the SEM images. For the EDX measurements from Chapter 2, 3 and 4, performed in the Molecular Cell Biology Group, I am very much grateful to Hans Meeldijk. The understanding of the reaction mechanisms wouldn't have been possible without the NMR investigations shown in Chapter 3, for which I thank Kees van Walree from the Organic Chemistry and Catalysis Group. We had interesting discussions and a fruitful collaboration. The experiments with surfactants included in Chapter 4 are partially due to the extensive work of my student, Patrick Steegstra. Thank you Patrick and good luck with your PhD. I enjoyed a lot the collaboration with Catherine Quilliet on buckling of colloids, which materialized in the second part of Chapter 5. Thank you Catherine for the scientific input but also for the nice time we spent together. A very interesting and rewarding experience I shared with Irena Ivanovska from Vrije Universiteit Amsterdam. The SFM nanoindentation experiments we did together were possible also due to the support of your supervisor, Gijs Wuite, and are shown in the first part of Chapter 5. The beautiful foam structures presented in Chapter 6 were possible using the spin-coating, method I've learned from Yu Ling Wu, who also successfully incorporated my shells in silica crystals. I want to mention also Benjamin Dollet,

the author of the software used to analyze the foam structures.

The special atmosphere in room 014 from Ornstein Laboratory was both inspiring and relaxing, thanks to the people who passed by. With Christina and Job I spent most of my time there. We shared many interesting discussions on various topics, scientific or not. I couldn't have wished for a better company. I think we've all learned a lot from each other. And Job, thank you for being always very helpful, for providing mathematica notebooks and a critical revision of my Dutch summary. I also shared the office with Jacob, for a short period of time in the beginning; in the end Teun brought something new to the office and contributed as well to the clarity of my Dutch summary.

The Soft Condensed Matter Group was a great place to work, with a stimulating atmosphere and enthusiastic people. I really had a wonderful time. Especially I thank Didi for being a good friend, for the fun we had with our experiments and for the squash lessons. I think I've learned some Dutch words almost from everybody, but I want to thank particularly to Mirjam, Astrid and Esther for their interesting and unusual advices. Joan, Marjolein, Alejandro, Eduardo, Michiel, Andrea, Peter, Andrew, Ahmet, Matthiew and Rene, thank you all for contributing to the group activities, which I enjoyed a lot. And Peter, our tweezers experiments were quite interesting, I hope something will come out of them. I shared many cakes and opinions with the members of the Molecular Biophysics Group, too. Especially with Dave I had interesting discussions and a lot of fun during the volleyball games. Maria was always helpful and Hans took good care of my computer and the SLS set-up. I had useful and pleasant discussions with former members of our group, among which I would like to mention Dirk, Krassimir, Patrick, Matthias, Paddy, Antti-Pekka and Slava. I would also like to thank our students, and in particular to Brian and Ronen, for their experiments on defects in photonic crystals. I also appreciated a lot the meetings with the FCC group; thank you all for the interesting discussions and for the nice moments we had together. The people from the P&O department were always helpful with various administrative problems, and in particular many thanks to Thea. As for my friends, the last years wouldn't have been the same without your presence. Thank you all!

Finally, but equally important, my gratitude goes to those who are dearest to me, my family. Close or far away, your love and support meant a lot to me. Dana, I will always be grateful for everything you did for me, at any moment, for being closer to me than ever, as two sisters should always be. You had a major contribution to the "positive output", so did Jacob, with the extremely inspired design of my cover.

And mostly, thank you Antoni for being there for me.

CURRICULUM VITAE

Carmen Iulia Zoldesi was born on 19th of August 1974 in Tăsnad, a small town situated in the north-west of Romania. In 1992, she graduated "Mihai Eminescu" high school from Satu Mare, the mathematics-physics section.

From the autumn of the same year, she studied physics at Babes-Bolyai University, Cluj-Napoca, which she graduated in 1996. In June 1997 she obtained her M.Sc. degree in materials science at the same university, in the group of prof. Ioan Ardelean, during which she did spectroscopic studies of glass systems containing vanadium and copper ions. After her master, she continued to collaborate with prof. Ardelean on various projects involving glassy systems containing iron ions, while working as a physics teacher in Satu Mare and later on as a physicist at Central Laboratory of National Administration of Roads in Cluj-Napoca.

In September 2002 she started her PhD at Utrecht University, in the Soft Condensed Matter Group of prof. dr. Alfons van Blaaderen, under the supervision of dr. Arnout Imhof. During this time, she developed a facile procedure to obtain new types of hollow colloidal particles with an elastically deformable shell. These interesting colloids were extensively characterized and used for fabrication of various materials, from crystalline to microcellular structures. The results of her research are described in this thesis and published in scientific journals. The author participated at various schools and workshops and presented her work at international conferences.

COLOPHON

The cover represents an artistic interpretation of Figure 3.6 of this thesis, where it is shown that the final shape of spherical hollow colloids depends on their relative shell thickness. In the drawing, a third dimension was added to depict the transition from colloidal foam to individual spheres.
Cover design by Jacob Kerssemakers, August 2006.

Printed by: Ipskamp